

Technical Report

TR-98-24

Investigation of the large scale regional hydrogeological situation at Beberg

Lee Hartley
AEA Technology, UK

Anders Boghammar, Bertil Grundfelt
Kemakta Konsult AB

December 1998

Svensk Kärnbränslehantering AB

Swedish Nuclear Fuel
and Waste Management Co
Box 5864
SE-102 40 Stockholm Sweden
Tel 08-459 84 00
+46 8 459 84 00
Fax 08-661 57 19
+46 8 661 57 19



Investigation of the large scale regional hydrogeological situation at Beberg

Lee Hartley
AEA Technology, UK

Anders Boghammar, Bertil Grundfelt
Kemakta Konsult AB

December 1998

This report concerns a study which was conducted for SKB. The conclusions and viewpoints presented in the report are those of the author(s) and do not necessarily coincide with those of the client.

Information on SKB technical reports from 1977-1978 (TR 121), 1979 (TR 79-28), 1980 (TR 80-26), 1981 (TR 81-17), 1982 (TR 82-28), 1983 (TR 83-77), 1984 (TR 85-01), 1985 (TR 85-20), 1986 (TR 86-31), 1987 (TR 87-33), 1988 (TR 88-32), 1989 (TR 89-40), 1990 (TR 90-46), 1991 (TR 91-64), 1992 (TR 92-46), 1993 (TR 93-34), 1994 (TR 94-33), 1995 (TR 95-37) and 1996 (TR 96-25) is available through SKB.

Abstract

The present study forms part of the large-scale groundwater flow studies within the SR 97 project. The site of interest is Beberg which is based on data from the Finnsjön site.

To understand the groundwater flow and salinity at present it is necessary to consider the history of the Finnsjön site over the last few thousand years. A numerical approach is developed to model a situation of transient variable density flow on a regional scale. The model is considered a reasonable representation of the real situation at the site, since it is consistent with the current conceptual understanding of the site and predictions of salinity are in broad agreement with field observations. The effects of post-glacial uplift on the hydrogeological conditions are considered. It is assumed that about 9,000–4,000 years BP the rock was completely infiltrated by saline groundwaters during the periods when the Yoldia and Litorina Seas covered the Finnsjön area. The model represents the interval from the end of this period up to the present day. During which time the recharge of fresh water in the form of rainfall flushed or displaced saline water from the near-surface. Many variants on the basic conceptual model are considered both to calibrate the model against field data and to quantify the sensitivities of groundwater pathways.

The present study shows that:

- Salinity and transient processes are very important in determining groundwater pathways in the deep rock. Salinity drives flow downwards increasing the length of pathways and groundwater travel times.
- A high contrast in hydraulic conductivity between major structures and the rock mass results in the fractures zones being the dominant flow paths, in particular Zone 1 and Imundbo.
- There are two distinct flow paths. In the east of the hypothetical repository the path is short along Zone 1, for the west the path is longer through the rock mass.
- Fractures zones are flushed of salt on a time-scale of 10-100 years. For the rock mass it takes a few thousand years in the near-surface and about 10,000 years for the deep rock.
- The model can only be calibrated by including a semi-impermeable band in Zone 2, and truncating the fracture Zones around the northern block below Zone 2.
- The total porosity is an important parameter to calibrate. A value of 2% was used for the rock mass and 5% for the fracture zones.
- Approximate boundary conditions may be supplied to the site model by transferring the environmental pressure (density adjusted) obtained on the regional scale model.

Abstract (Swedish)

Den aktuella studien är en del av den storskaliga grundvattenmodellering som utförs inom SR 97. Den aktuella platsen för denna studie är Beberg som baseras på data från Finnsjön.

För att förstå grundvattensituationen vid Beberg vad avser nuvarande strömning och salthaltsfördelning är det nödvändigt att ta med Finnsjöområdets historiska utveckling över de senaste årtusendena. Ett numeriskt angreppssätt har utvecklats för att kunna studera transient flöde med variabel densitet i en regional skala. Modellen bedöms utgöra en rimlig representation av de verkliga förhållandena i området, eftersom den står i överensstämmelse med den rådande konceptuella förståelsen av området och eftersom de med hjälp av modellen framtagna förutsägelserna av salthaltsfördelningen står i rimligt god överensstämmelse med gjorda fältobservationer. I modellen har hänsyn tagits till effekterna av den postglaciala landhöjningen på de hydrologiska förhållandena i området. I studien antas att berget för 9000-4000 år sedan, då Yoldia- och Litorinahaven täckte Finnsjö- området, helt mättades upp med salt grundvatten. Modellen representerar utvecklingen under tidsperioden från Litorina till nutid. Under denna period har sött regnvatten infiltrerat berggrunden och successivt spolat ut saltvatten från de övre delarna av berget. I studien har många varianter körts för att kalibrera modellen mot fältdata och för att kvantifiera strömningsvägarnas känslighet för olika modellantaganden.

Studien visar:

- Inverkan av salt och transienta processer är mycket viktiga mekanismer som styr grundvattenflödet djupt ner i berget. Salt grundvatten strävar att strömma neråt varigenom strömningsvägarnas längd och grundvattnets strömningstid förlängs.
- Hög permeabilitetskontrast mellan bergmassa och sprickzoner leder till att sprickzonerna blir dominerande strömningsvägar, särskilt Zon 1 och Imundbo.
- Det finns i området två distinkta flödesvägar. Öster om det hypotetiska förvaret återfinns en kort strömningsväg som följer Zon 1, och väster om förvaret återfinns en längre strömningsväg genom bergmassan.
- Den tid det tar att spola ut saltvattnet ur sprickzonerna är i storleksordningen 10-100 år. För den yt nära bergmassan är motsvarande tid några få tusen år medan tiden för att spola ur de djupare liggande bergpartierna är ca 10 000 år.
- Modellen kan tillfredsställande kalibreras mot fältobservationer endast om ett lågpermeabelt skikt inkluderas i Zon 2 och om de zoner som omger det norra blocket trunkeras under zon 2.
- Den totala porositeten är en viktig kalibreringsparameter. För bergmassan används ett värde på 2% och i sprickzonerna 5%.
- Rimliga ungefärliga randvillkor till en lokalmodell kan fås genom att överföra "environmental pressure" (densitetsjusterat) som beräknats i den regionala modellen.

Contents

1	BACKGROUND AND OBJECTIVES	1
2	INTRODUCTION	3
2.1	Site Location	3
2.2	Modelling Techniques	3
2.3	Effects of Salinity	5
2.4	Natural Transient Processes	5
2.4.1	Post-Glacial Conditions	5
2.4.2	Transient Salt Evolution	6
2.4.3	Initial Condition	10
2.5	Boundary Conditions	10
2.5.1	Pressure Boundary Conditions	11
2.5.2	Salt Boundary Conditions	12
3	HYDROGEOLOGY AT THE BEBERG SITE	15
3.1	Topography	15
3.2	Structural Model	15
3.3	Hydrogeological Properties	20
3.4	Salinity Data	24
4	REGIONAL MODEL	27
4.1	Location and Size	27
4.2	Finite-Element Mesh	28
4.3	Boundary Conditions	31
4.3.1	Salt Boundary Conditions	32
4.4	Base Case Hydrogeological Properties	35
4.5	Time-Steps	36
4.6	Evolution of Salinity and Pressure	37
5	CALIBRATION	41
5.1	Near Surface Flows	41
5.2	Salinity Pattern	42
5.2.1	Base Case - Salinity on Vertical Sections	42
5.2.2	Base Case - Salinity in Boreholes	43
5.3	Calibration Variants	45
5.3.1	Depth of Local Fracture Zones (Zdeep)	46
5.3.2	Extra Fracture Zones in South (Zsouth)	48

5.3.3	Higher Hydraulic Connectivity Across Zone 2 (Z2highK)	50
5.3.4	Lower contrast between Rock Mass and Fracture Zones (ZlowK + ZlowK ϕ)	51
5.3.5	Inclusion of Zone 11 in Southern Rock Block (Z11)	52
5.3.6	Specified Salinity on Upstream Boundary (Csouth)	53
5.3.7	Lower Porosity (ϕ low)	55
5.3.8	Lower Dispersion Length (Dlow)	55
5.3.9	Implicit Inclusion of Local Fracture Zones (Zlocal)	57
5.3.10	Horizontal Anisotropy (RRD3)	59
5.3.11	Hydraulic Conductivity in fracture Zones (AltK)	60
6	LOCATION OF SITE SCALE MODEL	65
6.1	Groundwater Flow Pathways at Repository Level	65
6.1.1	Base Case	65
6.1.2	Sensitivities	67
6.1.3	Freshwater (Uniform density) Case	75
6.2	Choice of Local Scale Model and Summary	76
6.3	Boundary Conditions	77
6.4	Comparison of Saline and Non-Saline Cases	78
7	DETAILED MODEL WITH LAND-RISE	81
7.1	Finer Interpolation of Topography	81
7.2	Representation of Land-Rise	84
8	CONCLUSIONS	91
8.1	Future Work	94
9	REFERENCES	97
A	COUPLED GROUNDWATER FLOW AND SALT TRANSPORT EQUATIONS	99
B	DATA	101
C	QUALITY ASSURANCE	105
C.1	File Locations	105
C.2	NAMMU Input Files	105

List of Tables

3.1	Fracture zones in the Beberg area as modelled within the present study.	20
3.2	Salinity in boreholes at the Finnsjön site.	24
4.1	Keyvalues for the finite-element grid.	29
4.2	Sequence of time-steps used in the transient modelling.	37
5.1	The set of calibration and sensitivity variants.	46
5.2	Local fracture zones represented implicitly in the Zlocal variant.	58
5.3	Hydraulic conductivities used in the Zlocal variant.	58
5.4	Hydraulic conductivities for the AltK variant. The same inference between zones is applied as for [<i>Walker et al., 1997</i>]	61
6.1	Summary of travel times for the sensitivity variants for 16 pathlines.	76
7.1	Summary of travel times for the two detailed variants.	84
B.1	Summary of hydrogeological data used in the modelling.	102
B.2	Hydrogeological parameters used in the modelling.	103
C.1	Input files for main cases	106

List of Figures

2.1	Location of the Beberg site. The boundaries of the regional and site scale models are shown in green and yellow, respectively.	4
2.2	Schematic evolution of saline transition zone for a homogeneous rock with a hydraulic gradient from left to right.	7
2.3	Schematic evolution of saline transition zone for a case with vertical fracture zones.	8
2.4	Sketch of evolution of saline transition zone for a case with vertical fracture zones and the sub-horizontal Zone 2.	9
3.1	Topography on a large scale. Data has been supplied by the SKB GIS system. Contours are shown at 10m, 20m, 30m and 40masl (as shown in the legend). The approximate location of fractures zones is indicated by the annotation (see Figure fig:StructModel for the detailed structural map).	16
3.2	Rock block map of the regional model (Lövstabruk area) including the Finnsjön Rock Block (rastered).	18
3.3	A schematic of the structural model used. Based on Walker et al. [1997]. The outer boundary indicates the extent of the regional scale model.	19
3.4	Hydraulic conductivities for the rock mass (long vertical lines) used in the modelling. The dots show the measured hydraulic conductivities in 3m sections of rock upscaled to the SGU data scale (100m) [Walker et al., 1997]. The horizontal lines show the mean and a 95% confidence bound (calculated as $\pm 2\sigma$, where σ is the standard deviation) of the logarithm of hydraulic conductivity.	21
3.5	Map of fracture zones and boreholes in the vicinity of the Finnsjön rock block. Reproduced from [Andersson et al., 1991].	26
4.1	Oblique view of the finite-element mesh as seen from the south. The location of the model is shown in Figure fig:StructModel. Boundary conditions used in the modelling are indicated.	28
4.2	Plan view of the finite-element mesh for the base case showing the fracture zones and hydrogeological properties in the top elements. The positions of the 3 vertical slices a-A, b-B and c-C used in the calibration are indicated. Three lakes and road 76 are also shown as a reference.	30
4.3	Oblique view of seven vertical slices through the finite-element mesh showing the hydrogeological properties. This plot was produced using the Avizier geovisualisation software.	31

4.4	Plan view of the head boundary condition on the top surface of the model. The numbers shown in the key are in units of metres. The positions of the 3 vertical slices a-A, b-B and c-C used in the calibration are indicated. Three lakes and road 76 are also shown as a reference.	32
4.5	Plan view of the flow field for a slice near the top surface. The calculation is for the initial condition at 4,000 years BP. The key indicates the logarithm and sign of the vertical component of darcy velocity in units of ms^{-1} . Three lakes and road 76 are also shown as a reference.	33
4.6	The locations of recharge and discharge areas used in defining the salt boundary conditions on the top surface. The northern rock block, three lakes and road 76 are also shown as a reference.	34
4.7	Plan view of the flow field for a slice near the top surface. The calculation is for the base case for present day conditions. The key indicates the logarithm and sign of the vertical component of darcy velocity in units of ms^{-1} . Three lakes and road 76 are also shown as a reference.	35
4.8	Evolution of salinity in time on the slice a(left)-A(right) (see Figure 4.2) through the northern rock block for the base case. The contours of salinity shown correspond to 5%, 25%, 50%, 75% and 95% of the maximum salinity (corresponding to 6,500mg/l). From bottom to top, the plots correspond to density at 3,000 years BP, 2,000 years BP, 1,000 years BP and the present day. Zone 2 is the narrow feature dipping in the upper central part of the slice. The colours indicate different hydrogeological properties (see Figure 4.2 for a key). Note the vertical scale is exaggerated by a factor of 2.	38
4.9	Evolution of head in time on the slice a(left)-A(right) (see Figure 4.2) through the northern rock block for the base case. Contours of head are plotted at intervals of 1.5m between 13m and 43m. From bottom to top, the plots correspond to density at 3,000 years BP, 2,000 years BP, 1,000 years BP and the present day. Zone 2 is the narrow feature dipping in the upper central part of the slice. Note the vertical scale is exaggerated by a factor of 2.	39
5.1	Salinity on vertical slices along a-A, b-B, c-C (see Figure 4.2) for the base case. The contours of salinity shown correspond to 5%, 25%, 50%, 75% and 95% of the maximum salinity (corresponding to 6,500mg/l). Note the vertical scale is exaggerated by a factor of 2.	42
5.2	Salinity in the boreholes BFI01, KFI04, KFI06, KFI07 (from bottom to top) for the base case. The solid lines represent the model results. The red crosses are experimental data. The shaded bar across the top indicates the modelled lithology down the borehole. The range of density shown on vertical axis is 996 to 1010 kgm^{-3}	44
5.3	Salinity on vertical slices along a-A, b-B, c-C (see Figure 4.2) for Zdeep variant. The contours of salinity shown correspond to 5%, 25%, 50%, 75% and 95% of the maximum salinity (corresponding to 6,500mg/l). Note the vertical scale is exaggerated by a factor of 2.	47

5.4	Plan view of the finite-element mesh for the Zsouth variant showing the fracture zones and hydrogeological properties on the top elements. The positions of the 3 vertical slices a-A, b-B and c-C used in the calibration are indicated. Three lakes and road 76 are also shown as a reference.	48
5.5	Salinity on vertical slices along a-A, b-B, c-C (see Figure 4.2) for Zsouth variant. The contours of salinity shown correspond to 5%, 25%, 50%, 75% and 95% of the maximum salinity (corresponding to 6, 500mg/l). Note the vertical scale is exaggerated by a factor of 2.	49
5.6	salinity on vertical slices along a-A, b-B, c-C (see Figure 4.2) for Z2highK variant. The contours of salinity shown correspond to 5%, 25%, 50%, 75% and 95% of the maximum salinity (corresponding to 6, 500mg/l). Note the vertical scale is exaggerated by a factor of 2.	50
5.7	Salinity on vertical slices along a-A, b-B, c-C (see Figure 4.2) for ZlowK variant. The contours of salinity shown correspond to 5%, 25%, 50%, 75% and 95% of the maximum salinity (corresponding to 6, 500mg/l). Note the vertical scale is exaggerated by a factor of 2.	51
5.8	Salinity on vertical slices along a-A, b-B, c-C (see Figure 4.2) for ZlowK ϕ variant. The contours of salinity shown correspond to 5%, 25%, 50%, 75% and 95% of the maximum salinity (corresponding to 6, 500mg/l). Note the vertical scale is exaggerated by a factor of 2.	52
5.9	Salinity on vertical slices along a-A, b-B, c-C (see Figure 4.2) for Z11 variant. The contours of salinity shown correspond to 5%, 25%, 50%, 75% and 95% of the maximum salinity (corresponding to 6, 500mg/l). Note the vertical scale is exaggerated by a factor of 2.	53
5.10	Salinity on vertical slices along a-A, b-B, c-C (see Figure 4.2) for Csouth variant. The contours of salinity shown correspond to 5%, 25%, 50%, 75% and 95% of the maximum salinity (corresponding to 6, 500mg/l). Note the vertical scale is exaggerated by a factor of 2.	54
5.11	Salinity on vertical slices along a-A, b-B, c-C (see Figure 4.2) for ϕ low variant. The contours of salinity shown correspond to 5%, 25%, 50%, 75% and 95% of the maximum salinity (corresponding to 6, 500mg/l). Note the vertical scale is exaggerated by a factor of 2.	56
5.12	Salinity on vertical slices along a-A, b-B, c-C (see Figure 4.2) for Dlow variant. The contours of salinity shown correspond to 5%, 25%, 50%, 75% and 95% of the maximum salinity (corresponding to 6, 500mg/l). Note the vertical scale is exaggerated by a factor of 2.	57
5.13	Salinity on vertical slices along a-A, b-B, c-C (see Figure 4.2) for Zlocal variant. The contours of salinity shown correspond to 5%, 25%, 50%, 75% and 95% of the maximum salinity (corresponding to 6, 500mg/l). Note the vertical scale is exaggerated by a factor of 2.	59
5.14	Salinity on vertical slices along a-A, b-B, c-C (see Figure 4.2) for RRD3 variant. The contours of salinity shown correspond to 5%, 25%, 50%, 75% and 95% of the maximum salinity (corresponding to 6, 500mg/l). Note the vertical scale is exaggerated by a factor of 2.	60

5.15	Salinity on vertical slices along a-A, b-B, c-C (see Figure 4.2) for AltK variant. The contours of salinity shown correspond to 5%, 25%, 50%, 75% and 95% of the maximum salinity (corresponding to 6,500mg/l). Note the vertical scale is exaggerated by a factor of 2.	62
6.1	Forward (blue) and backward (green) pathlines for the base case model. A set of 16 pathlines are started from the northern block at a depth of $z = -600\text{m}$. Points of origin, discharge and recharge for each path are shown by an asterix coloured pink, purple and orange, respectively. . .	66
6.2	Forward (blue) and backward (green) pathlines for the Zsouth variant. A set of 16 pathlines are started from the northern block at a depth of $z = -600\text{m}$. Points of origin, discharge and recharge for each path are shown by an asterix coloured pink, purple and orange, respectively. . .	67
6.3	Forward (blue) and backward (green) pathlines for the ZlowK ϕ variant. A set of 16 pathlines are started from the northern block at a depth of $z = -600\text{m}$. Points of origin, discharge and recharge for each path are shown by an asterix coloured pink, purple and orange, respectively. . .	68
6.4	Forward (blue) and backward (green) pathlines for the Z11 variant. A set of 16 pathlines are started from the northern block at a depth of $z = -600\text{m}$. Points of origin, discharge and recharge for each path are shown by an asterix coloured pink, purple and orange, respectively. . .	69
6.5	Forward (blue) and backward (green) pathlines for the Csouth variant. A set of 16 pathlines are started from the northern block at a depth of $z = -600\text{m}$. Points of origin, discharge and recharge for each path are shown by an asterix coloured pink, purple and orange, respectively. . .	70
6.6	Forward (blue) and backward (green) pathlines for the Dlow variant. A set of 16 pathlines are started from the northern block at a depth of $z = -600\text{m}$. Points of origin, discharge and recharge for each path are shown by an asterix coloured pink, purple and orange, respectively. . .	71
6.7	Forward (blue) and backward (green) pathlines for the Zlocal variant. A set of 16 pathlines are started from the northern block at a depth of $z = -600\text{m}$. Points of origin, discharge and recharge for each path are shown by an asterix coloured pink, purple and orange, respectively. . .	72
6.8	Forward (blue) and backward (green) pathlines for the RRD3 variant. A set of 16 pathlines are started from the northern block at a depth of $z = -600\text{m}$. Points of origin, discharge and recharge for each path are shown by an asterix coloured pink, purple and orange, respectively. . .	73
6.9	Forward (blue) and backward (green) pathlines for the AltK variant. A set of 16 pathlines are started from the northern block at a depth of $z = -600\text{m}$. Points of origin, discharge and recharge for each path are shown by an asterix coloured pink, purple and orange, respectively. . .	74
6.10	Forward (blue) and backward (green) pathlines for the freshwater variant. A set of 16 pathlines are started from the northern block at a depth of $z = -600\text{m}$. Points of origin, discharge and recharge for each path are shown by an asterix coloured pink, purple and orange, respectively.	75

6.11	Three alternative prescriptions for defining pressure boundary conditions on the local scale model. Pressure contours are shown on the vertical slice a-A (see Figure 4.2). The plots are (bottom to top) for residual pressure, environmental pressure, and steady-state freshwater pressure. Contours of pressure are plotted in terms of the equivalent head $h = p/\rho_0g$ at intervals of 1.5m between 13m and 43m. Note the vertical scale is exaggerated by a factor of 2.	78
6.12	A comparison of velocity profiles for variable and constant density cases. The top profiles are the Darcy velocity at present day on a horizontal slice (left) at -600masl and on vertical slice a-A (right) for the base case. The bottom profiles are equivalent plots for the freshwater variant. The colours and key indicate the magnitude of velocity $\log(\mathbf{q})$. The vertical scale in the right hand plots is exaggerated by a factor 2.	80
7.1	Distribution of head on the top surface of the model based on a fine scale interpolation of the present day topography. The numbers shown in the key are in units of metres. The positions of the 3 vertical slices a-A, b-B and c-C used in the calibration are indicated. Three lakes and road 76 are also shown as a reference.	82
7.2	Forward (blue) and backward (green) pathlines detailed model without land-rise. A set of 16 pathlines are started from the northern block at a depth of $z = -600\text{m}$. Points of origin, discharge and recharge for each path are shown by an asterix coloured pink, purple and orange, respectively.	83
7.3	Distribution of head on the top surface of the model at 4,000 years BP (bottom), 2,000 years BP (centre) and at present (top). The numbers shown in the key are in units of metres. The same key is used for ewach time. The positions of the 3 vertical slices a-A, b-B and c-C used in the calibration are indicated. The northern rock block, three lakes and road 76 are also shown as a reference.	86
7.4	Plan view of the flow field for a slice near the top surface at 3,600 years BP (bottom) and at the present day (top). The key indicates the logarithm and sign of the vertical component of darcy velocity in units of ms^{-1} . Three lakes and road 76 are also shown as a reference.	87
7.5	Salinity on vertical slices along a-A, b-B, c-C (see Figure 4.2) for the base case. The contours of salinity shown correspond to 5%, 25%, 50%, 75% and 95% of the maximum salinity (corresponding to 6,500mg/l). Note the vertical scale is exaggerated by a factor of 2.	88
7.6	Forward (blue) and backward (green) pathlines for the detailed model with land-rise. A set of 16 pathlines are started from the northern block at a depth of $z = -600\text{m}$. Points of origin, discharge and recharge for each path are shown by an asterix coloured pink, purple and orange, respectively.	89

1 BACKGROUND AND OBJECTIVES

The Swedish Nuclear Fuel and Waste Management Company (SKB) has initiated a safety assessment project called SR 97, which is related to safety assessment of hypothetical disposal sites for spent nuclear fuel. SR 97 is part of several performance assessments and will focus on the long term safety of disposed nuclear fuel. Three hypothetical sites will be studied, Aberg, Beberg and Ceberg, data for these three sites have been taken from three real sites where SKB has performed extensive investigations. The three sites are Äspö, Finnsjön and Gideå respectively.

The present report concerns the large-scale regional groundwater flow at the Beberg site.

The main objectives of this project are to:

1. Understand the large-scale groundwater flow and salinity patterns within the area under natural conditions.
2. Examine the effects of natural transient processes on the groundwater flow and salinity patterns.
3. Identify locations of significant recharge and discharge under present conditions.
4. Determine the most appropriate boundary conditions to describe transient variable density groundwater flow in a regional scale model.
5. Calibrate the model against current day measurements of salinity in boreholes to establish a combination of hydrogeological parameters, such as hydraulic conductivities and porosities, that adequately describe the present situation at the site.
6. Determine the spatial extent of the regional model required to predict groundwater flow patterns in the vicinity of the site.
7. select the location of a site scale model based on the results of this work, and also supply such a model with appropriate boundary conditions.

A short introduction and an overview of the approach used in modelling the site is described in Chapter 2. The hydrogeological data as used in this project is described in Chapter 3. Chapter 4 presents a detailed description of the numerical model and how it was developed. Some predictions of the transient evolution of pressure and salinity over the last 4000 years are also given in Chapter 4. The calibration of the model for water balance and salinity distribution is discussed in Chapter 5. In Chapter 6 the results are discussed in the context of selecting a domain appropriate for the site scale. The work is summarise in Chapter 7.

2 INTRODUCTION

The following Sections describe the concepts, methods and assumptions used.

2.1 Site Location

The modelling performed concerned the Beberg site within SR 97. The Beberg site is located in northern Uppland, in a region of low topographical relief about 15km from the coast. The elevation at the site is about 35m above sea level. Figure 2.1 shows the location of the Beberg site.

The regional hydraulic gradient is only about 0.2-0.3% [*Walker et al., 1997*]. The highest relief in the area is to the west and south west of the site with a further gentle ridge to the south east. Lake Finnsjön lies between these raised areas and just south of the site. Several small lakes are situated to the north east. The general pattern of surface drainage is toward the Bothnian Sea in the north east.

The coordinate system used is the National Swedish RAK-system, with offset in East-West of 1 600 000 m and in NorthSouth of 6 600 000 m. All plots in this report refers to this coordinate system.

2.2 Modelling Techniques

The modelling of the groundwater flow and salt transport has been carried out with the deterministic finite element code NAMMU [*Cliffe et al., 1995*]. NAMMU uses a porous medium approach.

The equations describing coupled groundwater flow and salt transport are given in Appendix A. Because these equations are non-linear, Newton-Raphson iteration is used to be obtain a solution to the equations. In this study transients are represented

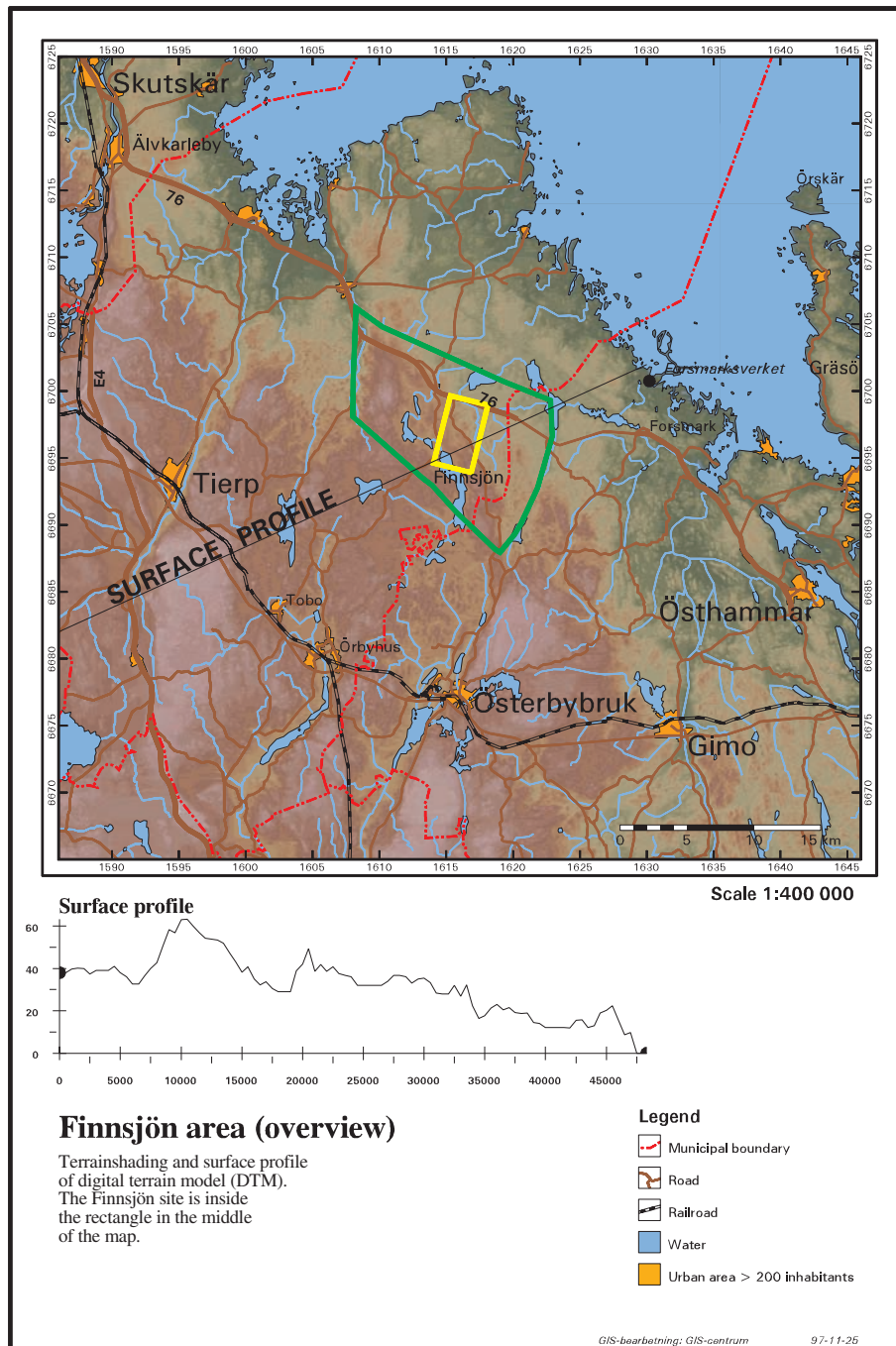


Figure 2.1: Location of the Beberg site. The boundaries of the regional and site scale models are shown in green and yellow, respectively.

using a fully implicit scheme.

2.3 Effects of Salinity

The presence of saline groundwater can cause significant modification to groundwater flow patterns due to buoyancy forces. Typically, dense saline water falls under gravity below less dense fresh water. Hence saline groundwater is often encountered at depth. Salinity modifies the pattern of flow in at least two ways. Firstly, by changing the distribution of driving forces. Secondly, by restricting the penetration of fresh groundwater to depth, effectively reducing the volume of subsurface accessible to flow.

In order to quantify the effects of salinity, one needs to consider the relative magnitudes of the two forces driving flow:

- 1) the pressure gradient, ∇p^r , where p^r is the dynamic (or residual) pressure;
- 2) the buoyancy force, $(\rho - \rho_0)\mathbf{g}$, where ρ is the fluid density, ρ_0 is the density of fresh water and \mathbf{g} is gravitational acceleration.

At Beberg, saline groundwater of up to 0.8% has been encountered at depths between 90-300m. This is equivalent to a density variation of about 8kg/m^3 . The resulting hydraulic gradient due to salinity is 0.008% per unit depth of salinity, or an increase of 0.8m in head per 100m depth of saline water. Given the very weak gradient in topography at this site (compare with Section 2.1), it is clear that salinity is a very important factor in the flow of deep groundwater at this site. If one were to neglect salinity and use a constant density model, then heads at a depth of 1km would generally be under-predicted by about 8m, for instance.

2.4 Natural Transient Processes

The hydrogeological situation at Beberg has undergone many significant changes as a consequence of the latest glacial event and post-glacial rebound. Here we summarise those changes and discuss their implications for modelling the site.

2.4.1 Post-Glacial Conditions

Immediately following deglaciation the Finnsjön site was covered by the brackish Yoldia Sea about 9,600 years BP. As the area rebounded and the land rose, the connection

to the Atlantic was closed and a non-saline lake covered the area (Ancyclus Lake at 9,000 years BP). Between 7,500-7,000 years BP the water became saline (Litorina Sea), which gradually transformed into the present brackish Baltic Sea. During this period the land around the Finnsjön site gradually uplifted to rise above sea level about 5,000-3,000 years BP [Almen *et al.*, 1978]. It is believed that the salt present at the site originated from the Yoldia and Litorina Sea waters. This conclusion was based on chemical analyses of deep groundwaters [Smellie and Wikberg, 1989; Laasoharju *et al.*, 1998].

2.4.2 Transient Salt Evolution

The current understanding of the history of the Finnsjön site then is that marine waters infiltrated the rock between about 10,000 to 4,000 years BP, as the land later rose above sea level, fresh water from rainfall gradually started to displace and flush the saline groundwater from the fractures and pores in the rock.

This hypothesis that the salinity distribution is controlled by transient processes is supported by field measurements. Saline groundwaters (>300mg/l of chloride) are encountered in a significant proportion of inland shallow (50-100m deep) wells in the region. Saline groundwater is also quite common in deep bedrock wells. Saline groundwater of 7000 mg/l of chloride occurs at 420m depth in the Dannemora mine and saline water of up to 6000 mg/l of chloride have been observed at about 50m depth at SFR. Several of the deep boreholes at the Finnsjön site have encountered salinity between 5000-6000 mg/l of chloride at depths ranging from 90-300m.

It is hard to imagine how such observations could be explained if it were assumed that the system is in a steady-state. The Ghyben-Herzberg (or sharp interface) formula predicts that for a steady-state system the depth, d , to the saline transition zone is given by

$$d = \frac{\rho_0 h}{\rho_s - \rho_0},$$

where h is the head at the surface and ρ_s is the density of saline water. For Beberg this becomes $d = 125 \times h$, so salinity would be present below about 3750m near the site and about 1250m in the potential discharge region to the north east. Clearly this is far from the real situation, and it is concluded that current groundwater flow at depth can only be understood by considering the transient processes that have taken place over the last few thousand years. This introduces significant complexity for the modelling, but it is necessary for the results to be considered meaningful.

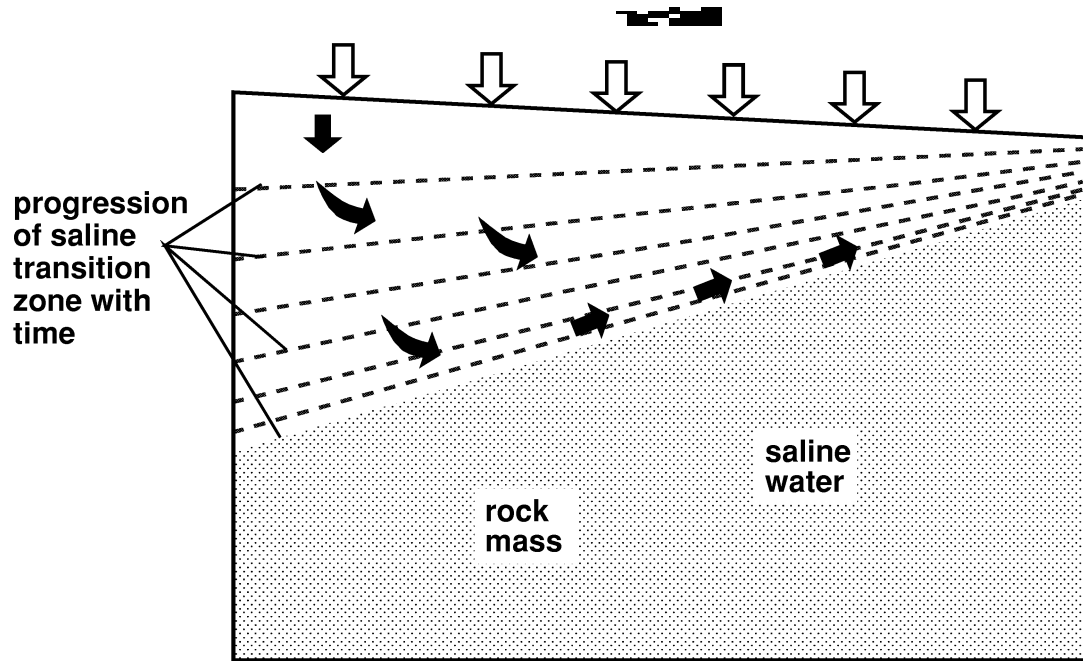


Figure 2.2: Schematic evolution of saline transition zone for a homogeneous rock with a hydraulic gradient from left to right.

An alternative steady-state hypothesis for the observed salinity distribution has been offered by Ahlbom [1991]. This proposes that saline waters have become trapped beneath a region of clay deposits slightly to the north east of the Finnsjön site. In fact, this is a related concept since it still relies on the infiltration and subsequent flushing of saline water as controlled by post-glacial marine transgressions. The difference being that clay deposits in the north east may reduce the discharge of saline waters downstream, and hence increase the residence time of salinity in the region of interest. At present, we see little possibility to either support or reject this assertion since there is insufficient data on the extent and thickness of the clay. However, it is remarked that in order for such a clay layer to prevent the rock from being flushed of salt, we believe that the clay must have a substantial horizontal continuity. Furthermore, as the clay is located downstream from the hypothetical repository area its potential for influencing the repository area is not obvious.

Heterogeneity has a strong influence in determining the evolution of salinity under transient conditions. Fresh water will displace or mix with saline water more rapidly in regions of relatively high hydraulic conductivity. At Beberg there are many regional and local scale fracture zones having hydraulic conductivities up to three orders of magnitude higher than the rock mass. The majority of zones are near vertical. One can expect that salt water will be flushed from these zones on a relatively short time-scale relative to the rock mass. Giving rise to phenomena such as vertical fingers or slabs of fresh water within the fracture zones dividing cells of saline water in the rock mass.

This has significance for the rate at which saline groundwater is exchanged for fresh.

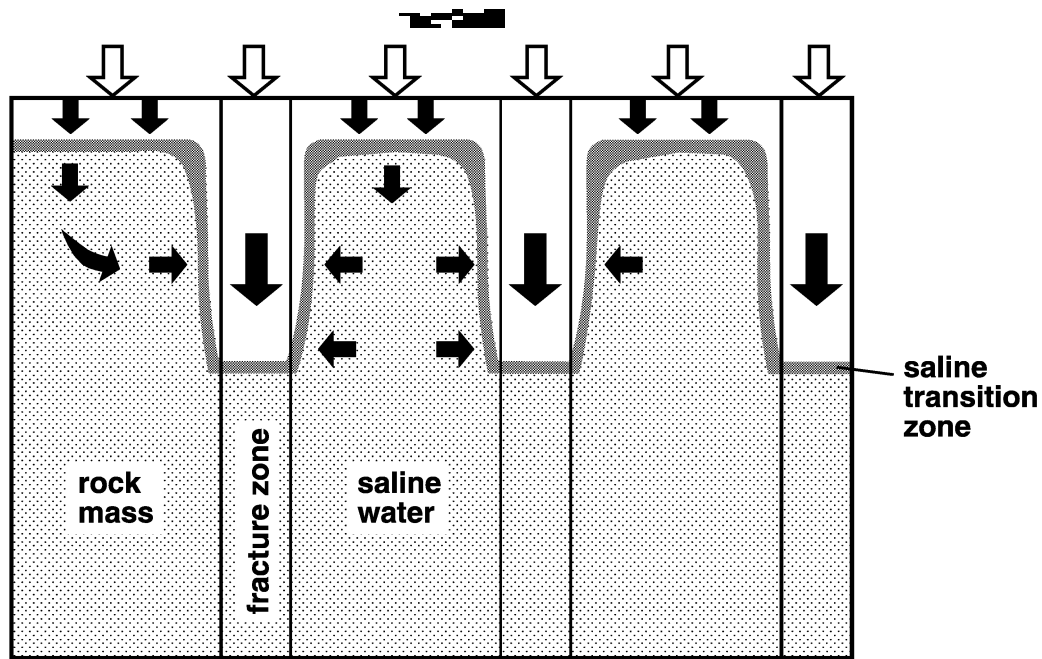


Figure 2.3: Schematic evolution of saline transition zone for a case with vertical fracture zones.

If the system were homogeneous, then the recharge of fresh water at the surface would gradually flush out salt water under the hydraulic gradient. Hence the evolution of the saline transition zone is mainly governed by topography. The higher the topography, the faster saline water is displaced by fresh, and the deeper the saline transition zone (see Figure 2.2). For a case with vertical fracture zones, the hydraulic gradient is augmented by buoyancy forces. Fresh water penetrates to depth relatively quickly in the vertical fracture zones. There is then a horizontal pressure gradient from the dense saline water in the rock mass toward the fresh water in the fractures zones (see Figure 2.3). The magnitude of this gradient being proportional to the difference in depth to the saline transition zone, and the difference in density between fresh and saline waters. Hence, one can expect groundwater to be fresh where there is a high frequency of fracture zones. A generic study of regional flow in the Baltic Shield by Voss and Andersson [1993] used numerical models to illustrate the importance of fracture zones, and their geometry, on the transport of saline groundwaters. The results confirm the assertions made above.

It is also interesting to consider how salt may have evolved in the region local to the Finnsjön site. The location of the hypothetical repository is situated below a well characterised sub-horizontal fracture zone (Zone 2). There is also a set of four vertical fracture zones surrounding the area forming the ‘northern rock block’. All of these zones are thought to be hydrogeologically significant and are spaced about 1.5-2km apart (see Section 3.2). It is probable then that at some stage in history, the water in the transmissive regions surrounding the rock block and in Zone 2 will have become fresh, while the rock block above Zone 2 remained saline (see Figure 2.4). This situation is unstable, as saline water will leak out into the fracture zones. The fact

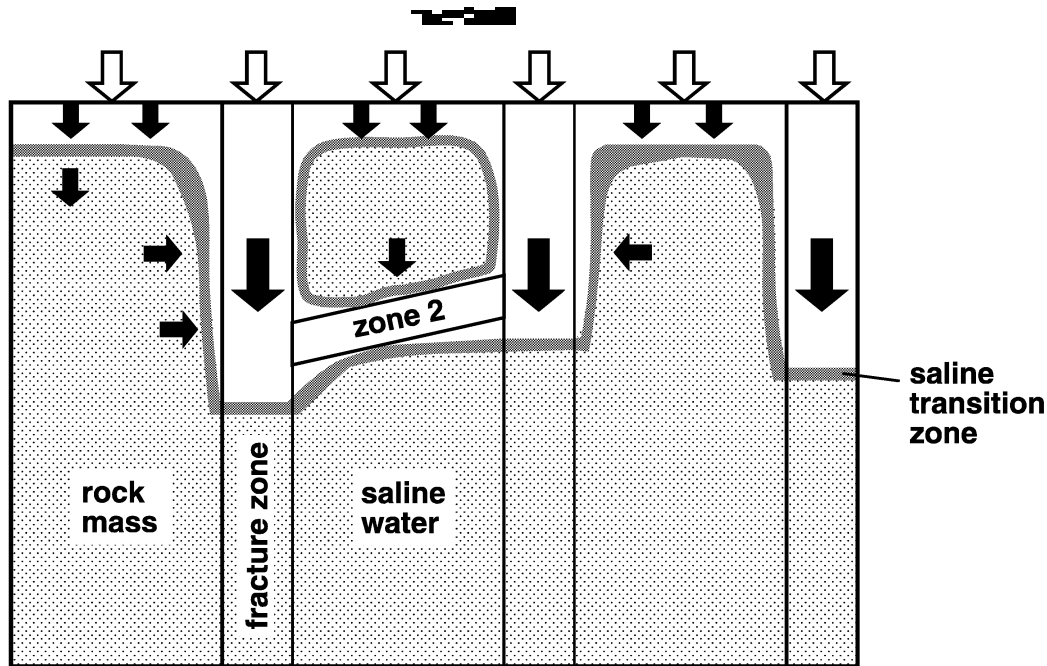


Figure 2.4: Sketch of evolution of saline transition zone for a case with vertical fracture zones and the sub-horizontal Zone 2.

that no significant salinity is observed above Zone 2 at the present day suggests that this situation could not have persisted for more than a few thousand years. This is clearly something we should aim to predict, and will assist in calibrating the model.

Modelling transients requires additional information to that for a steady-state calculation. This includes an initial condition, the variation of boundary conditions with time and the total, or transport porosity. Initial and boundary conditions are discussed in sections 2.4.3 and 2.5, respectively.

The total porosity is very important as, together with hydraulic conductivity, it controls the rate at which saline water in the pores and fractures is replaced by fresh water. The lower the total porosity, the quicker the salinity changes. It is important to make the distinction between total and flowing porosity. We define the total porosity as the total relative volume of accessible pore space. It includes the pore space occupied by relatively stagnant water such as in dead-ends or the rough sides of fractures. It can be measured in the laboratory by drying or carrying out diffusion experiments on rock samples. The flowing porosity is the relative volume of pore space through which significant flow takes place. This is a sub-set of the total porosity, and is often considerably smaller. It is usually measured by carrying out insitu hydraulic tests.

To predict the transport of salinity over the long time-scales of interest here, it is the total porosity which is the relevant parameter. This is because there is sufficient time for matrix diffusion to provide mixing of salinity at the micro-scale. However, the flowing porosity is the relevant quantity for predicting groundwater travel times. Since in the context of a safety assessment, we need to consider flow through the most rapid

flow channels, and hence the minimum groundwater travel times.

2.4.3 Initial Condition

Ideally the initial condition for a transient calculation is a well defined situation that occurred at some time in the geological history of the region. The period when the land around Beberg just began to rise above sea-level (3,000 to 5,000 years BP) is considered a reasonable approximation to such a situation. The Yoldia and Litorina Seas will have by then covered the region for about 5,000 years [*Walker et al., 1997*]. The rate at which marine water would infiltrate downwards in to the bedrock can be estimated by

$$v = \frac{k}{\mu\phi} (\rho_s - \rho_0) g,$$

where k is permeability, μ is the fluid viscosity and ϕ is the total porosity. For Beberg, the velocity is about 10^{-8}ms^{-1} for the rock mass and 10^{-5}ms^{-1} for the fractures zones. Thus, marine waters would occupy the top 1km of rock mass in about 3,000 years. The equivalent time period for the fracture zones is only a few years. These estimates are confirmed by the numerical results (see Subsection 6.1). It then appears reasonable to suppose that between about 10,000 to 3,000 years BP ancient marine water will have permeated down in to the deep bedrock. Hence, the initial condition is approximated to be that the entire pore space of the regional model was occupied by water of a constant salinity 4,000 years BP.

Of course, it would be interesting to consider the evolution over much longer time-scales consistent with the cycles of glacial and inter-glacial periods. The techniques used to carry out such a study would be similar to those reported here, except additional processes such as glacial loading would have to be modelled. It is probably inevitable that much a larger region would also have considered.

However, the above arguments suggest it is sufficient to model the history of salinity over the last 4,000 years. The model needs to represent the infiltration of fresh water from rainfall gradually flushing and diluting the old marine groundwaters. The model prediction of the salinity pattern at the present day can be compare with salinity measurements to calibrate the hydrogeological parameters used in the model until an acceptable match is found.

2.5 Boundary Conditions

A very important part of the specification of the model is defining boundary conditions for both pressure (or flow) and salinity. For a transient situation these may have both a spatial and time dependence. Here we describe the types of boundary conditions that are appropriate to this site, and how they might vary in time. The exact definition of the boundary conditions used in each calculation is given in Sections 4 and 5.

2.5.1 Pressure Boundary Conditions

The depth to the water table at the Finnsjön site is typically only 1-2m [Walker *et al.*, 1997]. Hence, it is reasonable to take the head on the top surface to equal the height of topography using sea level as a datum. NAMMU uses the dynamic pressure, p^r , so the boundary condition becomes

$$p^r = \rho_0 g h = \rho_0 g z_s.$$

where z_s is the elevation of the surface. This is based on the current elevation of topography. Of course, the topography would have been lower in the past. The land in this region has risen at a rate of about 6-8mm per year, and hence much of the area considered in this study would have been covered by marine water 4,000 years BP. While the land is covered by the sea the boundary condition has to be altered so that

$$p^r = h = 0 \quad \text{for } z_s \leq 0$$

However, it is considered unlikely that the gradual change in pressure on the top surface will have a substantial effect on the way the salinity pattern evolves. This is justified by remarking that on the scale of the regional model the rate of uplift will have been spatially uniform, and hence to first approximation the hydraulic gradient will not have changed greatly over the period of interest. For this type of boundary condition (specified pressure) the recharge and discharge areas can be identified by carrying out a groundwater flow calculation with constant density, and examining the direction (up or down) of flow vectors near the top surface.

A more sophisticated model is a time-dependent boundary condition for head on the top surface which accounts for changes in the position of the coast. By assuming a linear dependence on time, t , head becomes

$$h(t) = \begin{cases} z_s(0) + \epsilon t & z_s(0) > -\epsilon t \\ 0 & z_s(0) \leq -\epsilon t \end{cases}$$

where $z_s(0)$ is the elevation of the surface at present ($t = 0$), and ϵ is approximately $7.0\text{mm}/3.156 \cdot 10^7\text{s} = 2.2 \cdot 10^{-10}\text{ms}^{-1}$. It is likely that this will predict recharge and discharge areas that gradually change with time. Again the recharge and discharge areas can be determined by plotting flow vectors at any particular time.

The boundary condition on the bottom surface is zero flow in all cases considered. This is justified by placing the boundary well below the saline transition zone and the hypothetical repository depth.

It is difficult to identify any definite water divides in the region as relief is so flat. This is complicated further by the condition that any proposed water divides should have been so for the last 4,000 years. Thus, there is not an obvious feature where one can place a vertical boundary and impose no-flow. Instead the approach is to extend the model over a large regional area, about 20km by 10km, and specify a hydrostatic pressure on all vertical sides. This boundary condition allows either horizontal inflows or outflows across the boundary as determined by the pressure gradients within the domain. As such, it imposes quite a weak condition on the flow – no vertical flow on the sides. It is the most appropriate boundary condition for the transient situation at Beberg, since it allows the magnitude and direction of flow to change in time as the pressure in the model evolves.

For a variable density flow the hydrostatic pressure, p^h is a function of density. For any point the hydrostatic pressure is evaluated by integrating the deviation from freshwater density vertically downwards from the top surface. The value at the surface is equal to the dynamic pressure, so that

$$p^h(z) = p^r(z_s) + g \int_{z_s}^z (\rho - \rho_0) dz.$$

Hence, for a constant density saline groundwater, hydrostatic pressure increases linearly with depth. In the transient case density will obviously change in time, requiring the value of hydrostatic pressure on the boundary to be re-calculated every time-step. This is a very important step. Failure to do this results in flow being forced upwards at the sides, which is undesirable as it is unphysical, and creates numerical problems. The reason is that the hydrostatic pressure at depth generally decreases in time as salt water is flushed out, so if the hydrostatic pressure on the sides is not regularly up-dated, then the pressure on the boundary is higher than that within the domain. Numerical problems occur because the salt can no longer exit the model at the downstream boundary, causing salinity to gradually rise to unphysical values. NAMMU allows the hydrostatic pressure to be computed accurately by integrating density using the finite-element method.

2.5.2 Salt Boundary Conditions

Deriving realistic boundary conditions for salinity is equally complex in the transient case. The possibilities are specified concentration, no flux of salt, or advective flux of salt.

Where there is a recharge of fresh groundwater a condition of zero salinity is appropriate. That is,

$$c = 0.$$

Where there is a groundwater velocity out of the model, either on the sides or top, then an advective flux boundary condition is the most realistic. That is, salt is advected

out of the model at a rate equal to the darcy velocity normal to the boundary surface multiplied by the salt concentration on the boundary. Hence, the mass flux, $F_c(\mathbf{x}, t)$, at point \mathbf{x} and time t out of a boundary with outward unit normal vector $\mathbf{n}(\mathbf{x})$ is

$$F_c(\mathbf{x}, t) = \rho c \mathbf{q}(\mathbf{x}, t) \cdot \mathbf{n}(\mathbf{x}),$$

where $\mathbf{q}(\mathbf{x}, t)$ is the Darcy velocity distribution. Since the flow rate and salinity change in time, then the flux of salinity out of the boundary is time-dependent. Also, since ρ and \mathbf{q} are functions of salinity, this boundary condition is non-linear. Hence, it is necessary to know the position of the recharge and discharge areas in order to specify the boundary conditions. If the pressure boundary conditions on the top surface change with time, then it is likely that the distribution of recharge and discharge changes slightly, so the definition of the salt boundary conditions should strictly be changed also. Such a level of complexity becomes quite involved to implement in a numerical model.

For most of the calculations report here, the top surface boundary conditions are simplified. The pressures on the top surface are held constant at values appropriate to the present day. The recharge and discharge areas are estimated from a constant density steady-state flow calculation. This forms the basis for assigning boundary conditions for salt on the top surface. It implies, that the spatial definition of the salt boundary conditions is constant, but the actual values of flux vary in time. The approach is considered adequate since hydraulic gradients are thought not to have changed significantly over the period of interest.

On vertical boundaries where there is an inflow, for instance in the south, it is difficult to know the salinity of the groundwater entering the model. Further, for the transient situation the evolution of salinity upstream is more uncertain. This boundary condition is probably the hardest to define with confidence. The approach taken was to set an inflow of salinity equal to the darcy velocity across the boundary multiplied by the concentration at the boundary. In reality, the salinity in the region to the south of the model is likely to be deeper than that seen at the Finnsjön site. This is because the ground is generally higher to the south, and one may expect higher heads driving saline water deeper. The uncertainty associated with the upstream boundary condition motivates the model being extended well to the south of the site to prevent this boundary having a strong influence on the results. It is possible to quantify the effects of the southern boundary by specifying a guessed salinity profile as a variant calculation.

Zero-flux of salinity is specified on the bottom boundary as it is thought that flows at large depths are not significant.

3 HYDROGEOLOGY AT THE BEBERG SITE

3.1 Topography

Topography data was obtained using the SKB GIS database. The topography on the large scale is shown in Figure 3.1. The top surface of the finite-element mesh was adjusted according to a bi-linear interpolation of the topography data. The topography data has a horizontal resolution of 50m.

Due to the coarse discretisation used within the present model it captures the major topographical features, but not in as much detail as smaller steady-state models in the past [*Svensson, 1991; Lindbom et al., 1992*].

3.2 Structural Model

The structural model used within the present study is similar to the one used within previous studies of the Beberg area [*Lindbom et al., 1991, 1992*] and is based on the map shown in Figure 3.3. The fracture zones included within the model are shown in Figure 3.2. This is consistent with what is reported by Walker et al. [*1997*]. All regional zones within the modelled area have been included and some of the more important local zones. This gives a model with 14 regional fracture zones and 2 site scale zones (Zones 2 and a sub-horizontal zone in the Southern Rock Block).

Fracture zones were represented explicitly by creating a non-regular finite-element mesh to fit the pattern of lineaments. Each zone is at least one finite-element in width. The thicknesses and physical properties of the finite-elements representing the fracture zones are specified as in [*Walker et al., 1997*]. The Giboda fracture zone branches into two (Giboda and Giboda S) about 4km to the north-east of the site. It was considered adequate to merge these two zones into a single zone with the transmissivity of the merged zone equivalent to that for the two zones in parallel. This is justified as they are far from the site and relatively close to one another.

Topography

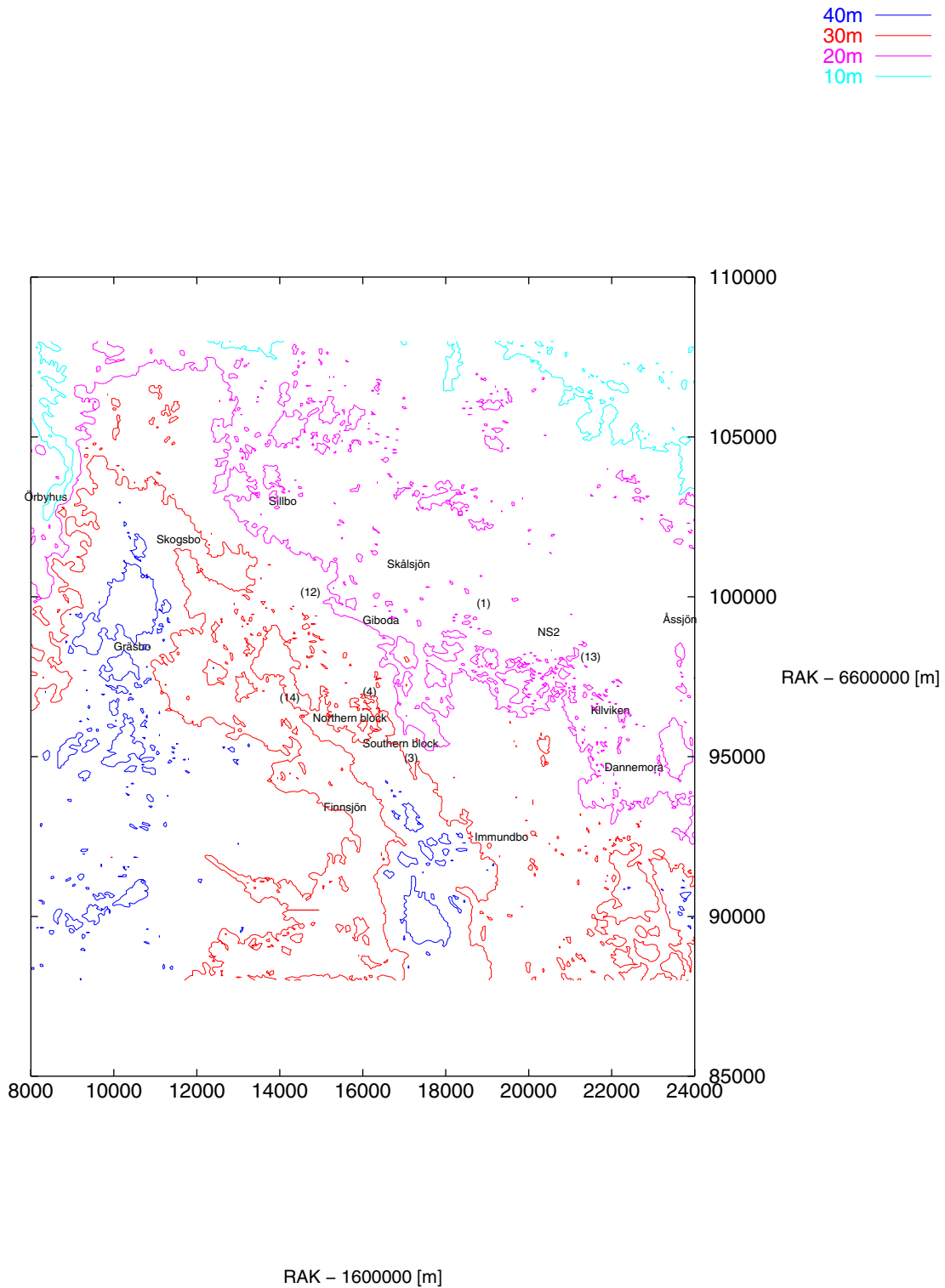
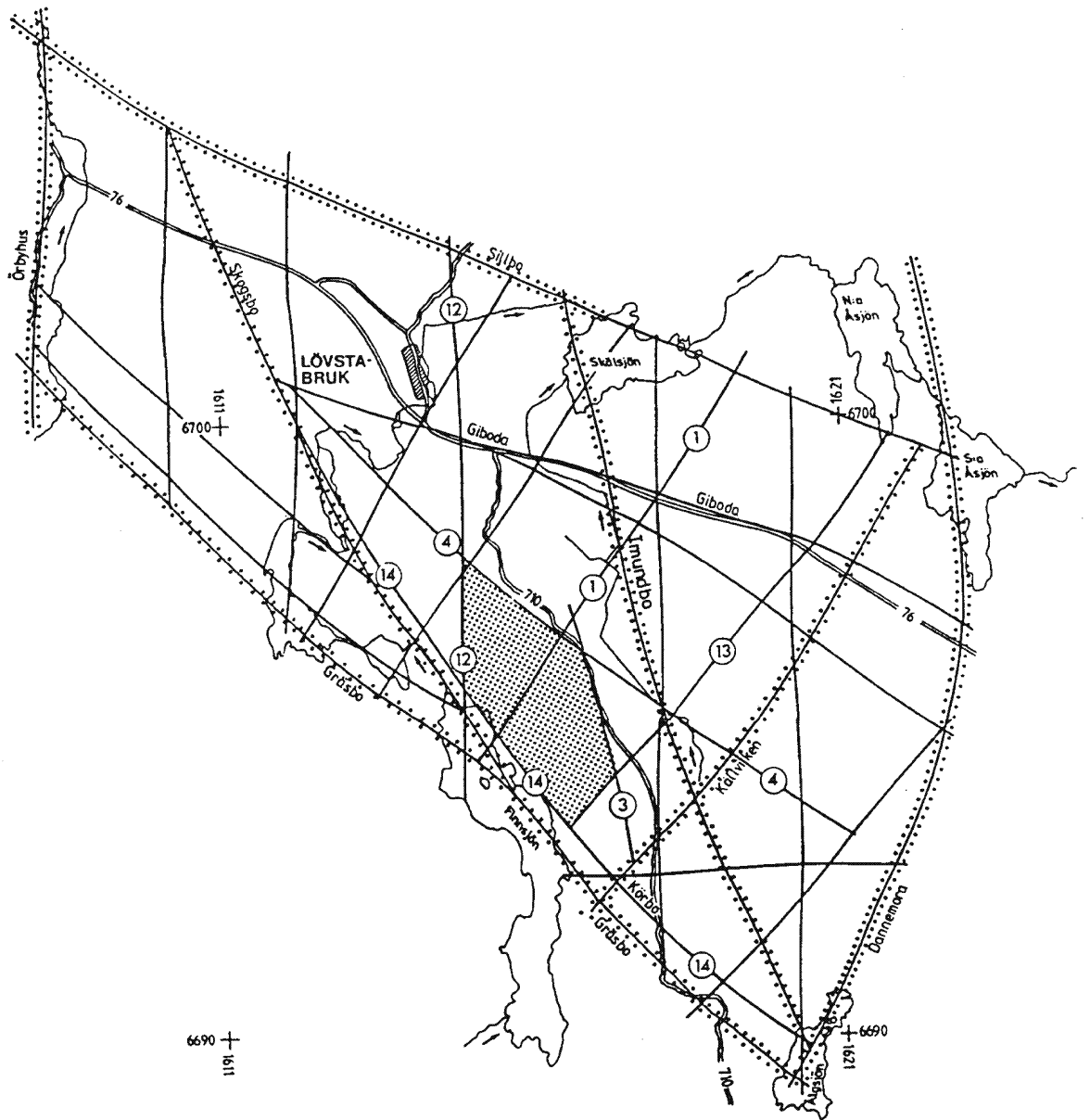


Figure 3.1: Topography on a large scale. Data has been supplied by the SKB GIS system. Contours are shown at 10m, 20m, 30m and 40masl (as shown in the legend). The approximate location of fractures zones is indicated by the annotation (see Figure 3.3 for the detailed structural map).

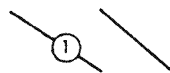


The majority of fractures zones are estimated to be vertical (dip 90 degrees). This simplifies the topology of the mesh. That is, the finite-element mesh can be constructed from a series of near-horizontal layers. Exceptions are Zone 2 which is sub-horizontal (dip 16 degrees SW) and Zone 4 which has significant slope (60 degrees SW). These 2 zones were modelled with the appropriate inclination by distorting the mesh. Zones 1 and 3 also have dips less than 90 degrees, 75 and 80 degrees, respectively. It was considered a fair assumption to model these as vertical. Including these two zones with the specified inclination would have added further complexity to the mesh.

An option to include a sub-horizontal fracture zone in the southern rock block was included by extending the geometrical representation of Zone 2 to the south west. The purpose of this is to enable us to consider qualitatively the effects of a generic sub-horizontal zone in the south. The site characterisation specifies that Zone 11 lies in this region. However, Zone 11 dips more steeply than Zone 2, 35 degrees SW, and hence the representation of Zone 11 should only be considered approximate. For the base case Zone 11 was specified as having rock mass properties. The widths and inclinations of the fractures zones represented are summarised in Table 3.1.

A number of smaller site scale fracture zones have been identified in the site characterisation. Some of these zones (Zones 5, 7 and 8) have hydraulic conductivities comparable with the regional fracture zones, but they are typically much narrower (only 5m), so less transmissive, and obviously less extensive. For these reasons, they are not expected to have a significant effect on regional flows. Hence, it was considered unnecessary to refine the mesh on the local scale to include these zones explicitly. A variant case is considered in which the local scale fracture zones are included implicitly to indicate qualitatively what effect the zones may have. This is achieved by adjusting the hydraulic conductivity tensor of the rock mass to represent the combined transmissivity of the fracture zones and rock mass. It results in an anisotropic hydraulic conductivity tensor with principal directions aligned with the fracture zones.



SIMPLIFIED ROCK BLOCK MAP , LÖVSTABRUK AREA

-  Fracture zones
-  Position of lineaments interpreted on regional scale
-  Finnsjön Rock Block

The glacial striation is north-south

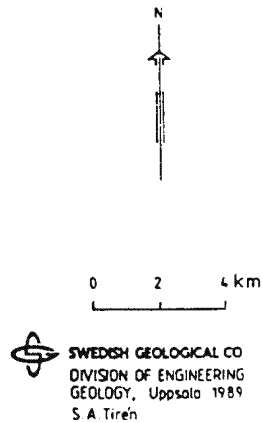


Figure 3.2: Rock block map of the regional model (Lövestabruk area) including the Finnsjön Rock Block (rastered).

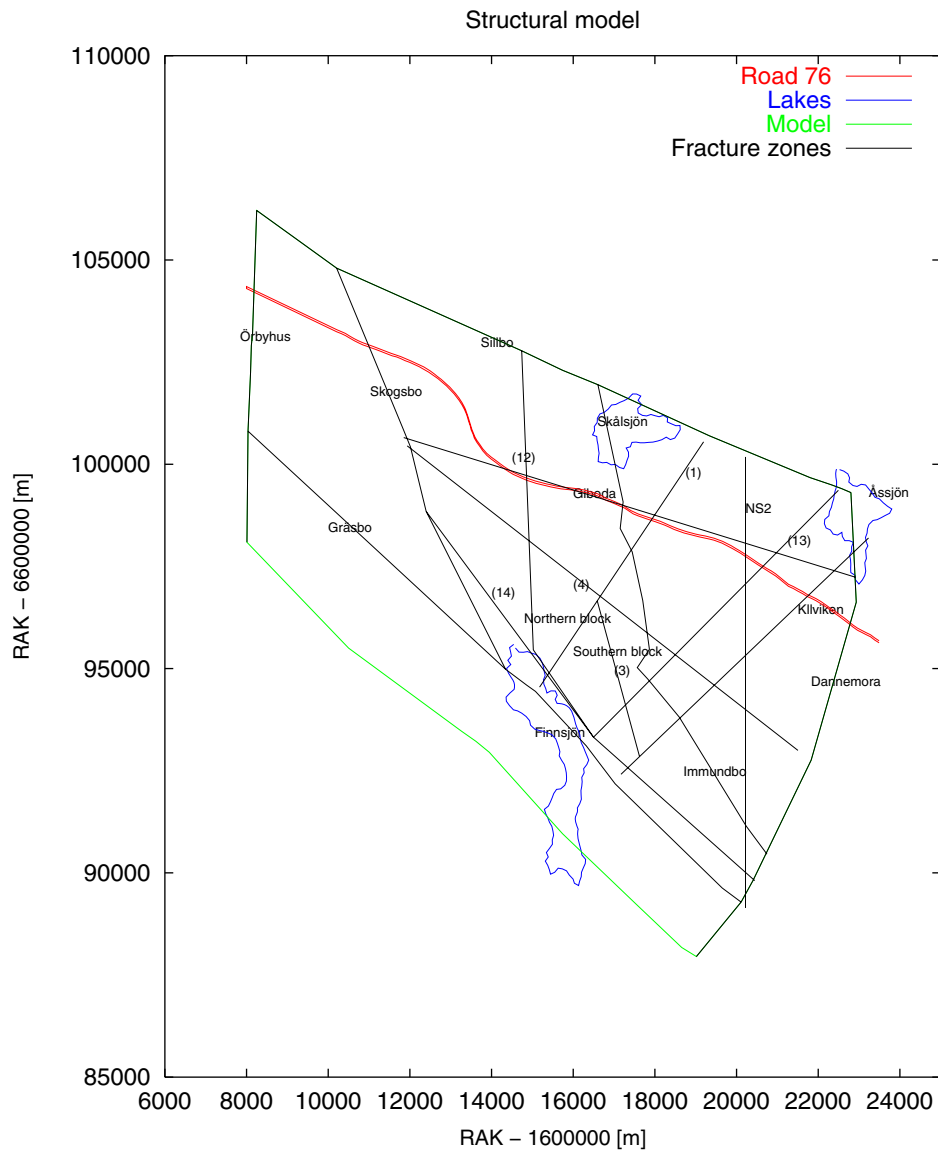


Figure 3.3: A schematic of the structural model used. Based on Walker et al. [1997]. The outer boundary indicates the extent of the regional scale model.

Table 3.1: Fracture zones in the Beberg area as modelled within the present study.

Zone	Width	Inclination	Comment
1	20	90	The actual inclination is 75 SE
2	100	16SW	
3	50	90	The actual inclination is 80SW
4	10	60SW	
11	100	16SW	Accounted for in the model but not included in base case The actual inclination is 35SW
12	25	90	
13	20	90	
14	100	90	
Skogsbo	100	90	
Giboda	100	90	Giboda and Giboda S merged
Imundbo	100	90	
Gräsbo	100	90	
Dannemora	100	90	
Källviken	100	90	Extended south in a variant
Örbyhus	10	90	
Silbo	100	90	
NS2	25	90	
Finnsjön	50	90	Only included in a variant

3.3 Hydrogeological Properties

The hydrogeological data requirements for this study are as follows:

- i) deterministic hydraulic conductivity and specific storativity for each fracture zone;
- ii) deterministic hydraulic conductivity and specific storativity, possibly as a function of depth for the rock mass;
- iii) total porosity for the fractures zones and rock mass for calculating salt transport;
- iv) hydrodynamic dispersion lengths for the fractures zones and rock mass;
- v) flowing porosity for rock mass and fracture zones for calculating groundwater travel times.

Hydraulic conductivities for the fracture zones and rock mass have been re-analysed and collated in [Walker *et al.*, 1197]. Properties for the rock mass were sub-divided into four vertical bands: above -100m, -100 to -200m, -200 to -400m, and below -400masl. Apart

from the upper most layer the variation with depth is only slight, ranging between $8.5 \cdot 10^{-9} \text{ms}^{-1}$ to $2.1 \cdot 10^{-8} \text{ms}^{-1}$. The hydraulic conductivity for the upper layer is an order of magnitude higher at $1.5 \cdot 10^{-7} \text{ms}^{-1}$.

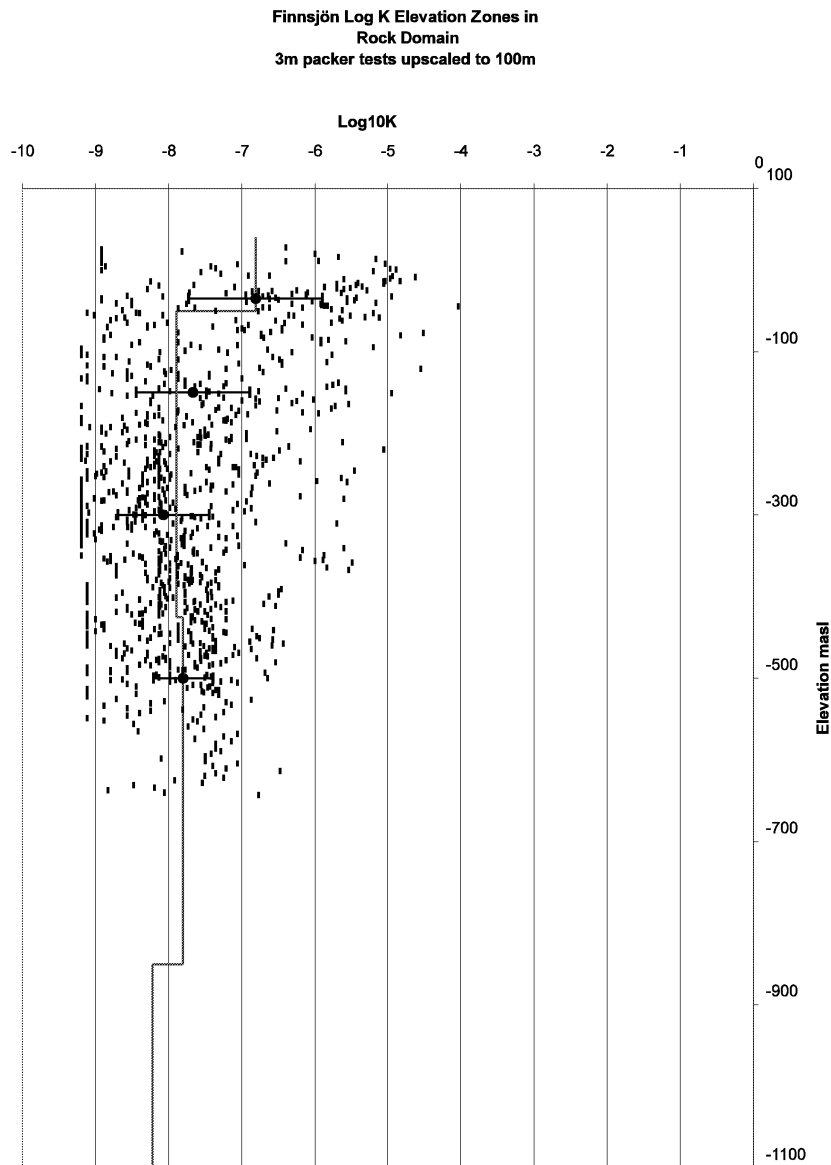


Figure 3.4: Hydraulic conductivities for the rock mass (long vertical lines) used in the modelling. The dots show the measured hydraulic conductivities in 3m sections of rock upscaled to the SGU data scale (100m) [Walker *et al.*, 1997]. The horizontal lines show the mean and a 95% confidence bound (calculated as $\pm 2\sigma$, where σ is the standard deviation) of the logarithm of hydraulic conductivity.

The hydraulic conductivities of rock mass as used in the base case model are shown in Figure 3.4. A comparison is made with the measured data for 3m sections upscaled to the SGU data scale as summarised in Appendix B of [Walker *et al.*, 1997]. The depth zonation proposed by [Walker *et al.*, 1997] is also shown. A log-normal distribution for hydraulic conductivity is assumed in estimating 95% confidence bounds (i.e. using

$\pm 2\sigma$, where σ is the standard deviation in the logarithm of conductivity). Clearly the values used in the model are consistent with [Walker *et al.*, 1997]. It is important to note that there is no data below about -700masl. Hence, the hydraulic conductivity at large depths has to be extrapolated from the top 700m, and hence is uncertain. In the model, a value of $6.0 \cdot 10^{-9} \text{ms}^{-1}$ is applied to all rock mass below about -850masl. This is about half the central value given in [Walker *et al.*, 1997] for rocks below -400masl, but is well within the 95% confidence limits (one standard deviation corresponds to a factor of about 1.6).

For SKB 91 a regression formula $K = Az^{-b}$ (with $b = 2.23$) was used to define the depth dependence of the hydraulic conductivity for both the rock mass and fracture zones [Ahlbom *et al.*, 1992; Lindbom *et al.*, 1992; Boghammar *et al.*, 1993]. This resulted in a value of about $1 \cdot 10^{-8} \text{ms}^{-1}$ at the depth of the hypothetical repository (-500 to -600masl) compared with about $1 \cdot 10^{-8} \text{ms}^{-1}$ for the current study. The near surface hydraulic conductivity was about one order of the magnitude higher in the top 100m for SKB 91 than in the current study. At large depths the hydraulic conductivity was about $1 \cdot 10^{-9} \text{ms}^{-1}$ for SKB 91, and hence an order of magnitude lower than is used here. In summary, the hydraulic conductivity for the rock mass is broadly consistent with that used in SKB 91, although it has significantly less variation with depth.

For the fracture zones, the current data is substantially different to that used in SKB 91. The contrast in hydraulic conductivity is up to three orders of magnitude compared with just over one order of magnitude for SKB 91. This has great significance, since it implies that the fracture zones are the dominant medium for flow on the regional scale. In order to make this conclusion one needs to consider the relative transmissivity (width multiplied by hydraulic conductivity) of the fracture zones and rock mass. The width of the fracture zones is 10-100m, and the width of the rock mass between is a few kilometres, on average. Thus, when the contrast in conductivities becomes more than about two orders of magnitude, one can expect the main medium for flow to change from being the rock mass to the fracture zones. Of the variants considered in SKB 91 [Lindbom *et al.*, 1992], X36FR had properties most similar to those used in the current study. To assist comparison with SKB 91 a variant is considered in which the contrast in hydraulic conductivity is only about one order of magnitude.

Again, the depth dependence of the hydraulic conductivity of the fracture zones is not known. When a case with constant fracture zone properties was considered (case RCD1 in [Walker *et al.*, 1997]), the contrast in hydraulic conductivity at depth was over three orders of magnitude. This led to sharp changes in salinity and pressure at large depths and in consequence rapid mixing of saline and non-saline waters. The reason is that in continuing the zones to depth, freshwater is being piped rapidly to the base of the model, -2kmasl. It was concluded that for RCD1 the predicted salinity distribution did not appear to be consistent with measurements, and it leads to a solution with sharp spatial variations which is difficult to resolve numerically. This prompted an alternative case in which the hydraulic conductivity of each fracture zone was reduced by 1.5 orders of magnitude below a depth of about -850masl. This allows the possibility for freshwater to penetrate below Zone 2 and to the depth of the hypothetical repository, but at greater depths the fracture zones are less dominant as

conduits for flow. The contrast in hydraulic conductivity between the fracture zones and rock mass at depth becomes two orders of magnitude. This depth zonation was used in the base case and most variants. It is similar to the RCD2 case proposed in [Walker et al., 1997], except in that case the major reduction in hydraulic conductivity would occur much higher at about -100masl. An alternative structural model proposed by [Walker, 1998] is consider in the AltK variant to scope this very important aspect of the hydrogeological data.

The specific storativity of the rock is an uncertain parameter. Some data for specific storativities obtained from interference tests in boreholes [Ahbolm et al. 1988; Andersson et al., 1989] suggest hydraulic diffusivities, D , in the range 1 to 100 m²s⁻¹. One can estimate how far, Δx , a pressure pulse has propagated in time, Δt , from the relation

$$\Delta x^2 \sim D\Delta t$$

Therefore, even if $D = 1 \text{ m}^2\text{s}^{-1}$ a pressure pulse will propagate over 1km in a year. This implies that pressure equilibrates in response to transients on the order of a year or less. For this study the time-scales are thousands of years, and hence storage is not a significant parameter here. In other words, pressure transients diffuse much more rapidly than salt is advected. In consequence, the pressure can be considered to be instantaneously in equilibrium with the distribution of salinity at any time. The storativity was specified such that the hydraulic diffusivity was about 1 m²s⁻¹ throughout the model.

The most important parameter then in determining the rate at which the system changes is the total porosity. Laboratory measurements of porosity on rock samples from the Finnsjön site have suggested values of 0.5-3% for the rock mass, and 1-5% for fracture material [Brandberg and Skagius, 1991]. This gives us a way of checking the consistency of our model. Our approach is to calibrate the values of total porosity in order to predict a realistic evolution of salinity from the initial condition 4,000 years BP to the current day. If the values we obtain from the calibration agree with those from the laboratory experiments then it helps to build confidence in the relevance of the conceptual model.

NAMMU uses a Fickian model of hydrodynamic dispersion to model the spreading of salinity due to heterogeneity in the rock. Dispersion is specified in terms of a longitudinal and transverse dispersion length (see Appendix A). Although there have been some field tracer tests to determine hydrodynamic dispersivity [Ahlbom et al., 1992], it is very unclear whether these are appropriate for predicting the dispersion of salinity on a large regional scale. The values of dispersivity reported range between about 1m to 100m. Hence, the dispersion parameters are very uncertain. Values of longitudinal and transverse dispersion length are chosen about 80m and 40m, respectively. A variant case with smaller dispersion is considered to scope the effect of these parameters.

3.4 Salinity Data

Salinity has been measured in all the deep boreholes at the Finnsjön site. The positions of the boreholes are shown in Figure 3.5. Table 3.2 summarises the data for nine of the boreholes. The salinity data suggests several features:

- i) there is little salinity above Zone 2 in the northern block;
- ii) in the northern rock block salinity increases across Zone 2 and is about 5500mg/l of Chloride below Zone 2;
- iii) very little salinity is present in the southern block;
- iv) significant salinity is found at shallow depths east of Zone 3 or Zone 11.

It is the purpose of the calibration exercise to identify what combinations of values for the hydrogeological properties gives a model which broadly reproduces these features of the salinity distribution. The presence of salinity in near surface wells (see Section 2.4.2) suggests that ancient marine water may still be discharging salinity to the environment. This is another feature we should aim to reproduce in the model.

Table 3.2: Salinity in boreholes at the Finnsjön site.

Borehole	Depth to salt (masl)	Maximum Chloride (mg/l of Chloride)	Comment
BFI01	-150 to -250	5600	salt in and below Zone 2 northern block
KFI01		37	no salt found to a depth of -262masl southern block
KFI02		32	no salt found to a depth of -264masl southern block
KFI04		360	no salt found to a depth of -498masl southern block
KFI05	-130 to -270	5650	salt increases below Zones 1 and 2 from southern to northern block
KFI06	-150 to -370	5800	gradual increase in salt with depth northern block
KFI07		665	no salt found to a depth of -478masl northern block
KFI08	-140	4600	salt east of Zone 3 (or Zone 11) southern block to east
KFI09	-130 to -280	5100	salt in and below Zone 2 northern block

The relationship between density, mass fraction of salinity (c) and Chloride concentration used is detailed in Appendix A. A mass fraction relationship is used, but for brackish sea water this approximates to the following linear relationship

$$\rho \sim 998.3(1 + 0.008c).$$

Equivalently, density can be related to the concentration of Chloride, X (mg/l),

$$\rho \sim 998.3 + 0.00123X,$$

or salinity, S (%),

$$\rho \sim 998.3 + 7.46S.$$

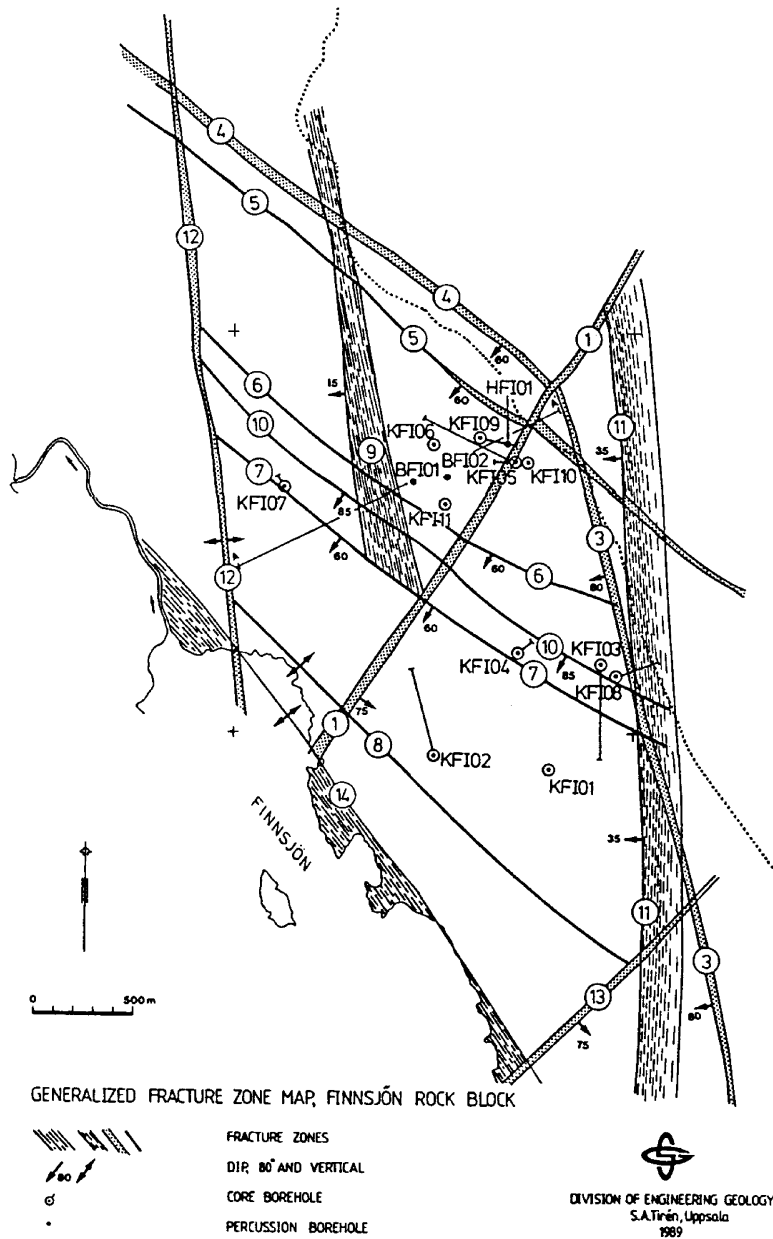


Figure 3.5: Map of fracture zones and boreholes in the vicinity of the Finnsjön rock block. Reproduced from [Andersson et al., 1991].

4 REGIONAL MODEL

4.1 Location and Size

The boundaries of the regional model were chosen to be sufficiently distant so that all possible recharge and discharge areas, which might influence flow at the site, were within the simulation domain, see Figure 2.1.

The model extends from Örbyhus in the west 16km to Dannemora in the east, and from Silbo in the north about 10km to the southern shore of Lake Finnsjön. Hence, the north, east and west boundaries are formed by regional fracture zones far from the Finnsjön site. These fracture zones are possibly associated with water divides, but this is not crucial to the modelling since pressure is set to hydrostatic on the sides. In fact, Silbo is very unlikely to be a flow divide as it is orthogonal to the regional flow direction, and hence it is important that there is flow across the northern boundary. It is more difficult to find a basis for locating the southern boundary. Walker et al. [1997] suggest the nearest water divide to the south is about 15km away. It is infeasible to extend the model this far. Instead the model was extended about 2.5km south of Gräsbo to include two low hills in the south and south west. There is no significantly higher ground for at least 5km further south. Thus, it is argued that our choice of southern boundary is adequate to capture the areas giving the maximum hydraulic gradient, and sufficiently far from the site (about 4km). If the boundary were too close, the results might be dominated by the choice of boundary condition.

Several lakes are included within the region. Lake Finnsjön extends northwards from the southern boundary to just south of the site. This is at a relatively high elevation of about 28m, and possibly forms a source of groundwater recharge for the site. Skålsjön and Assjön are at a lower elevation to the north and north east of the model, respectively. These are likely discharge areas. Further potential discharge areas are the two lakes located around the west and south east boundaries of the model.

4.2 Finite-Element Mesh

An oblique view of the finite-element mesh from the south is shown in Figure 4.1. The keyvalues for this mesh are shown in Table 4.1. The NAMMU CBQL cuboid element type was used. This uses mixed interpolation of variables: quadratic interpolation of pressure at 27 nodes per element, and linear interpolation for salt at 8 nodes per element. Mixed interpolation is used to give a consistent level of accuracy for evaluation of both terms in the velocity equation (A.2).

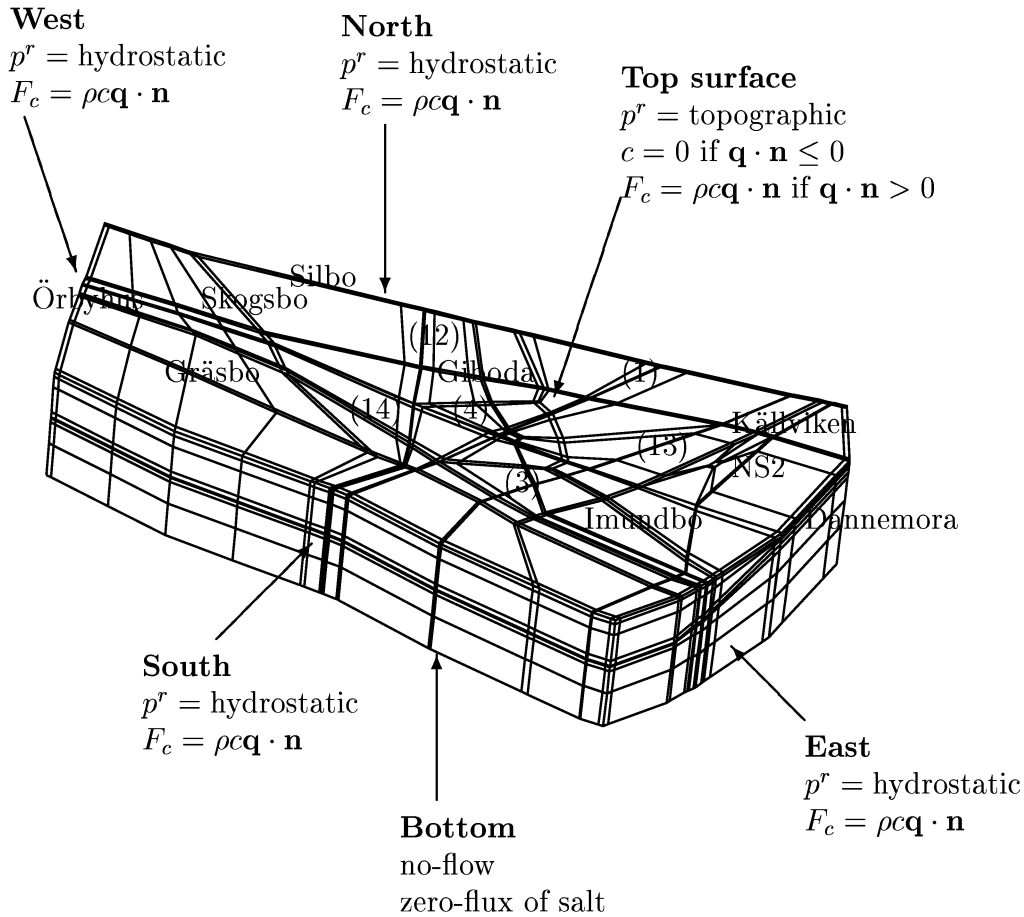


Figure 4.1: Oblique view of the finite-element mesh as seen from the south. The location of the model is shown in Figure 3.3. Boundary conditions used in the modelling are indicated.

The geometry of the mesh was based mainly on the lineament map. Some parts of the model were adjusted to represent the topography also. Figure 4.2 shows the representation of the fracture zones in the model. It is straightforward to construct a mesh when the lineaments are arranged in a fairly regular lattice, but becomes more difficult when fracture zones cross diagonally as well. In this case, Imundbo, Zone 3

Table 4.1: Keyvalues for the finite-element grid.

Item	Value
Number of elements	3478
Number of pressure freedoms	30963
Number of salt freedoms	4289
Depth	-2000 masl
Areal extent	20x10 km
Front width	1299

and NS2 cross several other lineaments diagonally. It was necessary to deviate the representation of these two zones slightly from the true lineament to avoid the finite-elements becoming heavily distorted.

The mesh is constructed from 5 vertical layers each with potentially different properties:

- i) an upper layer between the surface and $z = -50\text{m}$ to represent the more permeable near surface layer;
- ii) a layer above Zone 2, which has a base at $z = -750\text{m}$ south of Zone 2, and at $z = -100\text{m}$ north of Zone 2;
- iii) a 100m thick layer parallel to and including Zone 2 and other potential sub-horizontal zones;
- iv) a layer just below Zone 2 with a base at $z = -950\text{m}$ south of Zone 2, and at $z = -750\text{m}$ north of Zone 2;
- v) a bottom layer extending down to $z = -2000\text{m}$.

The definition of hydrogeological properties with depth is illustrated in Figure 4.3. Each of the three thick layers were refined vertically into 2 finite-elements to give a total of 8 elements in the vertical direction. This is considered adequate to represent changes in the vertical direction. In the horizontal directions refinement is reasonable in the vicinity of the site, but elements are much larger further out (up to 3km long). Ideally, there should be refinement of the finite-element mesh around the edges of each rock mass block to represent the rapid changes in salinity and flow that are likely as one moves from a fracture zone to the rock mass. For the transient non-linear physics considered such a level of refinement was not possible without run times becoming unacceptable. Typical run times per iteration were only about 5 minutes for the mesh shown in Figure 4.1 on a Silicon Graphics Power Challenge. However, about 4 iterations were required per time-step, and 47 time-steps were carried out giving run times of about 16 hours.

Thus, a pragmatic approach was taken in refining the grid. Most of the rock blocks close to the site were refined into several elements, and so one can expect reasonable

accuracy here. Further out, the lack of numerical resolution may result in the contrasts in salinity between fracture zones and the rock mass being smoother than in reality. This is not expected to effect the results on the local scale significantly, since the transport of salinity within a rock block is controlled mainly by the salinity in the surrounding fracture zones rather than in the salinity in distant rock blocks.

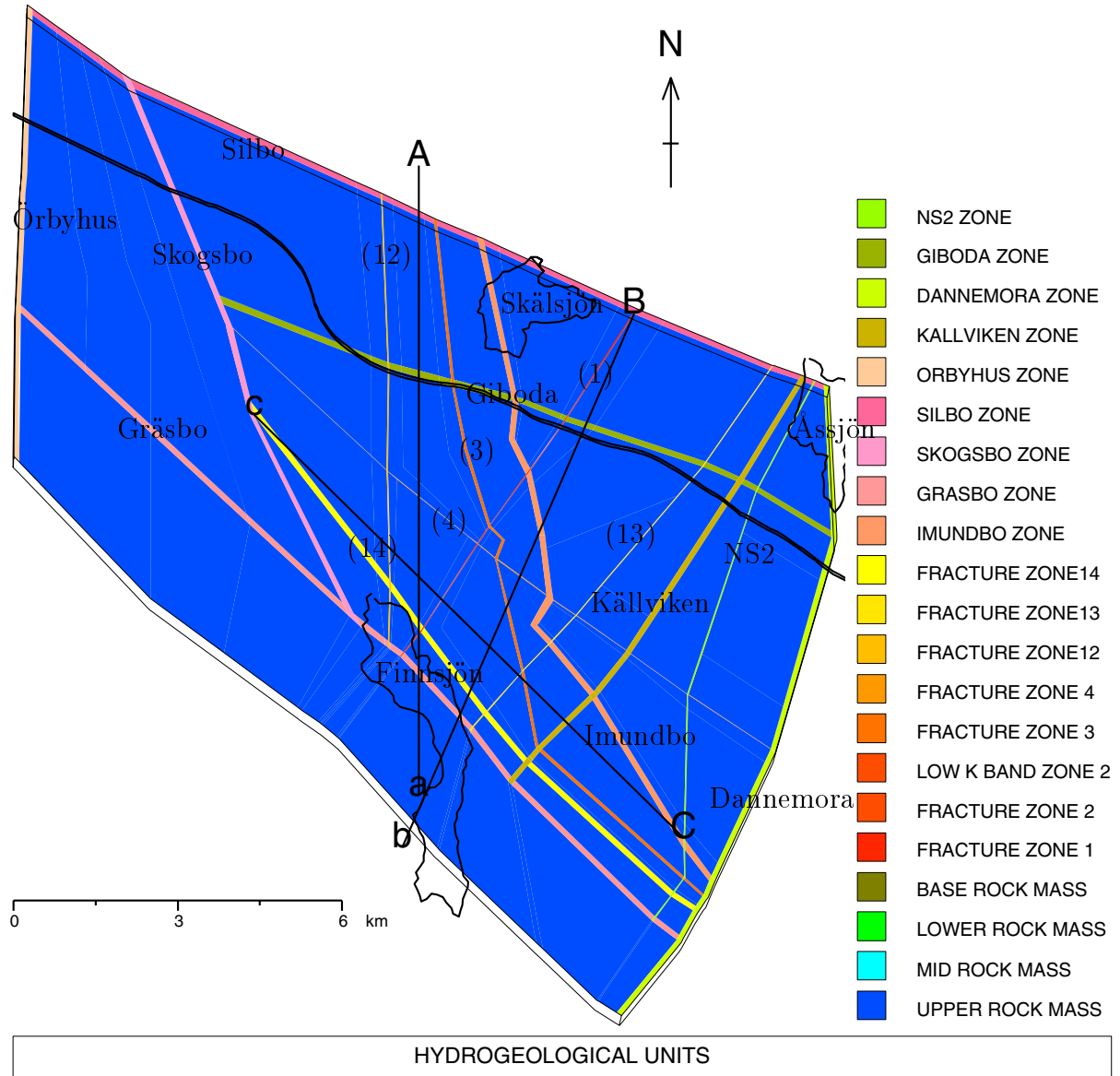


Figure 4.2: Plan view of the finite-element mesh for the base case showing the fracture zones and hydrogeological properties in the top elements. The positions of the 3 vertical slices a-A, b-B and c-C used in the calibration are indicated. Three lakes and road 76 are also shown as a reference.

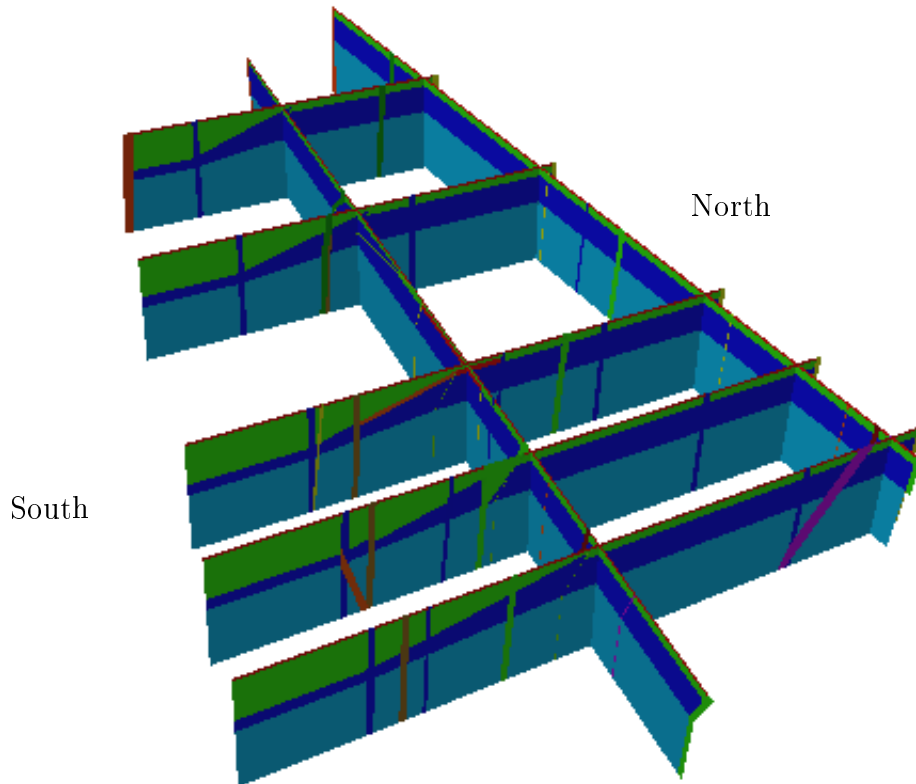


Figure 4.3: Oblique view of seven vertical slices through the finite-element mesh showing the hydrogeological properties. This plot was produced using the Avizier geovisualisation software.

4.3 Boundary Conditions

The boundary conditions used for the base case and the majority of variants are illustrated in Figure 4.1 (compare with Subsection 2.5). For the case described in this section the head on the top surface was constant in time and equal to present day topography. Figure 4.4 shows the head distribution set as a boundary condition on the top of the model. Topography data was obtained using the SKB GIS database.

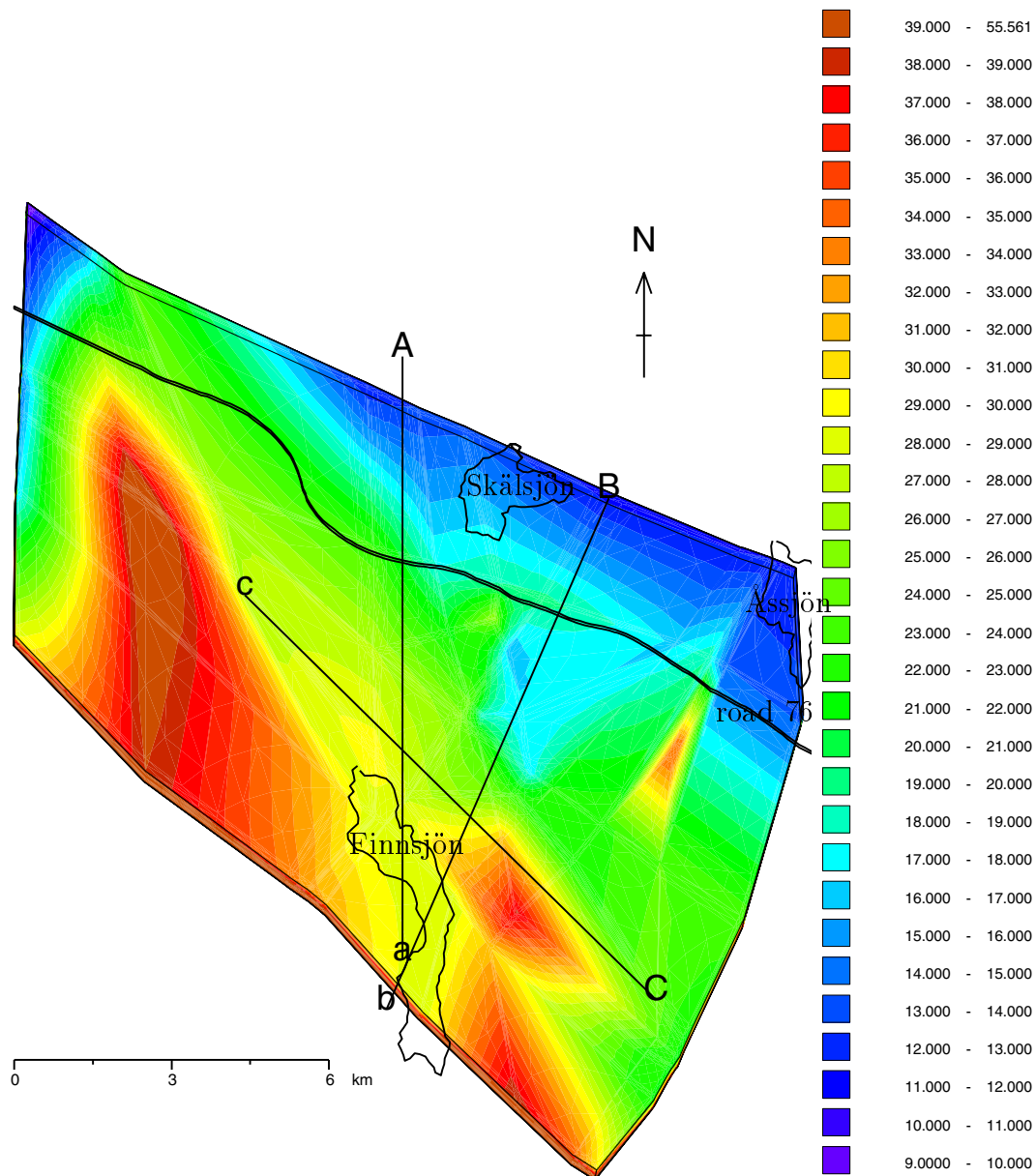


Figure 4.4: Plan view of the head boundary condition on the top surface of the model. The numbers shown in the key are in units of metres. The positions of the 3 vertical slices a-A, b-B and c-C used in the calibration are indicated. Three lakes and road 76 are also shown as a reference.

4.3.1 Salt Boundary Conditions

The recharge areas for which the boundary condition zero salinity is appropriate are determined on the basis of a constant density groundwater flow calculation (see Section 2.5). This was carried out for the initial condition where the whole domain is filled with saline water of density 1006.3kg m^{-3} . Figure 4.5 shows the flow field on a slice near the top surface of the model at $z = 8\text{m}$. The arrows indicate the direction of flow in three-dimensions, and are coloured according to the logarithm of the vertical flow component. Brown, red, orange, and yellow arrows are downwards indicating recharge

areas. Yellow is a high recharge $O(10^{-7})\text{ms}^{-1}$, while red is only $O(10^{-9})\text{ms}^{-1}$. Purple, blue, blue and green are upward flows indicating discharge areas. Green being the largest discharges. As expected, maximum recharge and discharge occur around the fracture zones.

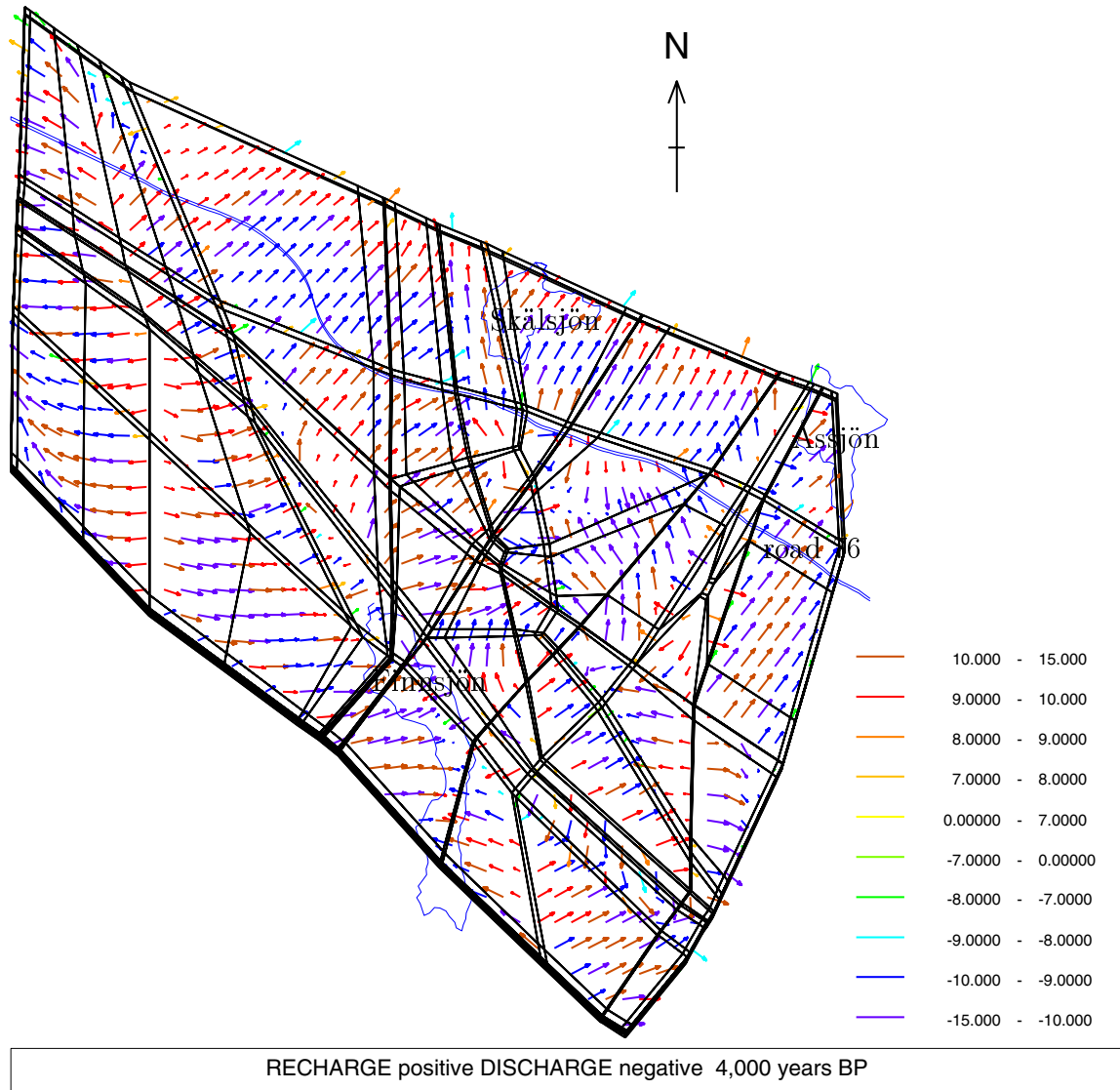


Figure 4.5: Plan view of the flow field for a slice near the top surface. The calculation is for the initial condition at 4,000 years BP. The key indicates the logarithm and sign of the vertical component of darcy velocity in units of ms^{-1} . Three lakes and road 76 are also shown as a reference.

This plot was used to establish visually what the appropriate boundary condition should be on the surface of sets of finite-elements (known as patches in NAMMU). Figure 4.6 shows the result of this manual process. As expected the recharge areas are mainly around high ground in the west and south east, but also the northern rock block. Discharge areas are mainly in the north and at the base of relatively steep slopes in the far west, east and the southern shores of Lake Finnsjön. For the recharge areas

(green) $c = 0$ was specified. In the discharge areas an advective outflow of salt was specified. However, it was found that the boundary condition in the discharge areas needs to be specified more carefully. There are some elements in which there is recharge on a part of the surface and discharge on the rest. The boundary condition specified in these elements was modified such that there was zero flux of salt if flow were inwards, and an advective discharge of salt otherwise.

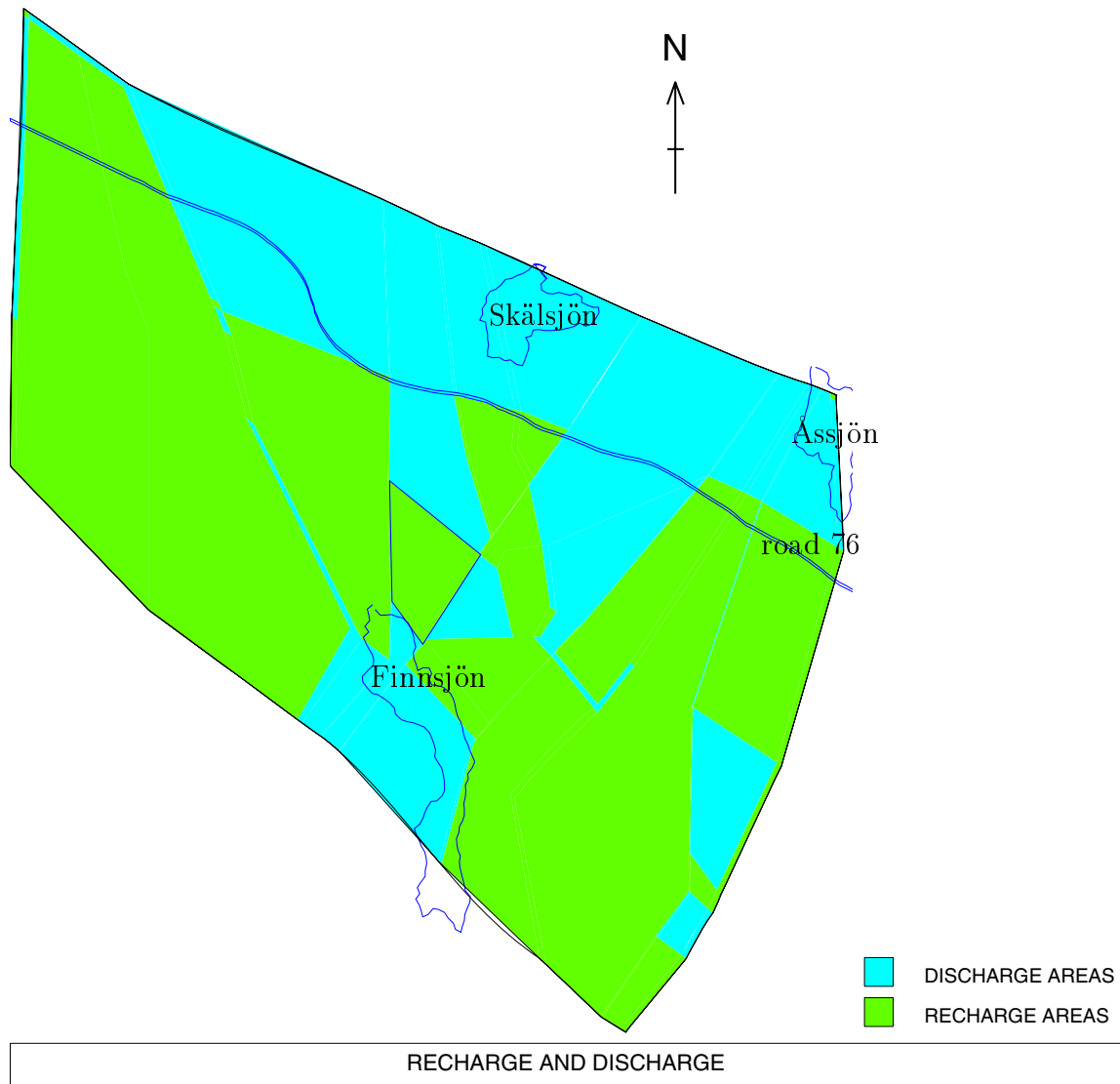


Figure 4.6: The locations of recharge and discharge areas used in defining the salt boundary conditions on the top surface. The northern rock block, three lakes and road 76 are also shown as a reference.

For the description of the boundary conditions to be self-consistent the recharge and discharge areas should not change significantly in time as the pattern of salinity evolves. This seemed to be the case. Presumably because the near surface flows are governed by topography rather than the salinity in the region beneath. Figure 4.7 shows the velocity arrows in the near surface at the present day for the base case run.

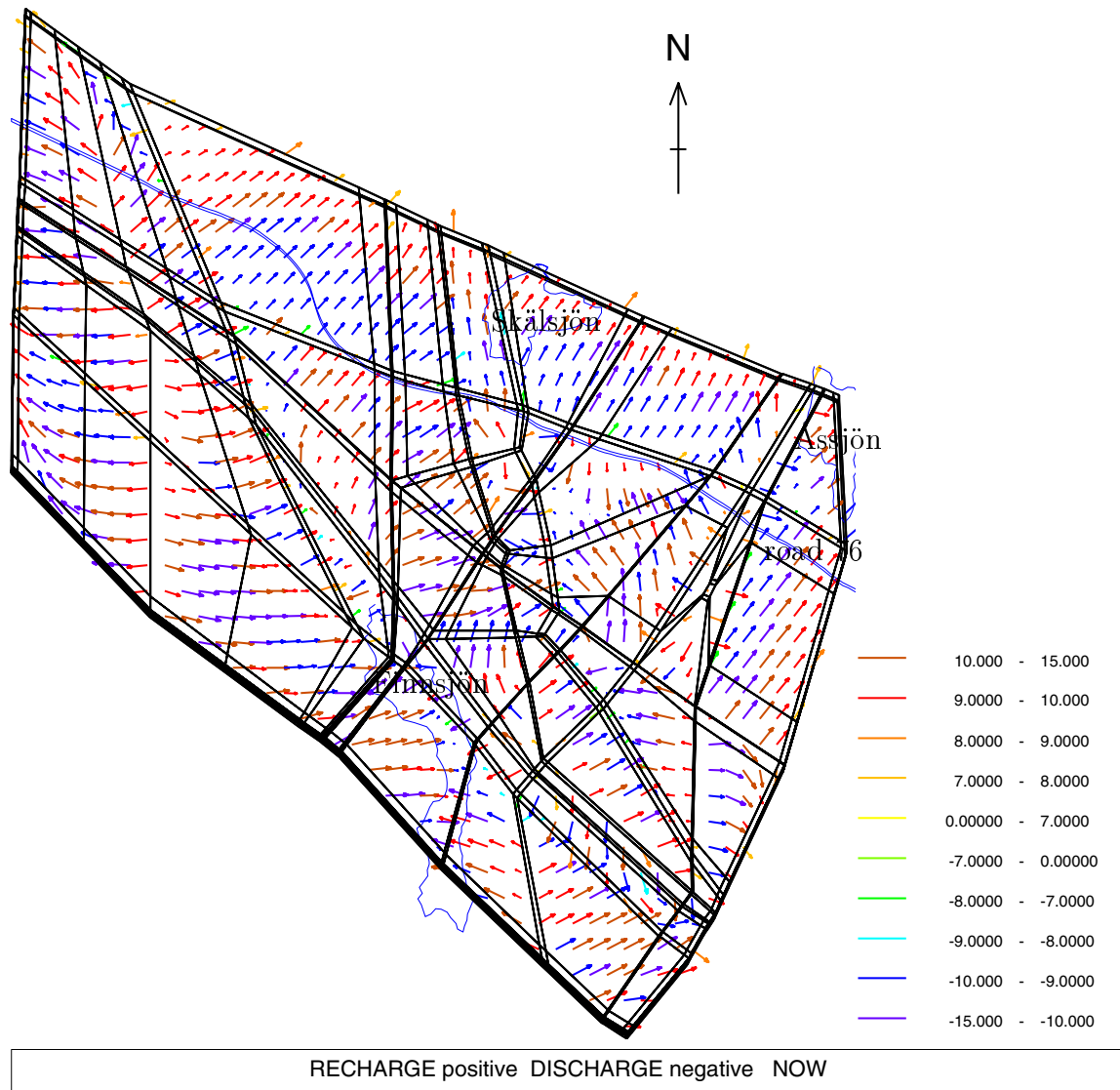


Figure 4.7: Plan view of the flow field for a slice near the top surface. The calculation is for the base case for present day conditions. The key indicates the logarithm and sign of the vertical component of darcy velocity in units of ms^{-1} . Three lakes and road 76 are also shown as a reference.

4.4 Base Case Hydrogeological Properties

In the following subsections we discuss some of the results for transient simulations of groundwater flow and salt transport. Those presented are for the base case model. It is important to note that the base case is not defined as that for which all values were set to central values, but is the result of a calibration exercise to obtain the best fit to observations. The calibration was qualitative, trying to match the broad features of the measured salinity pattern, and so it is by no means unique. There may be several

other combinations of parameters that give as good or a better match to reality. More detail on the calibration is given in Section 5.

The basic features required to achieve a good calibration were:

- i) truncate the vertical zones (Zone 4, 12 and 14) below Zone 2;
- ii) represent the semi-impermeable layer within Zone 2;
- iii) total porosity was set to 2% for the rock mass;
- iv) total porosity was set to 5% for the fracture zones;
- v) low dispersion lengths of 20m for longitudinal and 10m for transverse were set in Zone 2.

Zone 2 was in fact split into three vertical layers. Upper and lower layers are 25m thick and have high hydraulic conductivity $1.45 \cdot 10^{-5} \text{ms}^{-1}$. The middle layer is 50m thick and has a very low hydraulic conductivity $1.0 \cdot 10^{-9} \text{ms}^{-1}$. Hence, the combined horizontal transmissivity of Zone 2 is as specified by Walker et al. [1997], but the vertical conductivity is over three orders of magnitude less. This is consistent with conceptual models developed to analyse pump-tests in Zone 2 [Andersson et al., 1991]. This is only an idealised model of Zone 2 to represent the properties on the regional scale. Investigations of Zone 2 have revealed a lot of detailed structure with bands of permeable and semi-impermeable material, and fractures connecting the permeable bands. Hence, the calibration suggests that there is a relatively poor hydraulic connection vertically across Zone 2. This does not exclude the possibility of localised connections, it only implies that such connections are either infrequent or short and not interconnected.

A summary of all the hydrogeological properties used in the base case are summarised in Table B.2

4.5 Time-Steps

A fully implicit method was used for time-stepping. The large contrast in properties between the fracture zones and the rock mass implies that changes in the groundwater flow and salinity take place on different time-scales. It was found that initially the salinity evolved very rapidly in the fracture zones, so a time-step of a few years was appropriate. Later on, the changes in salinity were mainly in the rock mass and took place on a time-scale of hundreds of years. This suggested that the time-step size should gradually increase in time. A sequence of time-steps (see Table 4.2) was chosen manually (by experiment) on the basis that the maximum change in head between any two time-steps should not exceed a few metres. This condition should ensure reasonable accuracy. An alternative approach would have been to select the time-steps automatically using Gear's method, for example. This was avoided as it was

thought the method would prove to be too conservative in increasing the time-step size, resulting in extra time-steps and longer run times.

Table 4.2: Sequence of time-steps used in the transient modelling.

Number of steps	Size (years)	Elapsed time (years)
4	4	16
3	8	40
8	20	200
5	40	400
14	100	1800
11	200	4000

4.6 Evolution of Salinity and Pressure

Figures 4.8 and 4.9 show the evolution of salinity and pressure on the vertical slice a-A for the base case. Salinity is shown by plotting contours of equal groundwater density, while the pressure is represented by contours of equal head. Zone 2 is the gently dipping feature in the upper central part of the slice. The bands of high hydraulic conductivity are shaded orange, while the central low hydraulic conductivity band is shaded black.

The results reproduce a lot of the phenomena that were anticipated in Section 2.4.2. Salinity evolves most rapidly in the fracture zones. In fact, salt water is flushed from the upper parts of the fracture zones on a time-scale of 10-100 years. Salinity is retained in the rock mass for much longer time-scales, several thousands of years according to the model. There are several interesting features associated with Zone 2. Firstly, fresh water intrudes into the transmissive band at the top of Zone 2 at about 2,000 years BP giving rise to a cell of saline groundwater suspended in the rock mass above. The salinity of this cell decreasing substantially by the present day. Secondly, salinity varies rapidly across and below Zone 2. These profiles are broadly consistent with the borehole measurements in the northern block.

Figure 4.9 shows that pressure also changes significantly in time. In the upper layers contours change from being diagonal or near horizontal to become more vertical as fresh water replaces saline. It should be noted that the spacing between contours in the horizontal direction indicates the direction and magnitude of horizontal flows, but it is necessary to consider changes in density as well to predict vertical flows.

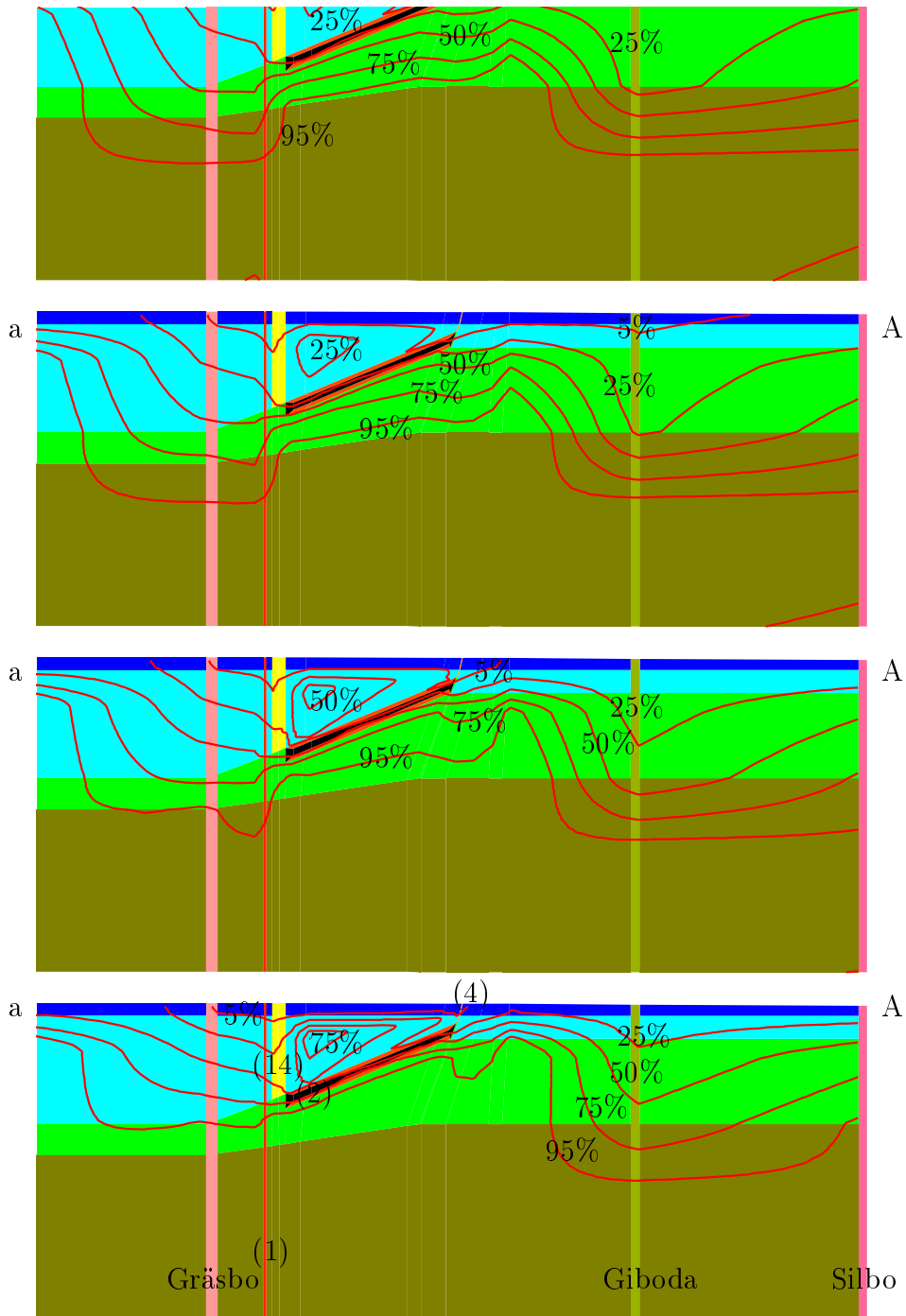


Figure 4.8: Evolution of salinity in time on the slice a(left)-A(right) (see Figure 4.2) through the northern rock block for the base case. The contours of salinity shown correspond to 5%, 25%, 50%, 75% and 95% of the maximum salinity (corresponding to 6,500mg/l). From bottom to top, the plots correspond to density at 3,000 years BP, 2,000 years BP, 1,000 years BP and the present day. Zone 2 is the narrow feature dipping in the upper central part of the slice. The colours indicate different hydrogeological properties (see Figure 4.2 for a key). Note the vertical scale is exaggerated by a factor of 2.

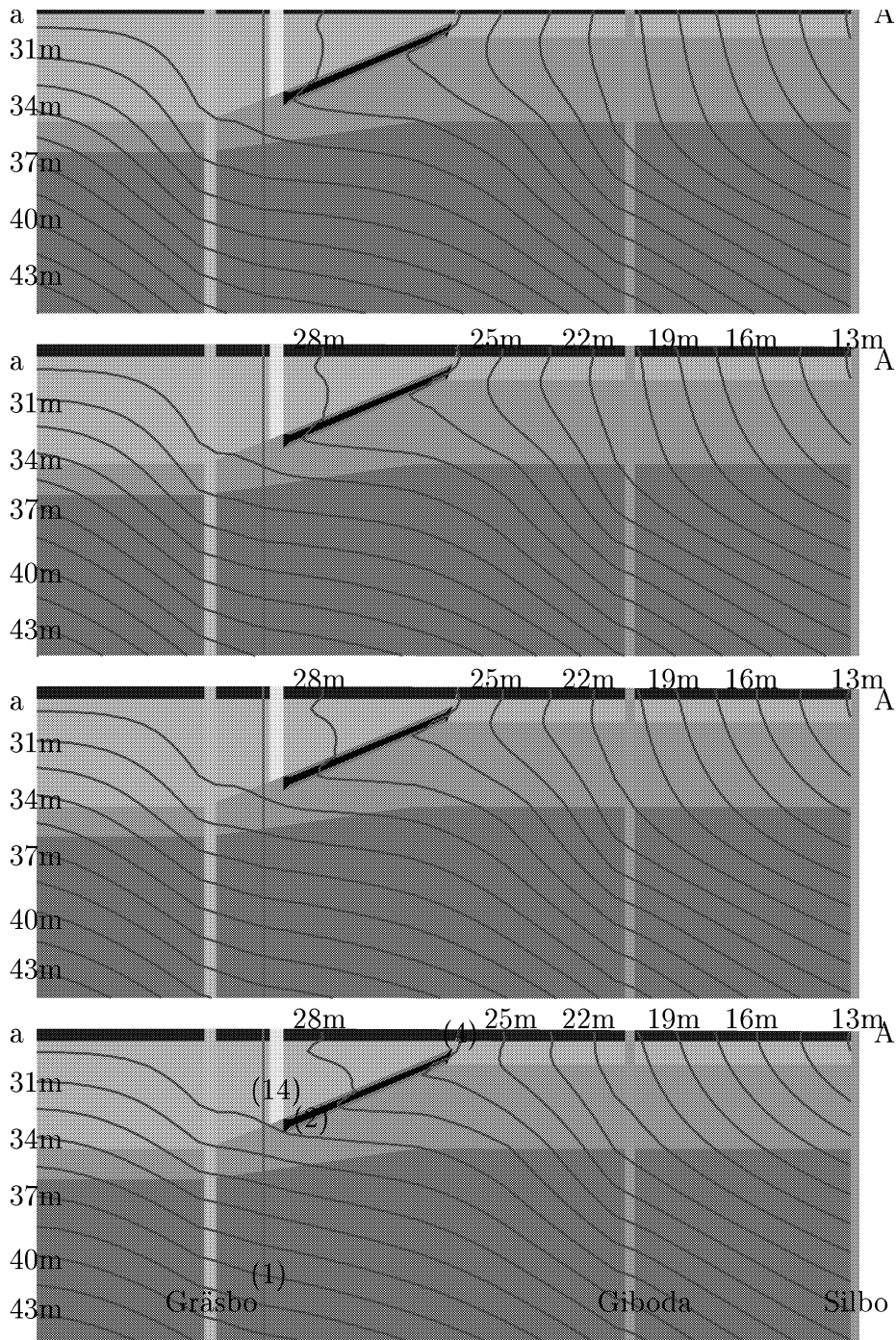


Figure 4.9: Evolution of head in time on the slice a(left)-A(right) (see Figure 4.2) through the northern rock block for the base case. Contours of head are plotted at intervals of 1.5m between 13m and 43m. From bottom to top, the plots correspond to density at 3,000 years BP, 2,000 years BP, 1,000 years BP and the present day. Zone 2 is the narrow feature dipping in the upper central part of the slice. Note the vertical scale is exaggerated by a factor of 2.

5 CALIBRATION

It is usually difficult to establish the reliability with which a model predicts quantities such as groundwater flow velocities at depth and regional scale groundwater flow patterns, since it is difficult to measure these quantities in situ. This is due to the long time-scales for transport at depth, and the lack of accessibility to the deep rock for conducting experiments. However, it is possible to measure the performance of a model by testing its ability to predict quantities that can be measured more readily. This may include recharge rates, discharge areas, and salinity profiles in deep boreholes. By comparing the model results against such data, an understanding of the combinations of hydrogeological features and parameters that give consistent results can be gained. Such a calibration helps to build confidence in the model by reducing the conceptual and parameter uncertainty.

The calibration against infiltration rates is described in Subsection 5.1. The way in which the salinity data in boreholes was used to calibrate the model is described in Subsection 5.2. The set of variants considered and the corresponding results are discussed in Subsection 5.3. A sub-set of these variants are identified as being ‘possible’ realisations of the regional groundwater flow and salinity patterns. These are the variants which predict salinity patterns which are considered to be broadly consistent with the salinity data available. Each of the variants which meet the calibration criteria are treated as sensitivity variants in the groundwater pathway calculations carried out in Subsection 6.1 to locate the local scale model.

5.1 Near Surface Flows

Although we are primarily interested in groundwater flow velocities at depth, it is important that the model should predict realistic flow rates and heads near the top surface. Since the head on the top surface is specified, the model can be calibrated by varying the hydraulic conductivity of the near surface and comparing the predicted recharge and discharge rates against those estimated in water balance calculations. Estimated recharge and discharge rates of 180 mm/year and 420 mm/year, respectively, for northern Upland are reported by Walker et al. [1997]. Figure 4.7 indicates the predicted magnitude of recharge and discharge in the near surface under present day conditions. Recharge and discharge rates are between 10^{-10} to 10^{-8}ms^{-1} (3 to 300

mm/year) for the rock mass, and about 10^{-8} to 10^{-7}ms^{-1} (300 to 3000 mm/year) for fracture zones. Thus, the magnitude of near surface flows predicted by the model appear realistic. This implies the values of hydraulic conductivity for the near surface and groundwater recharge rates proposed in [Walker *et al.*, 1997] are self-consistent.

5.2 Salinity Pattern

The main criterion for calibration of the model is that the profiles of salinity predicted in the site boreholes should approximate those observed. However, the pattern of salinity is only known in a localised area relative to the size of the regional model. Because the purpose of this study is to predict the large scale flow and salinity patterns, it is also important to consider results on the larger scale when comparing the variants.

5.2.1 Base Case - Salinity on Vertical Sections

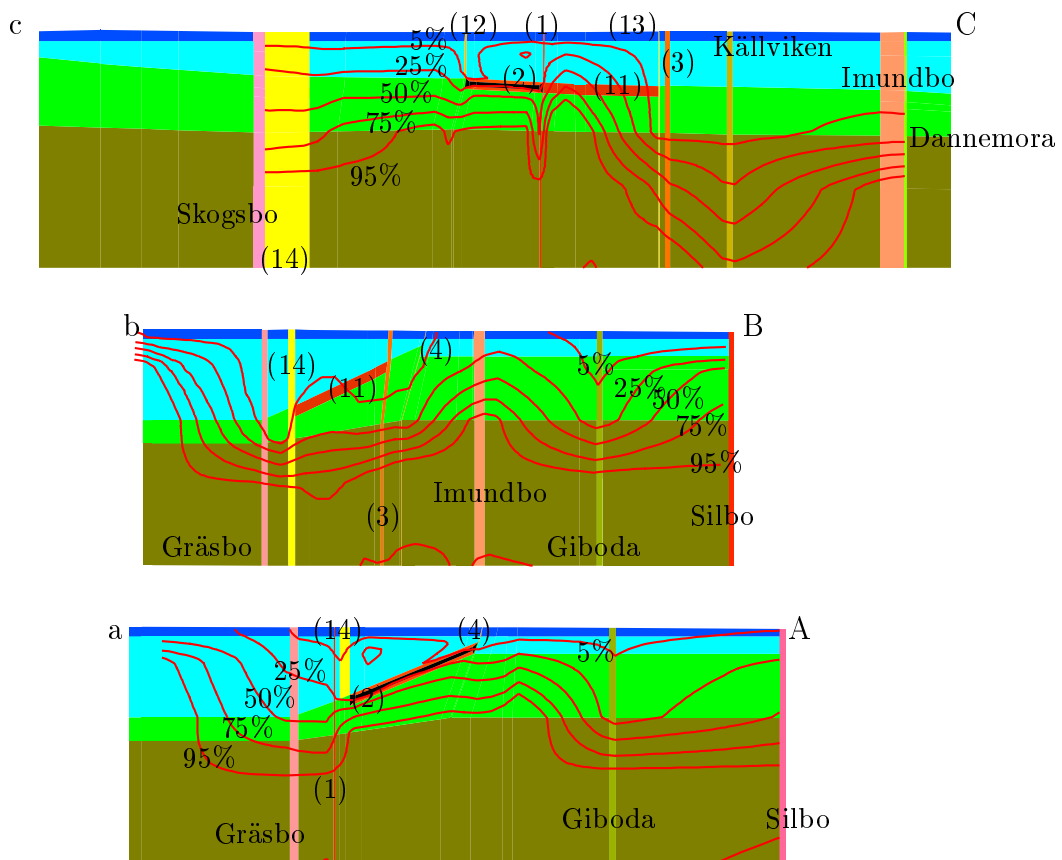


Figure 5.1: Salinity on vertical slices along a-A, b-B, c-C (see Figure 4.2) for the base case. The contours of salinity shown correspond to 5%, 25%, 50%, 75% and 95% of the maximum salinity (corresponding to 6,500mg/l). Note the vertical scale is exaggerated by a factor of 2.

Contours of salinity on each of the 3 vertical sections a-A, b-B, and c-C (as shown in Figure 4.2) are presented in Figure 5.1. The slice a-A cuts south-north through the northern rock block; b-B cuts SSW-NNE through the southern rock block; and c-C cuts NW-SE through both rock blocks. Very approximately, the slices a-A and b-B are aligned from upstream to downstream, while c-C is orthogonal to the regional flow direction. The profiles are shown for present day conditions.

The slice a-A cuts through Zone 2 (central upper part of the slice) showing the sharp transition in salinity across the zone. There is still low levels of salinity, about 1300mg/l of chloride, retained above Zone 2. Interestingly, salinity is relatively close to the surface to the north of Zone 2, where there is a discharge region. Salinity is much deeper to the north of Giboda. The saline transition zone is very diffuse to the south of Zone 2 (upstream). A later variant will scope how the prescription for the upstream salinity profile affects that in the vicinity of the Finnsjön site.

Slice b-B cuts through Zone 11 (shown in red) and shows that salinity is much deeper in the southern rock block. Again salinity ‘up-cones’ in the discharge region around Imundbo to the north.

Slice c-C confirms that there is a sharp saline transition zone below Zone 2. It is also apparent that the model predicts high salinity below about 200m in the western part of the southern rock block. This may just be result of the assumption that this area is a discharge area. Salinity is found to be much closer to the surface to the west of the site than to the east. This appears to be a result of the increased topographic gradient around the ridge in the south east corner of the model.

The rather coarse refinement of the grid is clearly apparent in some of the density contours shown in Figure 5.1, especially in the large finite-elements in the base layer. Due to the complexity of the model it would not be tangible to obtain a fully grid-converged set of results, and so there has to be some compromise in terms of accuracy. However, the representation of the physical processes is considered to be good, and there is a reasonable degree of grid refinement in the region of interest. Hence, it is believed the results are sufficiently indicative of the real situation that they can be used to explore the hydrogeological situation at Beberg.

5.2.2 Base Case - Salinity in Boreholes

In Figure 5.2 the performance of the model in predicting salinity in the site boreholes is measured. Profiles are shown for the boreholes BFI01, KFI04, KFI06, KFI07 (see Figure 3.5). These are four of the deeper site boreholes and are spread over a large area of the site. Boreholes BFI01, KFI06, KFI07 are in the northern rock block. KFI04 is in the southern rock block. The lithology down each of the boreholes (as observed in the model) is shown on a horizontal key.

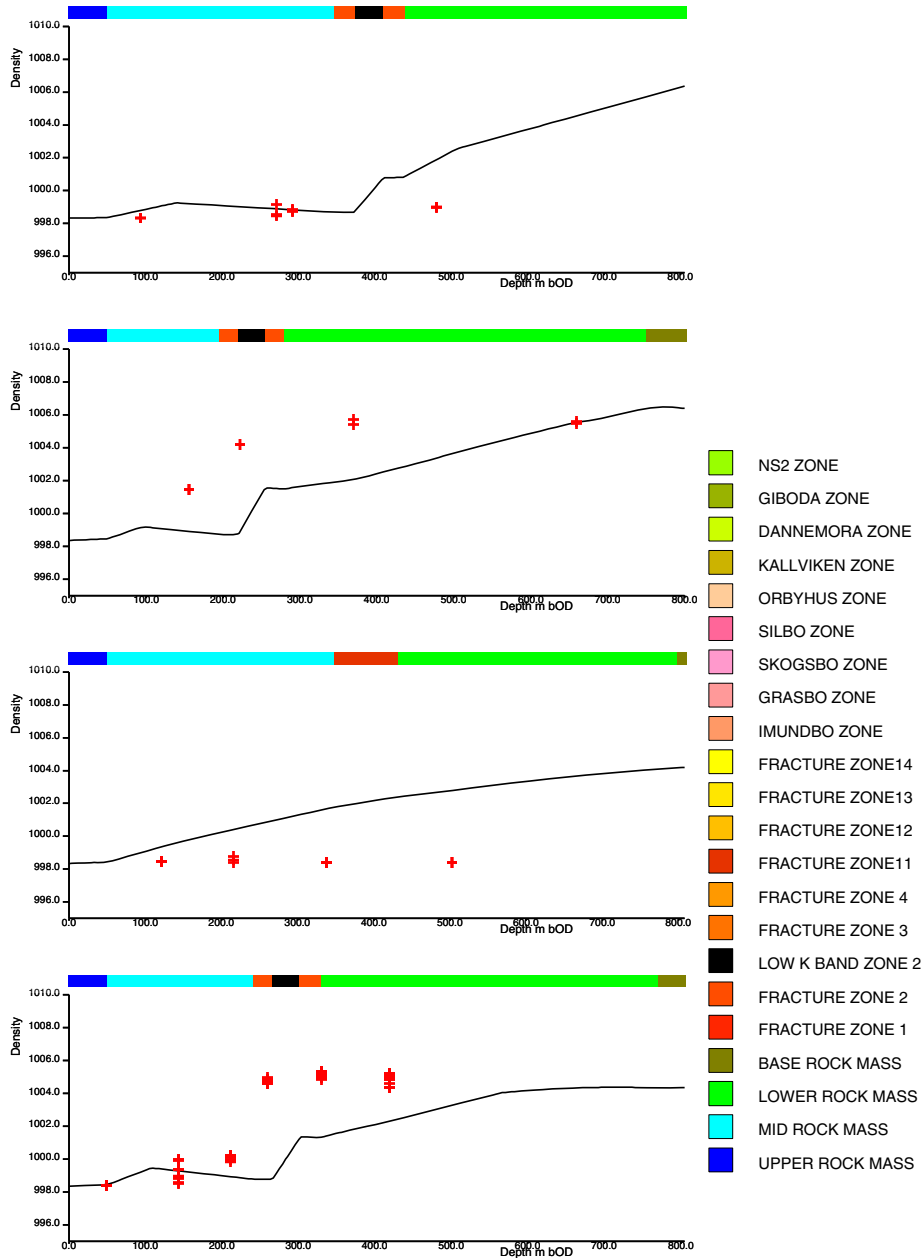


Figure 5.2: Salinity in the boreholes BFI01, KFI04, KFI06, KFI07 (from bottom to top) for the base case. The solid lines represent the model results. The red crosses are experimental data. The shaded bar across the top indicates the modelled lithology down the borehole. The range of density shown on vertical axis is 996 to 1010 kgm^{-3} .

The model reproduces the sharp increase in salinity across Zone 2 for each borehole seen in the experimental data. However, the size of this increase for the numerical results is less than in reality. The model predicts a further gradual increase in salinity below Zone 2. Observations suggest salinity reaches its maximum value just below Zone 2. This discrepancy may result from the lack of refinement within and below Zone 2. There are only 3 finite-elements in the vertical direction to represent the bands within Zone 2, and 4 finite-elements below Zone 2. The model predicts a gradual increase in salinity with depth in the southern rock block. This is not seen in the data from

KFI04. There are several possible ways in which the calibration might be improved in this region. These include:

1. by including local features within the southern rock block, such as Zone 11;
2. by changing the salt boundary condition in this region to be appropriate to recharge rather than discharge;
3. by improving the representation of the topography, such as including the low ridge which extends from the south east to this region.

The base case is judged a reasonable calibration against present day conditions given the complexity of the physical processes considered and coarse grid refinement.

5.3 Calibration Variants

The base case is one in a sequence of many calculations that were carried out in developing a calibrated model. These involved different combinations of boundary conditions as well as changes in physical properties. It is not practical to present all the models that were considered. Instead, we present here a set of variants that illustrate the effects of selected parameters and show why certain assumptions were necessary to calibrate the model. Additional variants are considered to quantify the sensitivity of the calibration to the salinity boundary condition on the southern boundary and additional regional fracture zones in the south.

In total eleven variants were considered, as summarised in Table 5.1. Each of these variants is described in detail in the following subsections. A label, such as Zdeep, is used as a short-hand reference for the variants in the following sections. Table 5.1 also indicates which of the variants were judged to be sufficiently calibrated to be treated as a sensitivity variant in the groundwater pathway calculations (see Subsection 6.1). This is indicated by a ‘Y’ in the sensitivity variant column. It can be seen that there are seven sensitivity variants. Seven of the calibration variants investigate aspects relating to the fracture zones. This reflects the importance of understanding the role of the fracture zones in determining the regional scale flow and salinity pattern. The remaining variants consider the effects of anisotropy, porosity, dispersion and the up-stream salinity boundary condition. A record of files relating to these variants is given Appendix C.

Comparison of the results for each variant is achieved by displaying salinity contours on the vertical slices a-A, b-B and c-C (see Figure 4.2). Although the profiles of salinity in the site boreholes give a more quantitative measure of model performance, in the context of this study, it is more important to assess the sensitivity of the salinity pattern on the regional scale, rather than focus on the local site scale.

Table 5.1: The set of calibration and sensitivity variants.

Identifier	Calibration activity	Calibration of	Sensitivity variant
Zdeep	Zones 4, 12 and 14 extended vertically to base	Depth of vertical zones	N
Zsouth	Källviken and Finnsjön zones extended south	Zones in south	Y
Z2highK	Higher permeability for middle band in Zone 2	Zone 2 vertical connectivity	N
ZlowK	Contrast in hydraulic conductivity reduced by 1/30	Fracture zone K	N
ZlowK ϕ	As for ZlowK, and lower porosity also	Fracture zone K + porosity	Y
Z11	Zone 11 made transmissive [Walker <i>et al.</i> , 1997]	Zone 11 K	Y
Csouth	Salinity specified constant on south boundary	Upstream salt b.c.	Y
ϕ low	Lower porosity for rock mass and fractures	Porosity	N
Dlow	Lower dispersion lengths in rock mass and fractures	Dispersion	Y
Zlocal	Include local fracture zones by implicit representation	K in local rock blocks	Y
RRD3	Anisotropy in the horizontal plane. NW-SE principal axis	K anisotropy in rock mass	Y
AltK	Alternative structural model similar to [Andersson <i>et al.</i> , 1991]	Depth dependent K in zones	Y

5.3.1 Depth of Local Fracture Zones (Zdeep)

The first variant is included to justify the decision to terminate fracture zones 4, 12 and 14 at Zone 2 in the base case. These three zones lie to the north, west and south, respectively, of the northern rock block. In Zdeep the only difference to the base case is that each of these zones is extended to the base of the model. None of the site boreholes intercept these zones, so there is a lot of uncertainty associated with both their vertical extent and hydrogeological properties. The characterisation of most fracture zones is only based on surface lineaments. Thus, the Zdeep variant and the base case can be considered equally plausible realisations of the geology.

Figure 5.3 presents salinity contours on the vertical slices for the Zdeep variant. The overall pattern of salinity is very similar to the base case, but there are significant differences below Zone 2. For Zdeep the rise in salinity across Zone 2 is much reduced, and the saline transition zone below Zone 2 is more diffuse. This makes the match

between the modelled and known salinity profile much worse than for the base case, and so Zdeep is not considered a legitimate calibrated variant.

The need to truncate fracture zones 4, 12 and 14 at Zone 2 is only a constraint on the hydrogeological description. It does not necessarily imply that the zones terminate against Zone 2, only that they are hydrogeologically insignificant below Zone 2. Other possibilities are that the fracture zones have very low hydraulic conductivity due to mineralisation or compression of fractures.

The reason for the differences is that Zones 4, 12 and 14 transmit fresh water to depth on the sides of the northern rock block, resulting in the saline water trapped below Zone 2 migrating sideways out of the rock mass due to the different hydrostatic pressures in the fracture zones and rock mass.

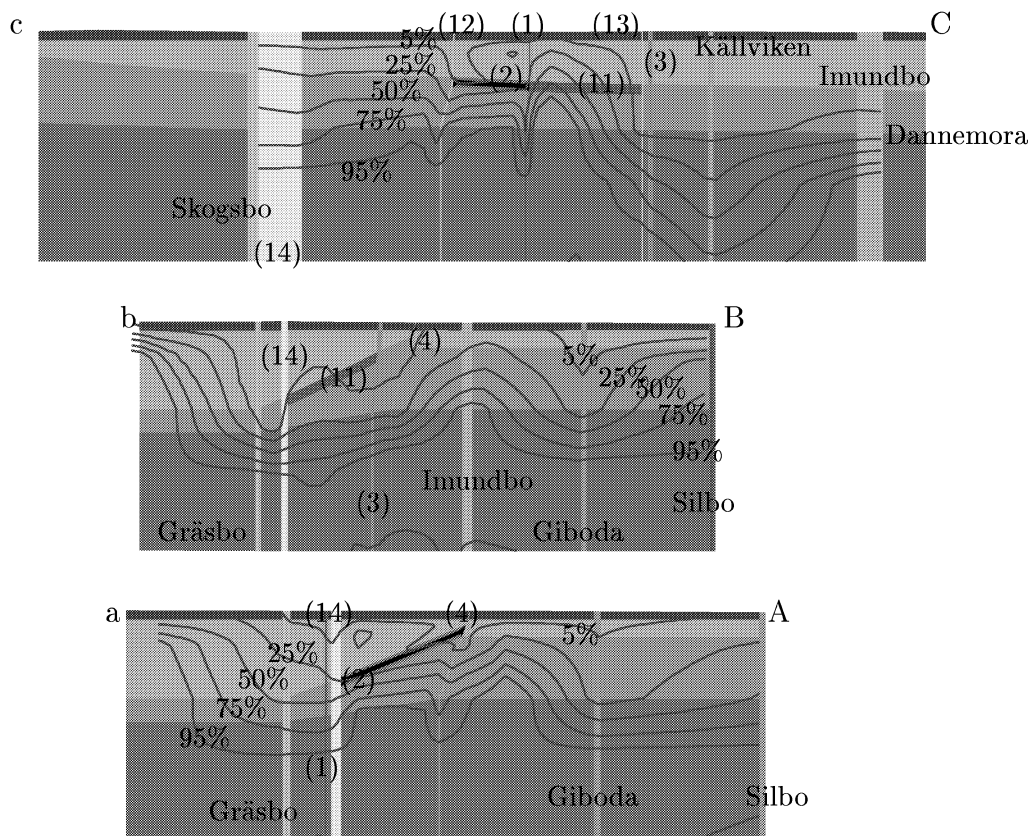


Figure 5.3: Salinity on vertical slices along a-A, b-B, c-C (see Figure 4.2) for Zdeep variant. The contours of salinity shown correspond to 5%, 25%, 50%, 75% and 95% of the maximum salinity (corresponding to 6,500mg/l). Note the vertical scale is exaggerated by a factor of 2.

5.3.2 Extra Fracture Zones in South (Zsouth)

In developing the base case model the domain was extended several kilometres south of the Finnsjön site to reduce the dependence of the results on the boundary condition for salinity upstream. However, fracture zones were not well characterised in this southern region. For the base case only the Örbyhus and Dannemora regional zones were extended to the south. Walker et al. [1997] present a regional lineament map showing two further features in the region. These are a southerly extension of Källviken and a well expressed zone running N-S under the southern section of Lake Finnsjön. These two zones were included in the Zsouth variant as shown in Figure 5.4.

The hydraulic conductivity for the Finnsjön Zone is $4.68 \cdot 10^{-5} \text{ms}^{-1}$, and it is 50m in width.

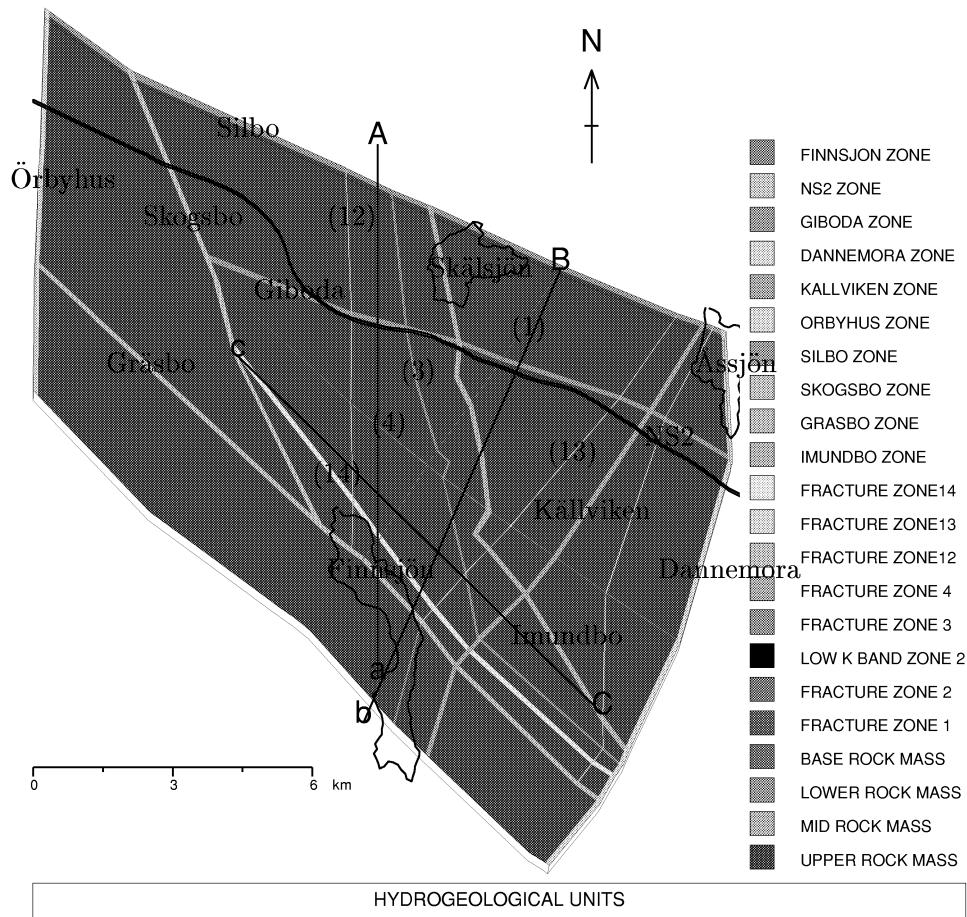


Figure 5.4: Plan view of the finite-element mesh for the Zsouth variant showing the fracture zones and hydrogeological properties on the top elements. The positions of the 3 vertical slices a-A, b-B and c-C used in the calibration are indicated. Three lakes and road 76 are also shown as a reference.

The specification of the boundary condition for salinity on the southern vertical bound-

ary including and between these two zones was changed to zero flux of salt. This again was a result of the difficulty in defining the salinity that enters the model in the south. In the base case the boundary condition was an advective inflow condition. For the Zsouth variant this boundary condition resulted in instabilities gradually arising around the two southern fracture zones. Given the uncertainty in the upstream boundary condition, it was considered legitimate to resolve the problem by re-defining the boundary condition locally. Figure 4.6 shows the region around the two new zones to be a recharge area. It was re-confirmed that this is still a recharge area for the Zsouth variant by re-calculating the near-surface flow distribution.

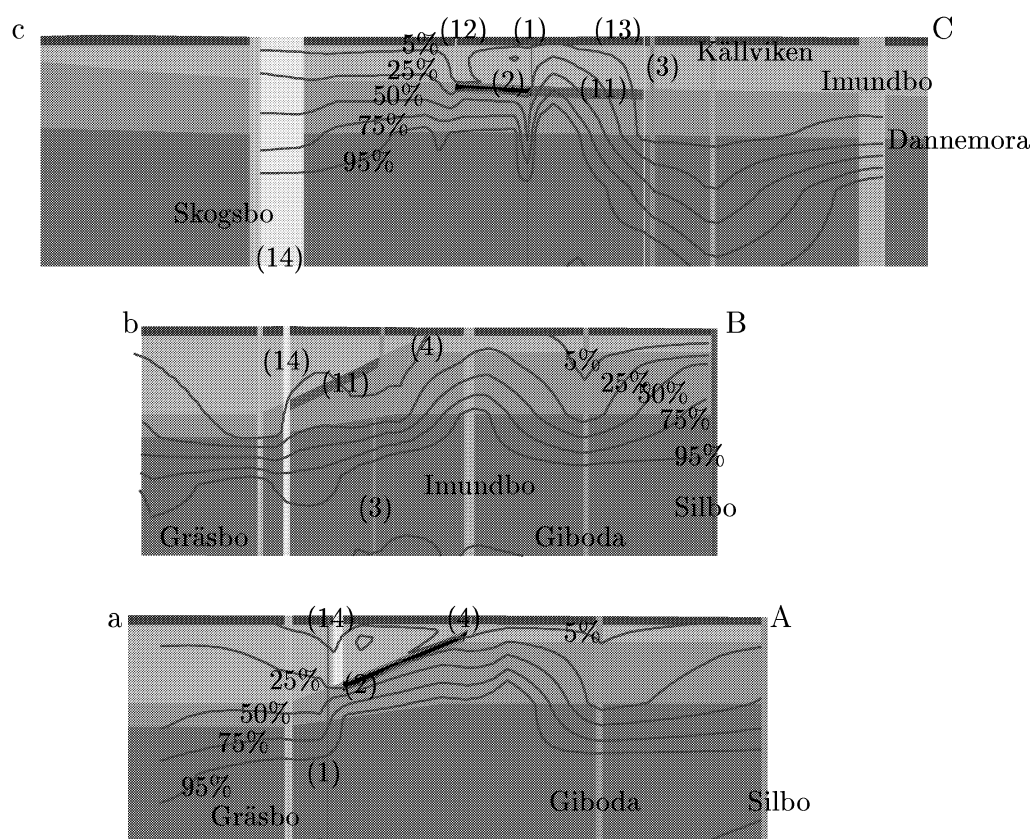


Figure 5.5: Salinity on vertical slices along a-A, b-B, c-C (see Figure 4.2) for Zsouth variant. The contours of salinity shown correspond to 5%, 25%, 50%, 75% and 95% of the maximum salinity (corresponding to 6,500mg/l). Note the vertical scale is exaggerated by a factor of 2.

Figure 5.5 shows the salinity on vertical slices for the Zsouth variant. Salinity is now much deeper upstream (south of Gräsbo) in both slices a-A and b-B. However, this does not appear to effect the salinity in the Finnsjön rock block. Hence, this variant is included as sensitivity variant to investigate if the change in upstream salinity effects groundwater pathways.

5.3.3 Higher Hydraulic Connectivity Across Zone 2 (Z2highK)

The variant Z2highK is included to justify the inclusion of a band of very low hydraulic conductivity within Zone 2. In this variant the hydraulic conductivity of the band is increased from $1 \cdot 10^{-9} \text{ms}^{-1}$ in the base case to $1 \cdot 10^{-7} \text{ms}^{-1}$. Figure 5.6 shows the salinity contours for the Z2highK variant. Again the sharp increase in density across Zone 2 is no longer seen, and salinity is significantly deeper around Zone 4. For these reasons the Z2highK variant is not considered calibrated or included in the sensitivity variants. As already discussed in Subsection 4.4, the implication is that the central band of Zone 2 must act as a barrier to vertical flow on the regional scale. The value of $1 \cdot 10^{-9} \text{ms}^{-1}$ for the effective hydraulic conductivity across Zone 2 is only speculative given the coarseness of the grid, but certainly it must be much less than that of rock mass to obtain a calibrated model.

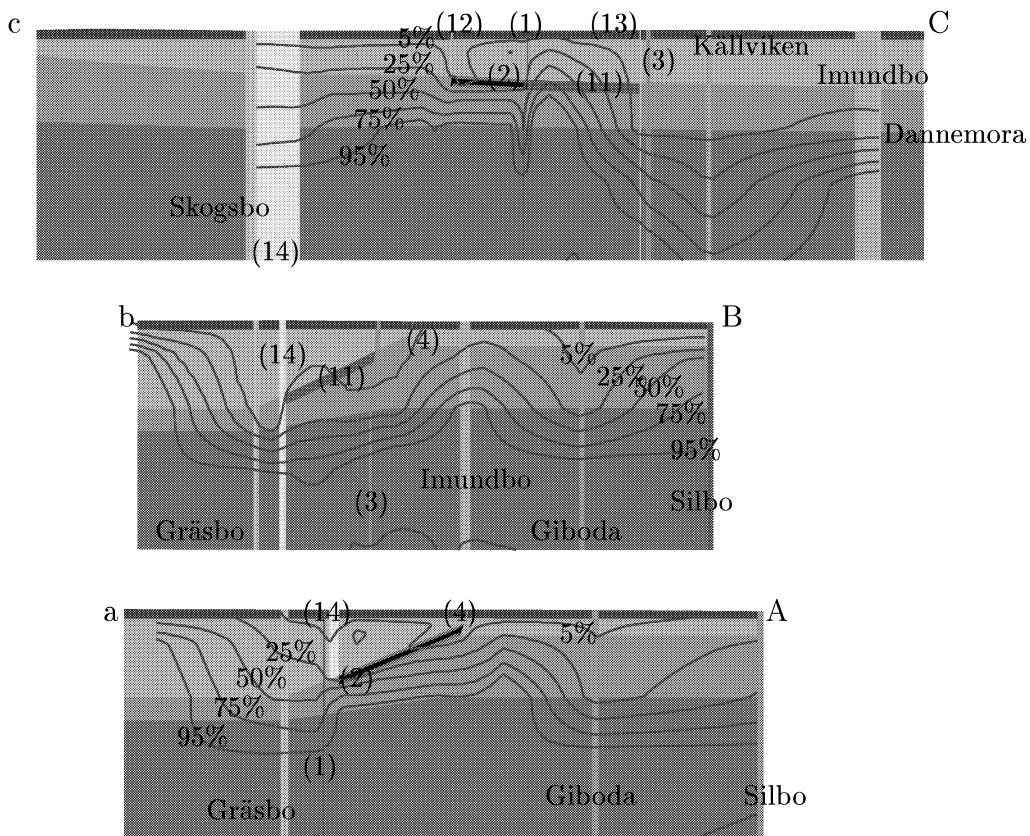


Figure 5.6: salinity on vertical slices along a-A, b-B, c-C (see Figure 4.2) for Z2highK variant. The contours of salinity shown correspond to 5%, 25%, 50%, 75% and 95% of the maximum salinity (corresponding to 6,500mg/l). Note the vertical scale is exaggerated by a factor of 2.

5.3.4 Lower contrast between Rock Mass and Fracture Zones (ZlowK + ZlowK ϕ)

The assumption that all lineaments are conductive fracture zones is highly uncertain. In general, the properties given in [Walker *et al.*, 1997] are extrapolated from tests carried out in lineaments with similar tectonic origin and orientation. The variant ZlowK is considered in order to evaluate the sensitivity to the contrast in hydraulic conductivity between the rock mass and fracture zones. The hydraulic conductivity of each fracture zone, except Zone 2, is a factor of 30 (1.5 orders of magnitude) down on the base case. This gives a contrast similar to that used in SKB 91. All other properties are identical to the base case.

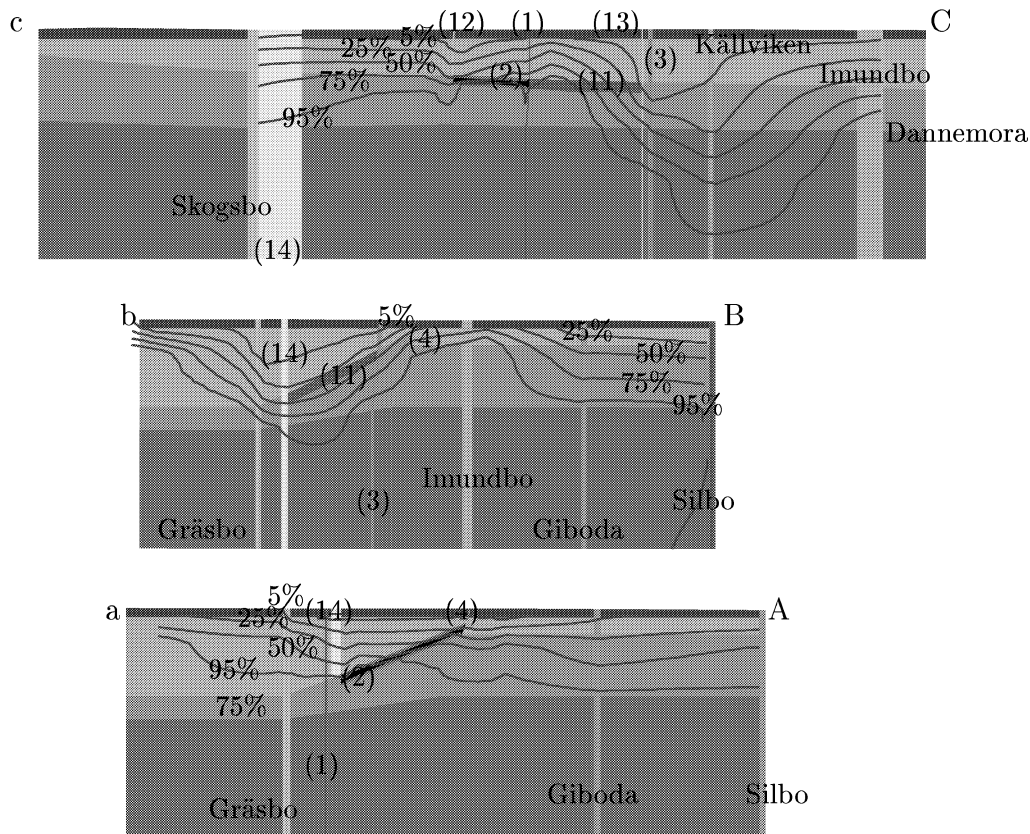


Figure 5.7: Salinity on vertical slices along a-A, b-B, c-C (see Figure 4.2) for ZlowK variant. The contours of salinity shown correspond to 5%, 25%, 50%, 75% and 95% of the maximum salinity (corresponding to 6,500mg/l). Note the vertical scale is exaggerated by a factor of 2.

salinity contours for ZlowK are shown in Figure 5.7. Clearly the salinity pattern is drastically different to the base case. Salinity is very shallow, suggesting that insufficient time has elapsed for fresh water to infiltrate to depth. It demonstrates how strongly dependent the transient evolution of salinity is on the transmissivity of the fracture

zones. Obviously this variant is not consistent with reality. In order to improve the calibration a second variant $ZlowK\phi$ is considered in which the porosity of the fracture zones is halved to 2.5%, and that of the rock mass to 1%. Since the time-scale for salt to evolve is proportional to porosity, this variant should give a more realistic salinity profile. The result is shown in Figure 5.8.

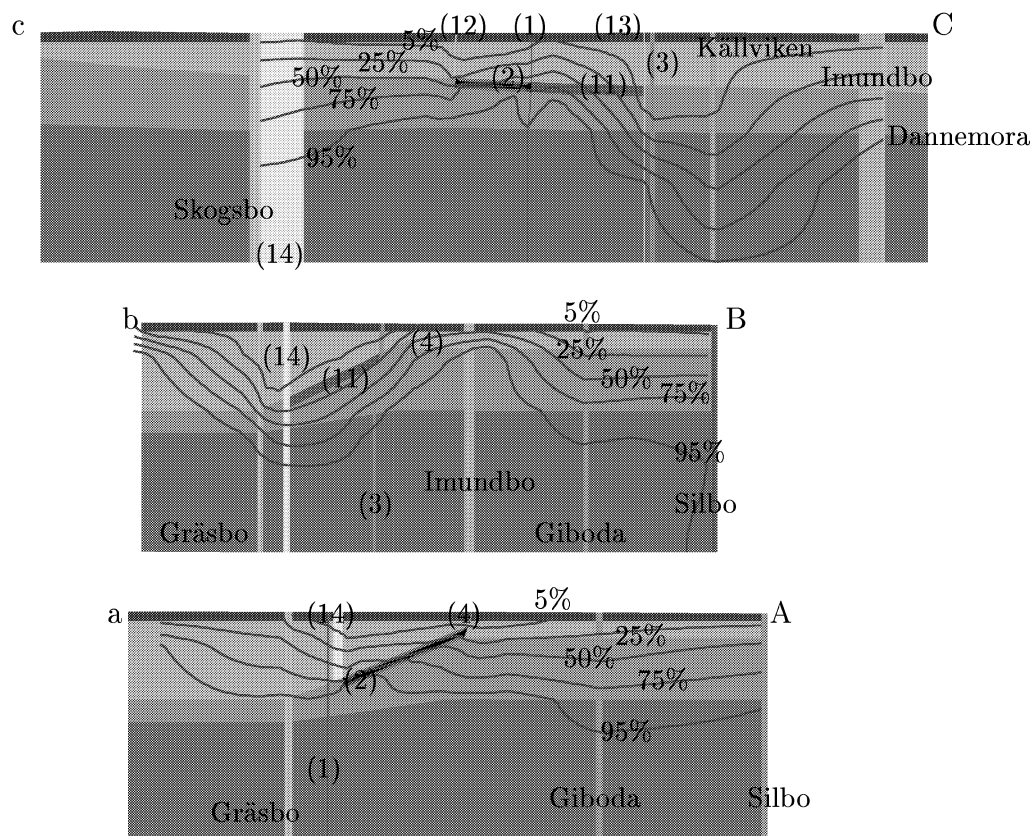


Figure 5.8: Salinity on vertical slices along a-A, b-B, c-C (see Figure 4.2) for $ZlowK\phi$ variant. The contours of salinity shown correspond to 5%, 25%, 50%, 75% and 95% of the maximum salinity (corresponding to 6,500mg/l). Note the vertical scale is exaggerated by a factor of 2.

Salinity is now much shallower, especially around Zones 2 and 11, but there is still significant salinity above Zone 2 and below Zone 11. Hence, the variant is not as well calibrated as the base case. However, since the regional scale salinity is substantially different to the base case, this variant provides an interesting test of the sensitivity of groundwater pathways to the salinity distribution.

5.3.5 Inclusion of Zone 11 in Southern Rock Block (Z11)

Zone 11 is not included in the base case model as a transmissive fracture zone. This is mainly due to the difficulty in representing the complex geometry of the local scale zones. The effects of a transmissive sub-horizontal feature in the southern rock block

are evaluated by changing the properties in a set of finite-elements adjacent to Zone 2. These elements have the appropriate thickness, 100m, but only dip at 16SW rather than the true dip of 35SW for Zone 11. Hence, the representation of Zone 11 is only notional. The hydraulic conductivity for Zone 11 is $9.6 \cdot 10^{-7} \text{ms}^{-1}$ [Walker *et al.*, 1997]. The rest around : ary localised y variant to investiga

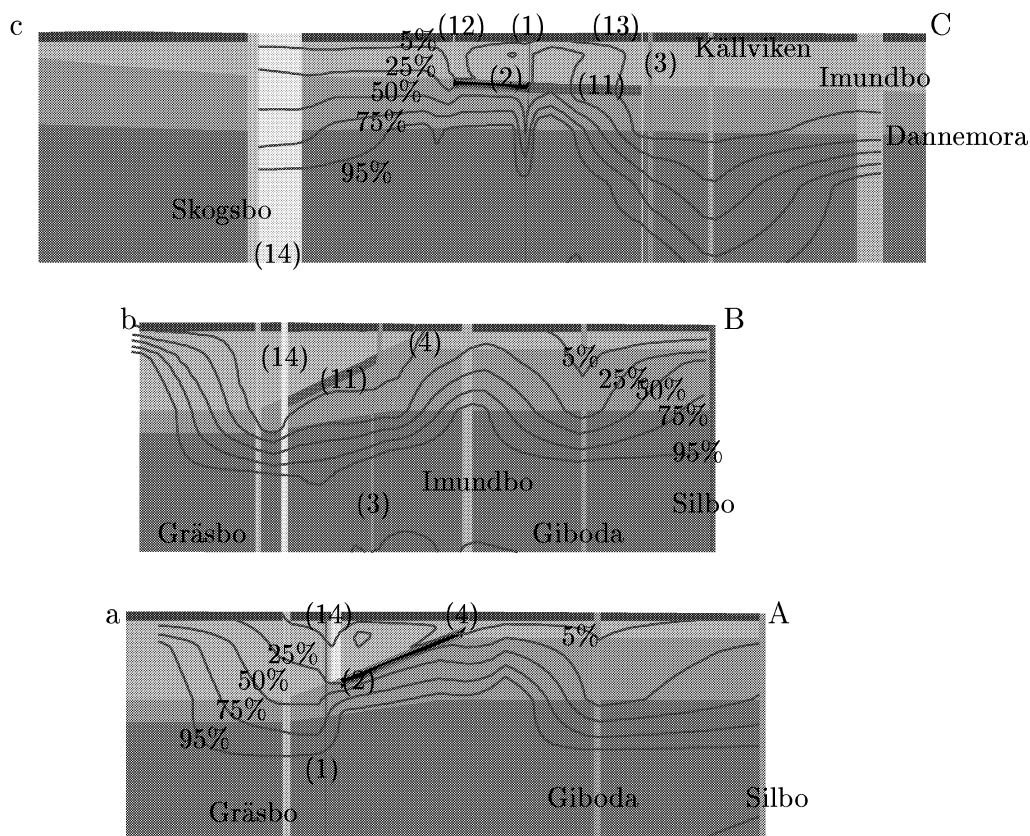


Figure 5.9: Salinity on vertical slices along a-A, b-B, c-C (see Figure 4.2) for Z11 variant. The contours of salinity shown correspond to 5%, 25%, 50%, 75% and 95% of the maximum salinity (corresponding to 6,500mg/l). Note the vertical scale is exaggerated by a factor of 2.

5.3.6 Specified Salinity on Upstream Boundary (Csouth)

Of the boundary conditions specified, the salinity on the southern boundary is the most uncertain. This is because groundwater is allowed to flow in at this boundary (pressure is specified as hydrostatic), but the salinity of this groundwater is poorly understood. In the base case the boundary condition is for an advective inflow of salinity equal to the instantaneous value of salinity on the boundary. The results

suggest this boundary condition leads to high levels of salinity south of the Finnsjön site. It is unclear whether this is realistic. Hence, it is important that the sensitivity of results to the salinity boundary condition in the south be quantified.

The C_{south} variant has a specified salinity on the southern boundary. The salt mass fraction variable c varies linearly with depth from 0 (fresh) at the surface to 1 (a salinity of 0.8%) at -750masl, and is equal to 1 down to the base. Salinity is also held constant in time in the south. Comparing with Subsection 2.5.2, rather than specifying the flux of salt F_c , we specify the salinity

$$c(\mathbf{x}, t) = c(z).$$

Figure 5.10 shows the results for the C_{south} variant. The only significant difference is that the saline transition zone is more diffuse south of Gräsbo. Salinity is unaffected around the Finnsjön rock block. Therefore, C_{south} is included in the sensitivity variants.

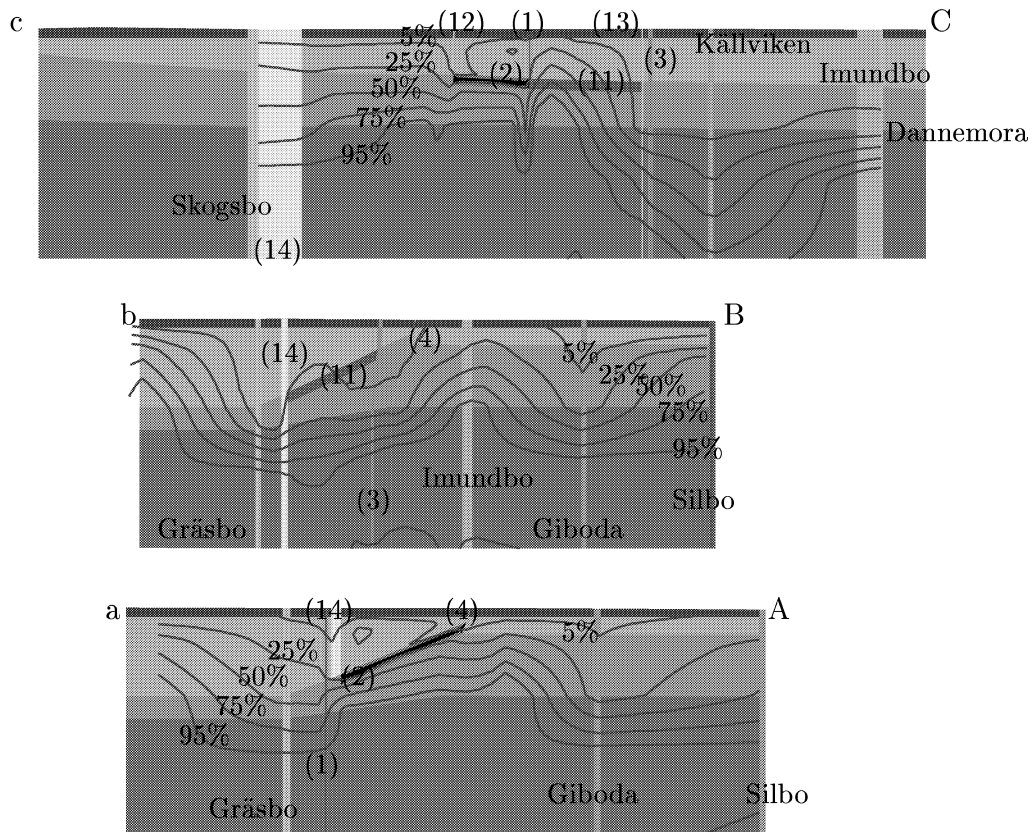


Figure 5.10: Salinity on vertical slices along a-A, b-B, c-C (see Figure 4.2) for C_{south} variant. The contours of salinity shown correspond to 5%, 25%, 50%, 75% and 95% of the maximum salinity (corresponding to 6,500mg/l). Note the vertical scale is exaggerated by a factor of 2.

5.3.7 Lower Porosity (ϕ_{low})

The total porosity is one of the key parameters to calibrate since it determines the rate at which the salinity pattern evolves. In order to show the effect of porosity the ϕ_{low} variant is presented. Here the porosity is halved to 1% for the rock mass and 2.5% for the fracture zones. These values are well within the possible range [*Brandberg and Skagius, 1991*]. Since the time-scale for the transport of salt is proportional to the total porosity, salinity evolves twice as rapidly for the ϕ_{low} variant. Alternatively, the results can be considered equivalent to running the base case for 8,000 years. That is, up until 4,000 years AP.

The results are shown in Figure 5.11. Salinity is now considerably deeper. In most regions, salinity is not encountered until the base layer at about -1kmasl. There is however still salinity below Zone 2, but the saline transition zone is more diffuse than for the base case. Although this variant provides a useful insight into how salinity might evolve in the future, it's prediction of the present day situation is not considered to be consistent with the data. Hence, it is not used as a sensitivity variant.

It is concluded that a total porosity of about 2% for the rock mass and 5% for the fracture zones are the calibrated values. However, as was demonstrated in the ZlowK variant, the calibration of total porosity is sensitive to the hydraulic conductivity of the fracture zones.

5.3.8 Lower Dispersion Length (Dlow)

Another uncertain property that had to be calibrated is the hydrodynamic dispersion length. For the base case, values of longitudinal and transverse dispersion lengths were guessed at 80m and 40m, respectively. Generally, dispersion tends to increase the thickness of the saline transition zone. This can also result in a change in the position of the saline transition zone, as fresh groundwater can penetrate to greater depths for a diffuse saline transition zone.

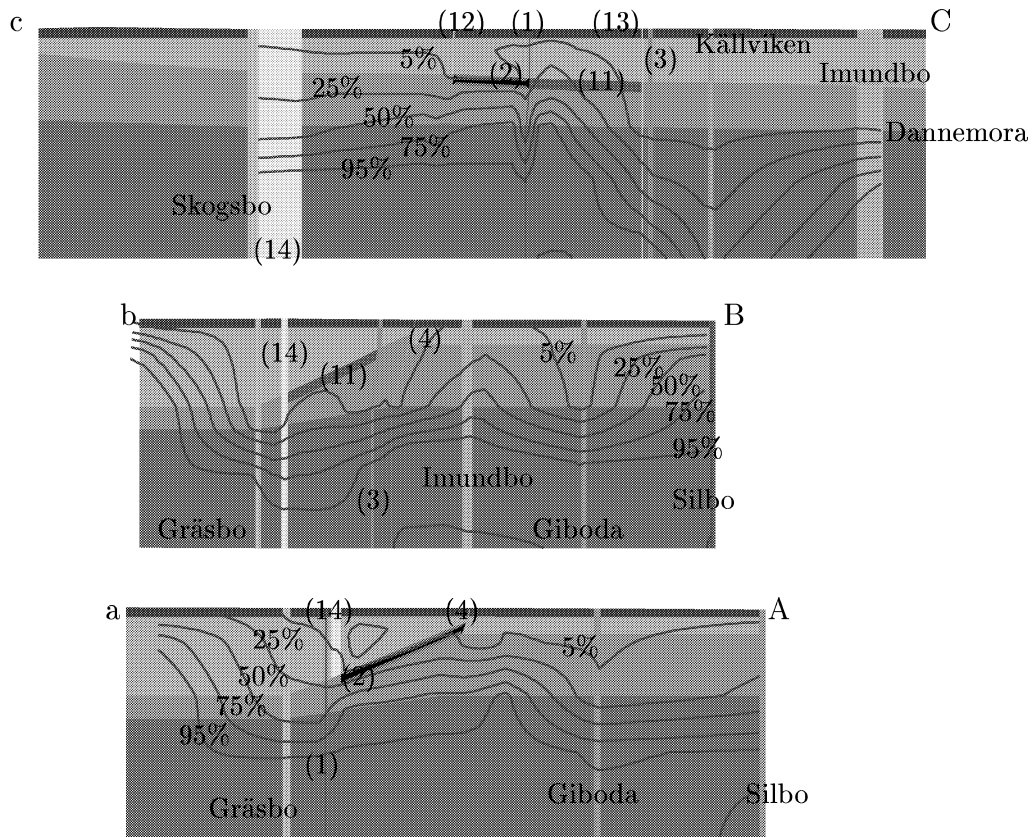


Figure 5.11: Salinity on vertical slices along a-A, b-B, c-C (see Figure 4.2) for ϕ low variant. The contours of salinity shown correspond to 5%, 25%, 50%, 75% and 95% of the maximum salinity (corresponding to 6,500mg/l). Note the vertical scale is exaggerated by a factor of 2.

Given the coarse grid it is not possible to represent very sharp transition zones, and so there is also a numerical component to dispersion due to the interpolation of salinity over the finite-elements. However, it is important to scope how dependent our results are on the choice of values for dispersion. The results for the Dlow variant are presented in Figure 5.12. The longitudinal and transverse dispersion lengths were set to 40m and 20m, respectively, in Dlow.

The results do not appear to be very sensitive to this parameter. There is a slight rise in salinity in the rock mass above Zone 2, which reduces the quality of the calibration. Dlow is included amongst the sensitivity variants to check if groundwater pathways are sensitive to salt dispersion.

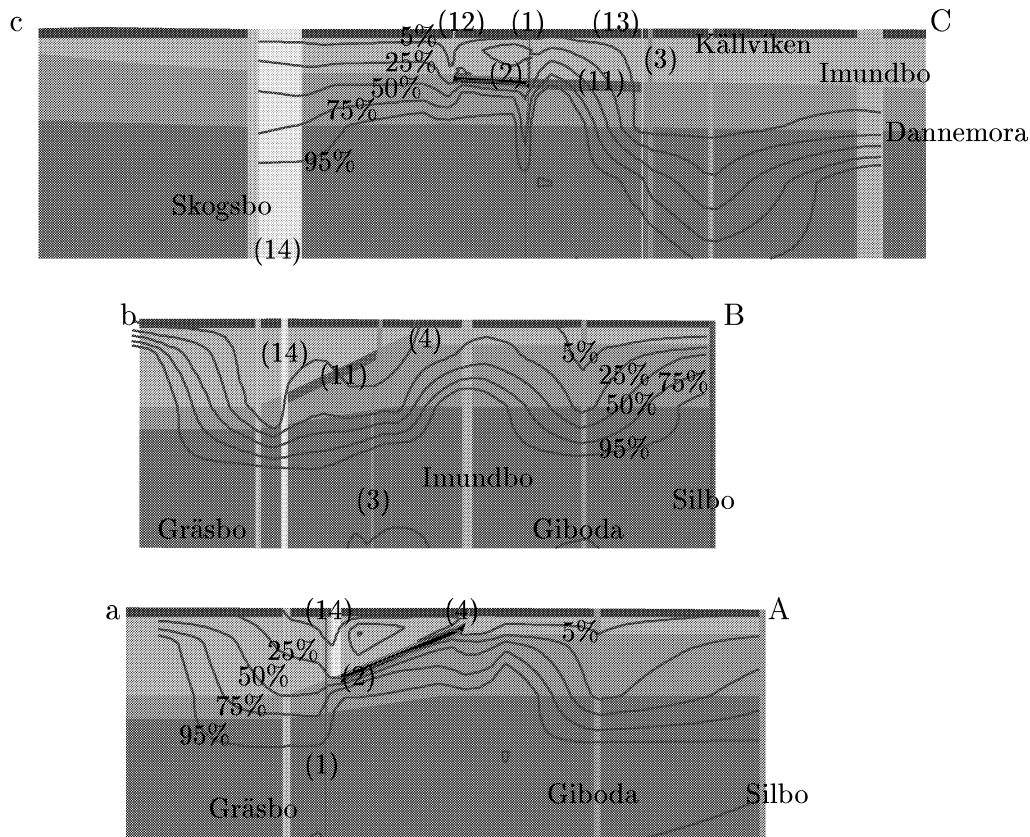


Figure 5.12: Salinity on vertical slices along a-A, b-B, c-C (see Figure 4.2) for Dlow variant. The contours of salinity shown correspond to 5%, 25%, 50%, 75% and 95% of the maximum salinity (corresponding to 6,500mg/l). Note the vertical scale is exaggerated by a factor of 2.

5.3.9 Implicit Inclusion of Local Fracture Zones (Zlocal)

Only Zones 2 and 11 of the local zones are included in the base case. However, there are several additional lineaments expressed in the Finnsjön rock block (see Figure 3.5). The widths and hydraulic conductivities [Walker *et al.*, 1997] are given in Table 5.2. All of these zones trend NW-SE and are near vertical.

Generally these zones have a lower transmissivity than the regional fracture zones, so they are unlikely to effect the large scale groundwater flow pattern. This is the justification for leaving them out of the base case. However, they may effect flow and salinity within the Finnsjön rock block. Much effort would be necessary to include each of zone explicitly within the existing grid. An alternative approach is to include the effect of the zones by representing them implicitly. This is achieved by calculating the effective hydraulic conductivity for Finnsjön rock block based on the combined properties of the each fracture zone and the rock mass between. For example, the effective hydraulic conductivity parallel to the local zones (NW-SE and vertical) is calculated as an arithmetic mean of the hydraulic conductivity for the zones and rock mass, with weights

Table 5.2: Local fracture zones represented implicitly in the Zlocal variant.

Zone	Width (m)	Hydraulic conductivity (ms ⁻¹)
5	5	6.9 10 ⁻⁶ ms ⁻¹
6	5	6.5 10 ⁻⁸ ms ⁻¹
7	5	6.3 10 ⁻⁷ ms ⁻¹
8	5	6.3 10 ⁻⁷ ms ⁻¹
10	5	3.2 10 ⁻⁸ ms ⁻¹

proportional to thicknesses of the zones and rock mass. In the direction orthogonal to the zones a weighted harmonic mean is used (see [*de Marsily, 1981*], for example). This results in an anisotropic effective permeability for the Finnsjön block. Because the local fractures trend NW-SE and are near vertical the principal directions for hydraulic conductivity are NW-SE and vertical, with the minor component SW-NE. The diagonal hydraulic conductivity tensor is first calculated relative to the principal directions and then a rotation operator is applied to map the tensor to the RAK coordinate system, which results in non-zero off-diagonal components in this anisotropic case.

Table 5.3: Hydraulic conductivities used in the Zlocal variant.

Hydrogeological unit	Hydraulic conductivity			
	KXX (ms ⁻¹)	KYY (ms ⁻¹)	KXY (ms ⁻¹)	KZZ (ms ⁻¹)
Near Surface	1.7 10 ⁻⁷	1.7 10 ⁻⁷	1.4 10 ⁻⁸	1.8 10 ⁻⁷
Above Zone 2	2.7 10 ⁻⁸	2.7 10 ⁻⁸	1.4 10 ⁻⁸	4.1 10 ⁻⁸
Below Zone 2	3.0 10 ⁻⁸	3.0 10 ⁻⁸	1.4 10 ⁻⁸	4.4 10 ⁻⁸

Table 5.3 presents the values used for the full anisotropic tensor in the northern and southern rock blocks. KXX is the hydraulic conductivity in the E-W direction, KYY is the component in the N-S direction, and KZZ is the vertical component. KXY is the horizontal off-diagonal component. The fractures zones have little effect on the overall hydraulic conductivity in the near surface, but result in an anisotropy ratio of 4:1 in the intermediate layer (-50masl to -850masl). The hydraulic conductivity of the base layer was not adjusted since it is uncertain whether the local zones extend to large depths.

The results for the Zlocal variant are shown in Figures 5.13. As expected, the effects are localised to the Finnsjön rock block. There is noticeably less salinity above Zones 2 and 11, which suggests this variant may be better calibrated than the base case. Hence, it is included in the sensitivity variants.

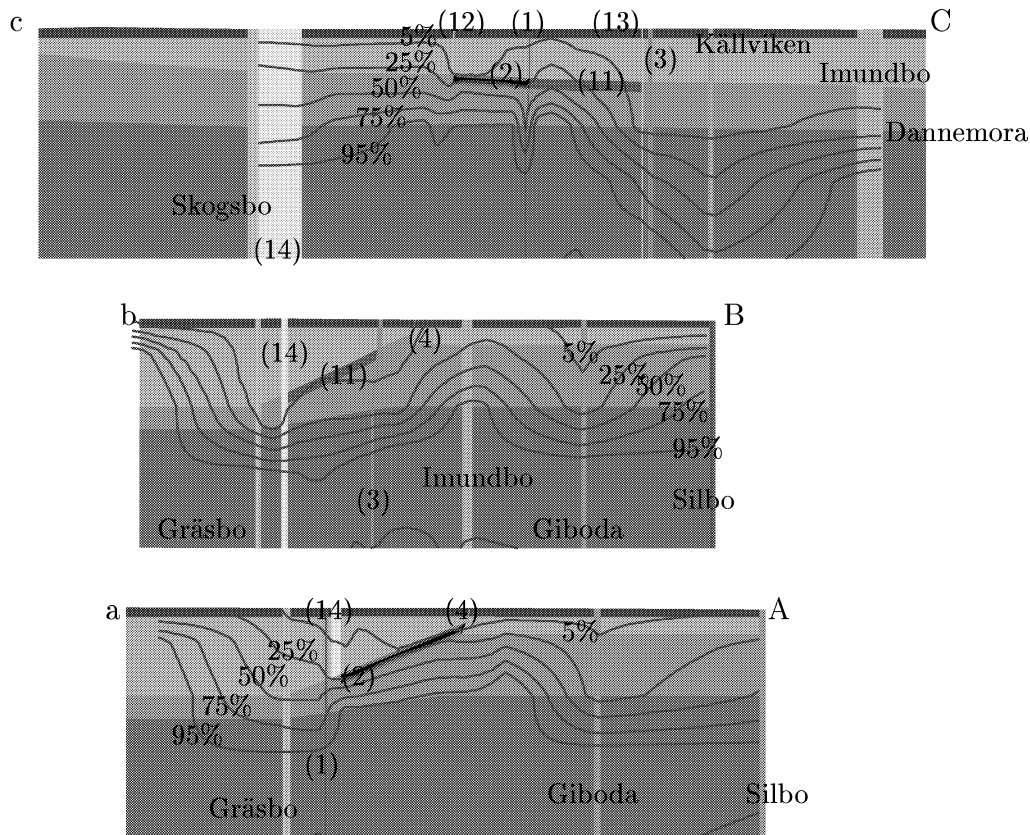


Figure 5.13: Salinity on vertical slices along a-A, b-B, c-C (see Figure 4.2) for Zlocal variant. The contours of salinity shown correspond to 5%, 25%, 50%, 75% and 95% of the maximum salinity (corresponding to 6,500mg/l). Note the vertical scale is exaggerated by a factor of 2.

5.3.10 Horizontal Anisotropy (RRD3)

The next variant examines the effects of anisotropy in the rock mass. This variant is the RRD3 case recommended by Walker et al. [1997] and later clarified [Walker, 1998]. Fracture mappings at the site, and on the regional scale, have indicated a trend in fracture orientation toward northwest-southeast. It is suggested that this will lead to anisotropy with the major axis aligned with the dominant fracture orientation. Further, this alignment is consistent with the direction of maximum horizontal rock stress in the region, N 48 W. Carlsson et al. [1986] proposed a degree of anisotropy in the horizontal hydraulic conductivity of 10:1:1 (horizontal major: horizontal minor: vertical) for SFR studies. The same ratio is used here. Under idealised conditions, the apparent isotropic conductivity K_a can be shown to be the geometric mean of the components of the anisotropic tensor of K [de Marsily, 1981 1998]. If we assume that the upscaled, normalised geometric mean of the 3m packer tests is K_a , we can use the anisotropy ratio to determine the components of the tensor. This yields $4.64K_a:0.464K_a:0.464K_a$. For the K_a is taken as the isotropic value used for the rock mass in the base case. Properties for the regional fracture zones are unchanged. It is important to note that

the major axis of hydraulic conductivity is orthogonal to the general regional hydraulic gradient.

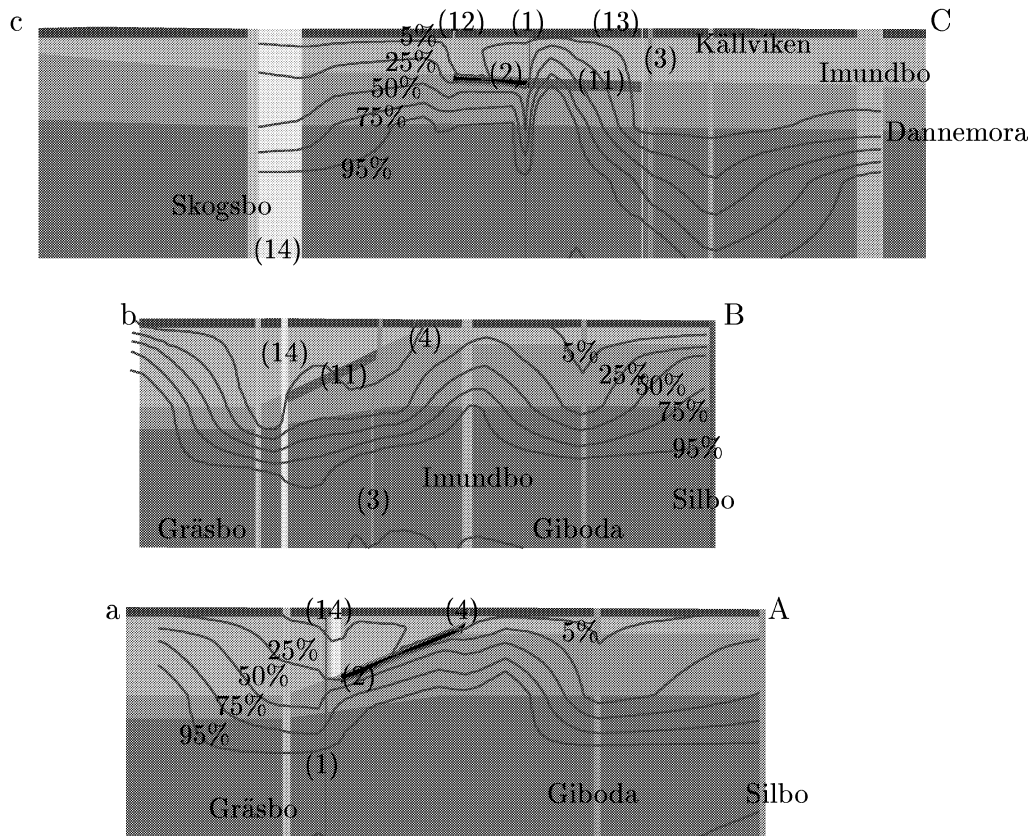


Figure 5.14: Salinity on vertical slices along a-A, b-B, c-C (see Figure 4.2) for RRD3 variant. The contours of salinity shown correspond to 5%, 25%, 50%, 75% and 95% of the maximum salinity (corresponding to 6,500mg/l). Note the vertical scale is exaggerated by a factor of 2.

The profiles of salinity are broadly similar to the base case, although the saline transition zone is slightly higher in the southern rock block. This is presumably due to reduced transport of salinity in the direction of the regional hydraulic gradient to the northeast. This case is considered amongst the sensitivity variants.

5.3.11 Hydraulic Conductivity in fracture Zones (AltK)

An additional variant has been suggested by Walker [1998] to address the conceptual uncertainty associated with the structural model for the fracture zones. The base case model for the fracture zones, RCD1, proposed that the hydraulic conductivity of the fracture zones be constant with depth. However, Subsection 4.4 concludes that the hydraulic connection to the subsurface is over-predicted if fracture zones have a constant hydraulic conductivity below the top of Zone 2. Further, in order to calibrate

RCD1 it is necessary that several vertical fracture zones adjacent to the northern rock block are terminated before connecting with Zone 2 (about -200 to -500masl).

Rather than terminate the fracture zones, their hydraulic conductivity may decrease with depth similar to the rock mass, as suggested in the alternative model RCD2. This may have the same effect of reducing freshwater recharge into Zone 2, without implying that the vertical fractures terminate abruptly. Such a conclusion is similar to that of Andersson et al. [1991].

Table 5.4: Hydraulic conductivities for the AltK variant. The same inference between zones is applied as for [Walker et al., 1997]

	Log(hydraulic conductivity)	
	(ms ⁻¹)	(ms ⁻¹)
RCD2	0 to -100masl	< -100masl
Zone		
1,13,Källviken	-4.33	-5.42
2		-4.50
3	-5.63	-6.72
4,Imundbo,Giboda, Skogbo	-3.90	-4.99
Singö,12,14, etc.	-4.91	-6.00
VAR(Log(K))	0.29	0.29
RRD1	-6.81	-7.90
VAR(Log(K))	0.21	0.086

To assess this possibility an alternative conceptual model (AltK) of the fracture zones is considered [Walker, 1998] with depth dependent hydraulic conductivity. This required a re-interpretation of the hydraulic data for the fracture zones. The median hydraulic conductivity of each fracture zone is generally measured from a single borehole intercept, and therefore the median value reported in [Walker et al., 1997] represents a single depth. To apply the stepwise relative changes in hydraulic conductivity, the measurements were indexed to their median depth then stepped up or down as necessary. That is, measurements taken near the surface are stepped downward to produce a decrease with depth, while measurements taken at depth are stepped upward with increasing elevation. Because there is little difference between -100masl (see Figure 3.3), both RRD1 and RCD2 may be simplified to only two zones by taking the weighted arithmetic average of zones below -100masl. The hydraulic conductivities prescribed by Walker [1998] for AltK are summarised in Table 5.4.

The significant changes between this interpretation and the base case are:

- the transmissivity of Zone 1 is less than those inferred from Zone 5 (Imundbo, Giboda, 4, Skogbo). In the base case Zone 1 was the dominant hydraulic feature;
- Although the fracture zones are still more conductive than the rock mass, the contrast is less below -100masl. Below this depth, typically the fracture zone conductivity is reduced by about one order of magnitude, which is sufficient for the

transmissivity of the fracture zones and rock to become comparable. Therefore, less freshwater penetrates below Zone 2;

- Zone 2 is more conductive by about half an order of magnitude.

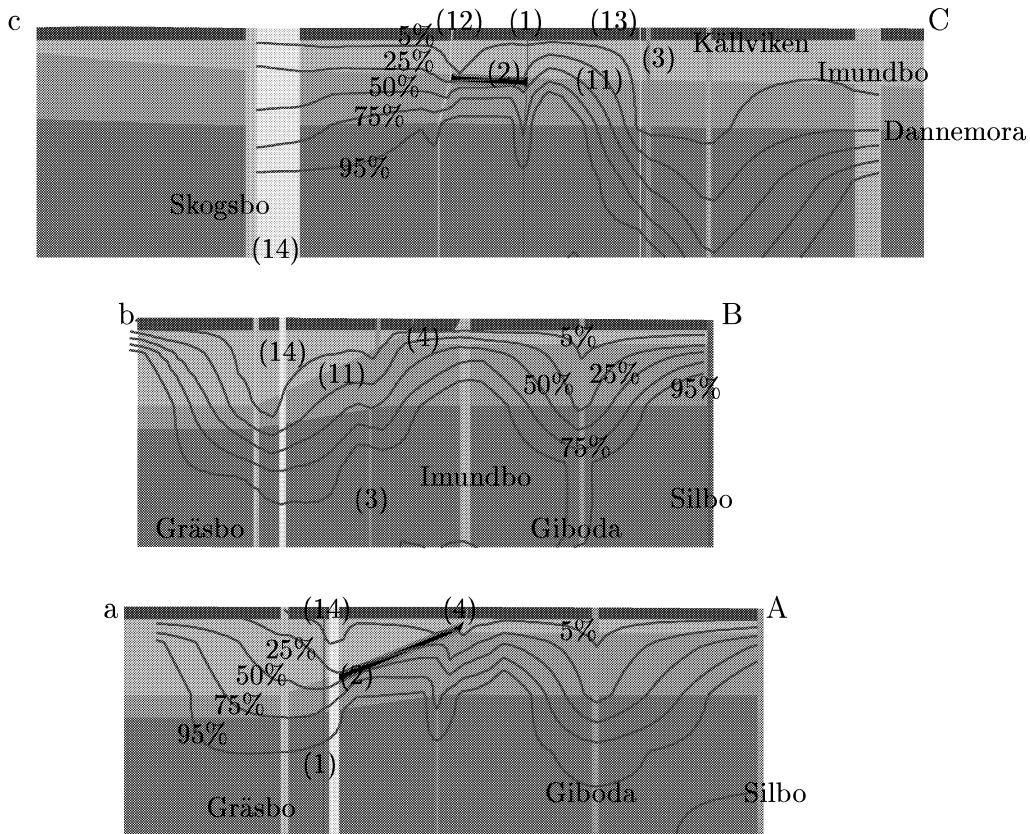


Figure 5.15: Salinity on vertical slices along a-A, b-B, c-C (see Figure 4.2) for AltK variant. The contours of salinity shown correspond to 5%, 25%, 50%, 75% and 95% of the maximum salinity (corresponding to 6,500mg/l). Note the vertical scale is exaggerated by a factor of 2.

As with the RCD1 model, some difficulties are encountered due to the large contrast in hydraulic conductivity persisting to the base of the model at -2000masl. Although the fracture zone conductivity is reduced, there is still a rapid intrusion of freshwater in the zones in the rock mass. This creates problems for both the calibration and numerics. For this reason two minor modifications are made to the AltK model in the lower finite-elements below -850masl:

1. the hydraulic conductivity for the rock mass is reduced to $6 \cdot 10^{-9} \text{ms}^{-1}$ for the rock mass, as for the base case, rather than $1.2 \cdot 10^{-8} \text{ms}^{-1}$;
2. the hydraulic conductivity of fracture zones based on Zone 5 (4, Imundbo, Giboda, Skogbo) is reduced to that of Singö, $1.0 \cdot 10^{-6} \text{ms}^{-1}$.

These modifications make AltK more comparable with the base case below -850masl, but are within the prescribed confidence limits in Table 5.4. The change to the rock mass is within one standard deviation. The change to fracture Zone 4, Imundbo, Giboda, Skogbo are within two standard deviations.

Salinity profiles for AltK are shown in Figure 5.15. This case needs to be compared with the base case (Figure 5.1) and the Zdeep variant (Figure 5.3). Comparing with the base case, salinity is generally deeper around the fracture zones, but there still high levels of salinity below Zone 2. Although the zones around the edge of the northern rock block (Zones 4, 14 and 12) lower the saline transition zone, the effects are not as dramatic as the Zdeep variant, and the variant calibrates. The fact that AltK calibrates suggests that it is only important that the fracture zones are of similar or less transmissivity than the rock mass below Zone 2, and that Zone 2 is the dominant hydrogeological feature.

6 LOCATION OF SITE SCALE MODEL

The two remaining objectives are to identify the locations of recharge and discharge areas relevant to a hypothetical repository below Zone 2, and on the basis of this locate a site scale model. In Subsection 6.1 we present the groundwater pathways and travel times for each of the sensitivity variants. The implications of these results and their sensitivities are summarised in Subsection 6.2. In addition to locating the local scale model, we also have to provide boundary conditions for a constant density stochastic continuum model. This issue is discussed in Subsection 6.3.

6.1 Groundwater Flow Pathways at Repository Level

The location and extent of a site scale model is guided by a set of pathlines starting at the hypothetical location of a repository. Pathlines show the advective transport of a tracer moving at the pore water velocity (forward pathlines). By mapping the positions where pathlines exit the boundaries of the model, discharge areas can be identified. Similarly, by calculating pathlines moving upstream or backwards in time (backward pathlines) areas of recharge relevant to the hypothetical repository can be identified.

6.1.1 Base Case

Figure 6.1 shows forward and backward pathlines seen from two projections. Firstly, on a plan view, and as viewed from the east. In the latter case, the pathlines are superimposed on the vertical section b-B to act as a reference. Pathlines are started at a depth of $z = -600\text{m}$ within the northern rock block. A flowing porosity of $1.0 \cdot 10^{-4}$ is used for all rocks. This is just a nominal value which has been used throughout the regional scale studies of SR 97.

The important features for flow appear to be Zone 1 and Imundbo. All forward pathlines go to the north east. Pathlines starting in the west move downwards and stay at depth beneath the saline transition zone, eventually intercepting either Imundbo or Zone 1. Several pathlines starting in the east move horizontally along Zone 1 and then discharge around the intersect with Imundbo. Some paths exit the northern vertical boundary at depth suggesting very long pathlengths. Note that some of the longer pathlines have been terminated before they reach a point on the boundary. These are deep paths and have long travel times of many hundreds of years. The paths are terminated in a relatively stagnant region within Giboda. Travel times for forward paths vary between 10 to 882 years. The shortest time is for pathlines starting in the east near Zone 4. The longest is for pathlines starting in the west. These times are notional as they are based on a very low flowing porosity of $1.0 \cdot 10^{-4}$. Note that travel times are directly proportional to flowing porosity.

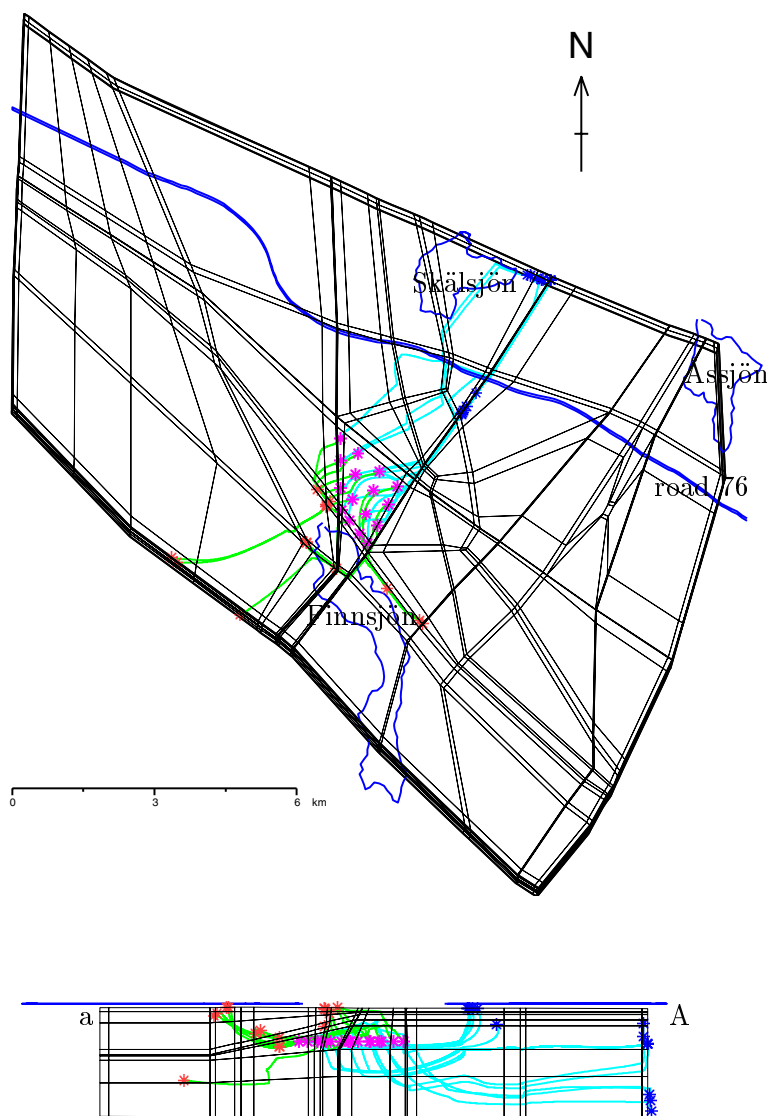


Figure 6.1: Forward (blue) and backward (green) pathlines for the base case model. A set of 16 pathlines are started from the northern block at a depth of $z = -600\text{m}$. Points of origin, discharge and recharge for each path are shown by an asterisk coloured pink, purple and orange, respectively.

Recharge areas for the northern rock block are very localised. Mostly they are around Zone 4 or Gräsbo, just south of the site. A single backward pathline suggests recharge from the low ridge to the south west may also be important. The travel time for backward pathlines is also of interest, since it gives us an indication of the residence time for water at repository depth to be replaced by water infiltrating from the environment. For a flowing porosity of $1.0 \cdot 10^{-4}$ it varies between 10 and 100 years. However, since we are interested in the time for the total water volume to be replenished then the total porosity ($\approx 10^{-2}$) should be used. Hence, the groundwater residence time is about 1,000 to 10,000 years.

6.1.2 Sensitivities

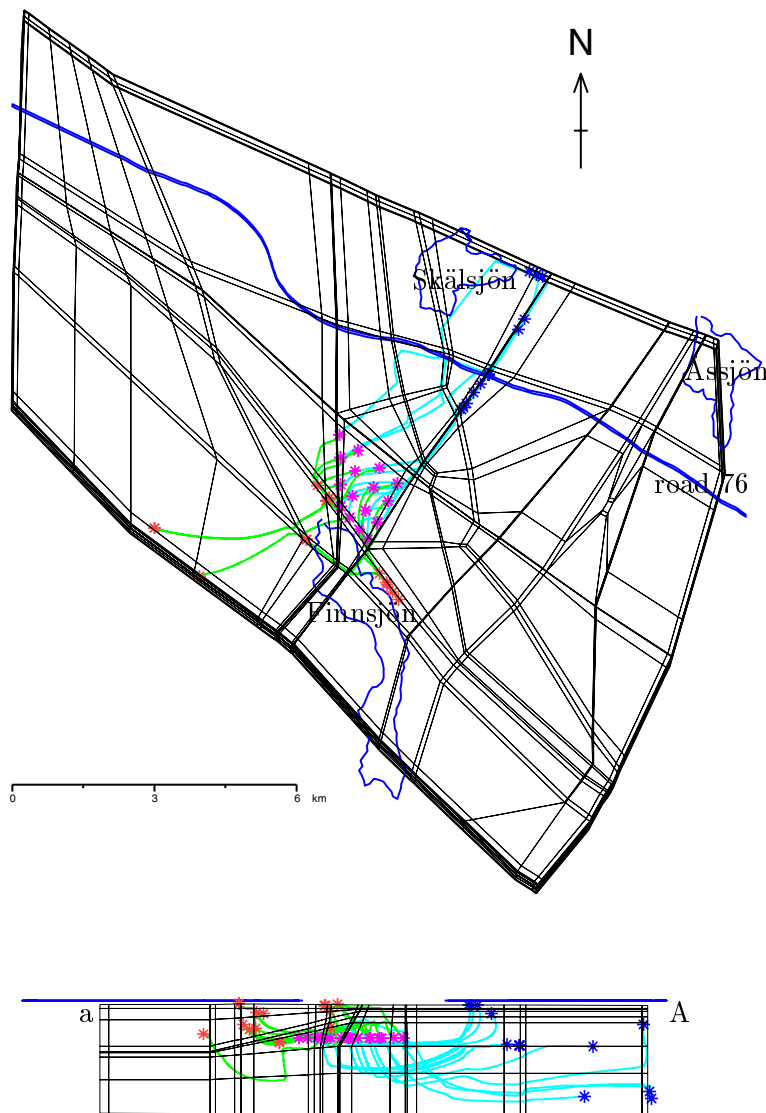


Figure 6.2: Forward (blue) and backward (green) pathlines for the Zsouth variant. A set of 16 pathlines are started from the northern block at a depth of $z = -600\text{m}$. Points of origin, discharge and recharge for each path are shown by an asterisk coloured pink, purple and orange, respectively.

In this section we investigate the sensitivity of the groundwater pathways. Only the calibrated or ‘sensitivity variants’ identified in Table 5.1 are considered.

Pathlines for the Zsouth variant are given in Figure 6.2. There is very little difference, suggesting that the results are relatively insensitive to the properties of the two additional fracture zones in the south. This is a consequence of the very localised recharge from Zone 4. Travel times vary between 10 and 765 years.

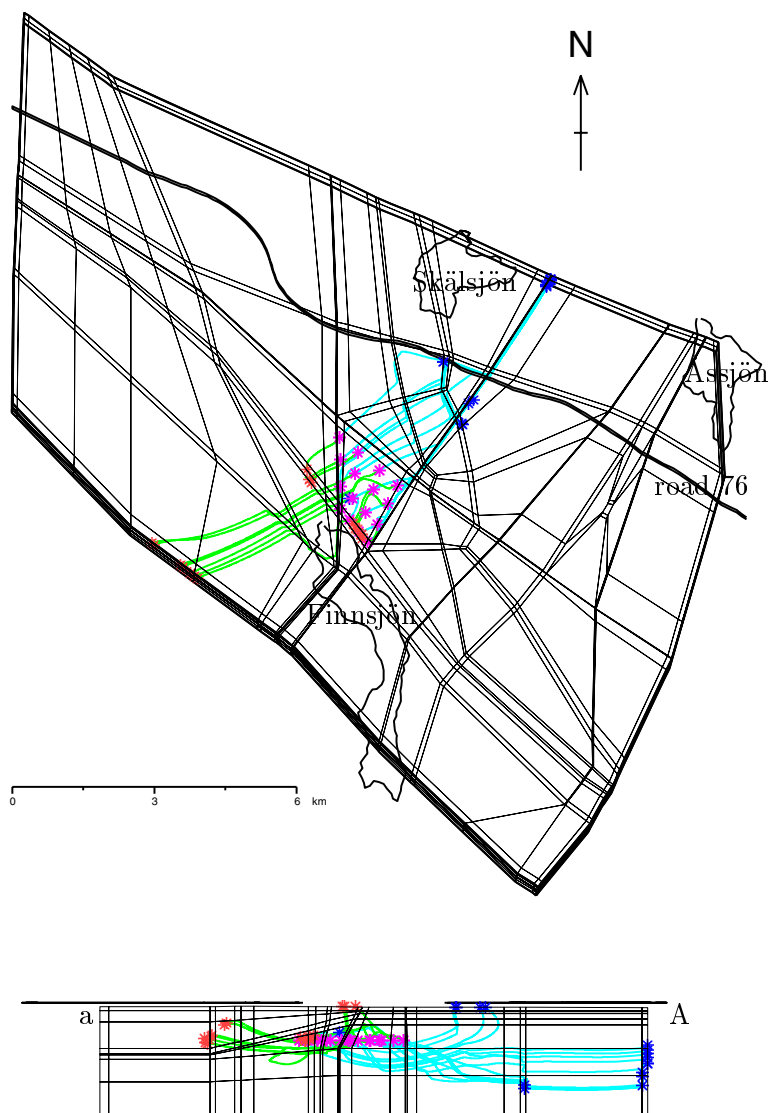


Figure 6.3: Forward (blue) and backward (green) pathlines for the ZlowK ϕ variant. A set of 16 pathlines are started from the northern block at a depth of $z = -600\text{m}$. Points of origin, discharge and recharge for each path are shown by an asterisk coloured pink, purple and orange, respectively.

The contrast in hydraulic conductivity between fracture zones and rock mass has much greater influence, as seen in Figure 6.3. This shows pathlines for the ZlowK ϕ variant. A greater number of pathlines pass through the rock mass to the north east rather than along Zone 1. Recharge from the low ridge to the south west has also become more important, although there is still substantial recharge locally from Zone 4. These

changes are a consequence of the reduced importance of the fracture zones. Travel times vary between 2 and 930 years.

Pathlines for the Z11 variant are shown in Figure 6.4. These are very similar to the base case. Hence, it can be concluded that Zone 11 is not a significant groundwater pathway for a hypothetical repository below Zone 2. The predominant direction for flow is north east and Zone 1 acts as a conduit for flow along the eastern edge of the hypothetical repository. Hence, there is effectively no flow from the northern to southern rock block. Travel times for Z11 vary between 10 to 876 years.

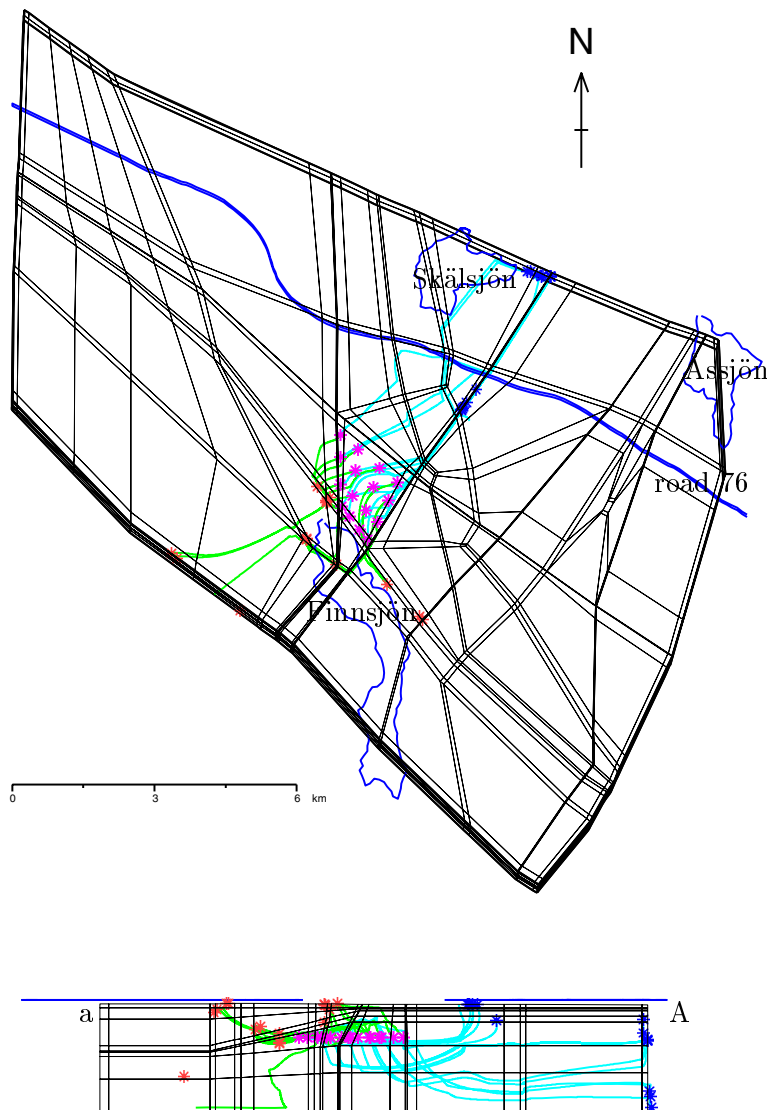


Figure 6.4: Forward (blue) and backward (green) pathlines for the Z11 variant. A set of 16 pathlines are started from the northern block at a depth of $z = -600\text{m}$. Points of origin, discharge and recharge for each path are shown by an asterisk coloured pink, purple and orange, respectively.

Again there is little change for the Csouth variant shown in Figure 6.5. There is one extra backward pathline from the low ridge to the south west, and an extra long forward pathline at depth. The results reinforce the conclusion that Zone 4 is the predominant feature affecting the upstream conditions at the hypothetical repository position. Travel times for Csouth vary between 10 and 763 years.

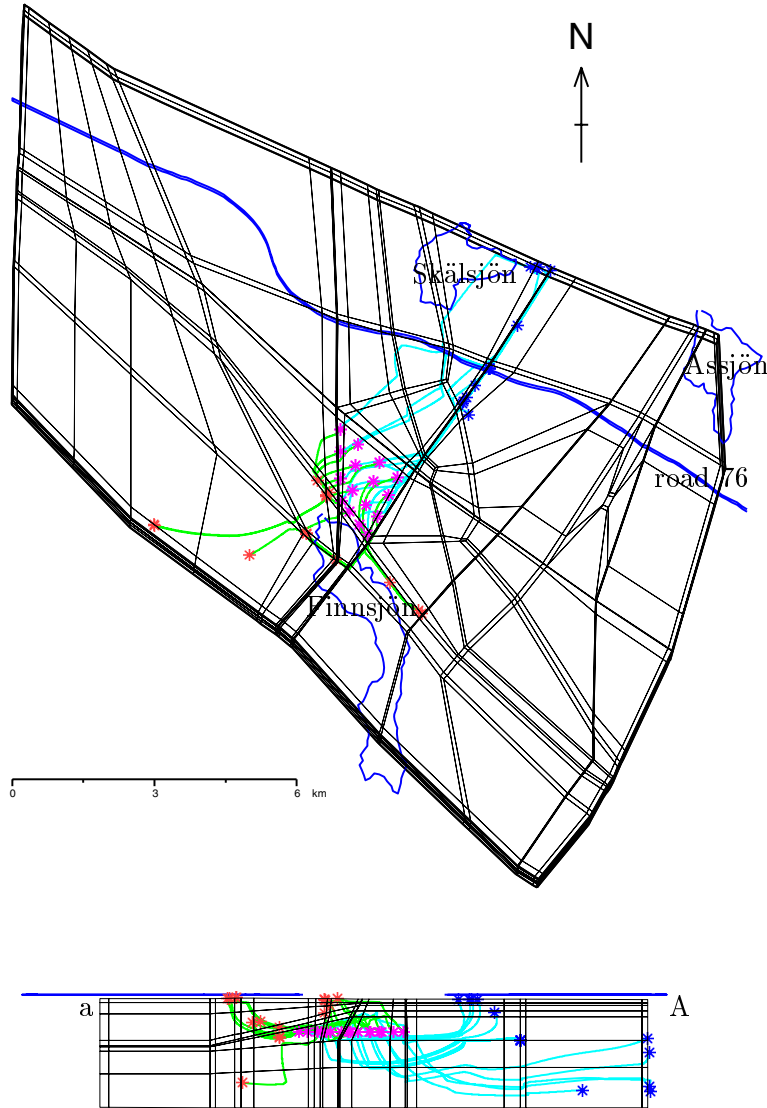


Figure 6.5: Forward (blue) and backward (green) pathlines for the Csouth variant. A set of 16 pathlines are started from the northern block at a depth of $z = -600\text{m}$. Points of origin, discharge and recharge for each path are shown by an asterisk coloured pink, purple and orange, respectively.

Figure 6.6 shows pathlines for the Dlow variant. In this case there is a slight increase in discharge around the intersect between Zone 1 and Imundbo. Recharge from the low ridge in the south west is also increased. This implies dispersion does not have a strong influence on these results. The range of travel times is between 2 and 1870 years.

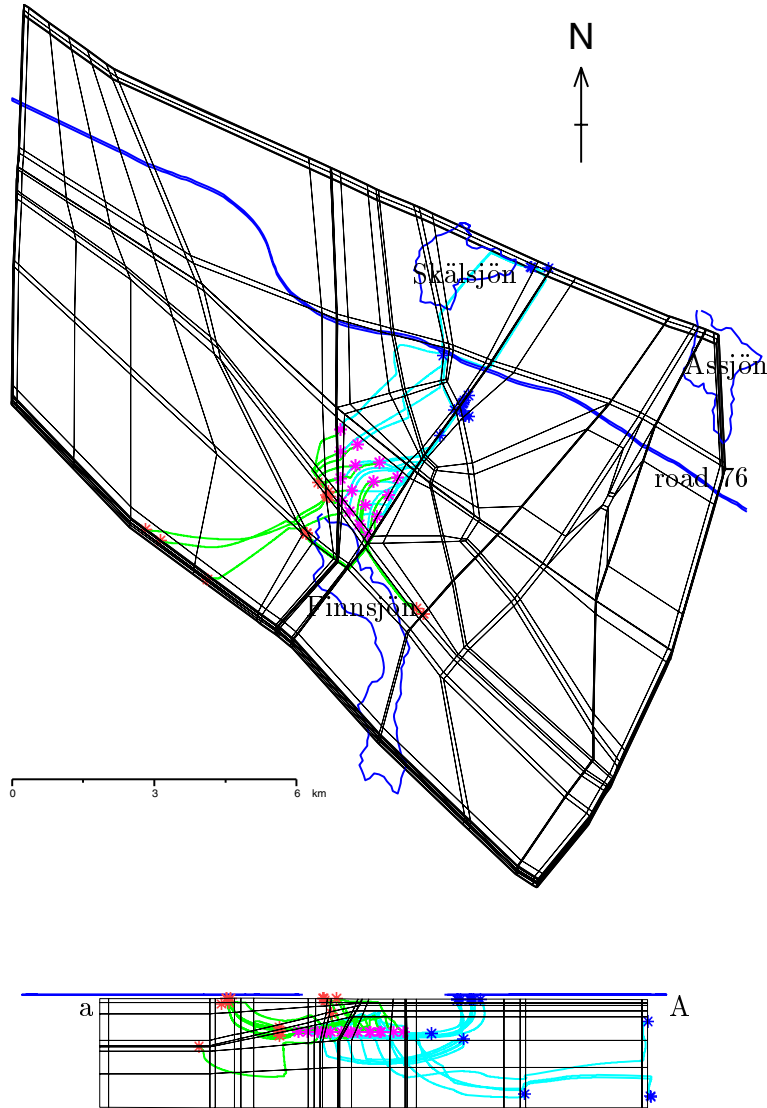


Figure 6.6: Forward (blue) and backward (green) pathlines for the Dlow variant. A set of 16 pathlines are started from the northern block at a depth of $z = -600\text{m}$. Points of origin, discharge and recharge for each path are shown by an asterisk coloured pink, purple and orange, respectively.

The effect of the local zones on groundwater pathways is insignificant. The results for the Zlocal variant are given in Figure 6.7. This was expected since the local zones effect the groundwater velocities most above Zone 2. The effect on pathlines below Zone 2 is small as a result of the poor hydraulic connection across Zone 2. Travel times for Zlocal vary between 2 and 762 years.

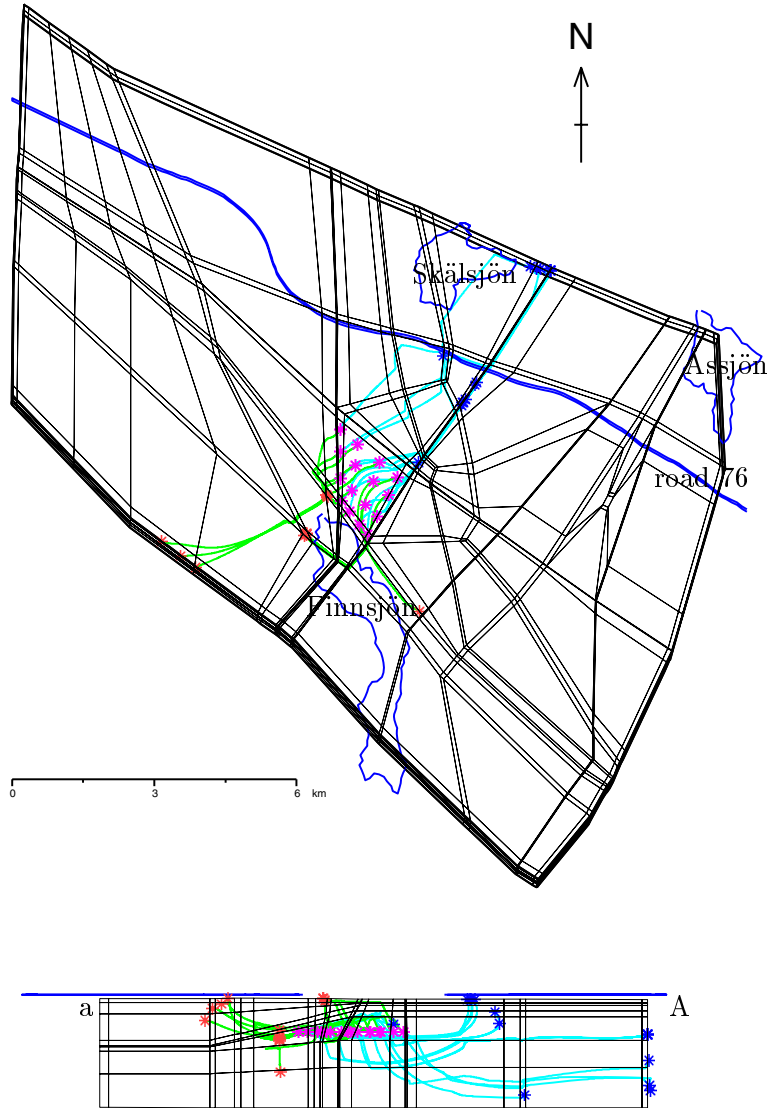


Figure 6.7: Forward (blue) and backward (green) pathlines for the Zlocal variant. A set of 16 pathlines are started from the northern block at a depth of $z = -600\text{m}$. Points of origin, discharge and recharge for each path are shown by an asterix coloured pink, purple and orange, respectively.

Anisotropy has a significant effect on pathlines. The results for the RRD3 variant are shown in Figure 6.8. The anisotropy in the rock mass channels all groundwater flow in the northern rock block southeast toward Zone 1. All pathlines now enter Zone 1, even those starting 2km away to the west. This is reflected in the traveled times. The minimum time is only 1 year and the average travel time is about 35% that of the base case. Hence, this is the worst case in terms of a performance assessment. The very short travel time is probably a result of the principal direction of hydraulic conductivity (NW-SE) channelling flow in the rock mass toward Zone 1. The fracture zones oriented SW-NE are likely to have higher velocities than in other variants because the contrast in hydraulic conductivity parallel to the hydraulic gradient is increased.

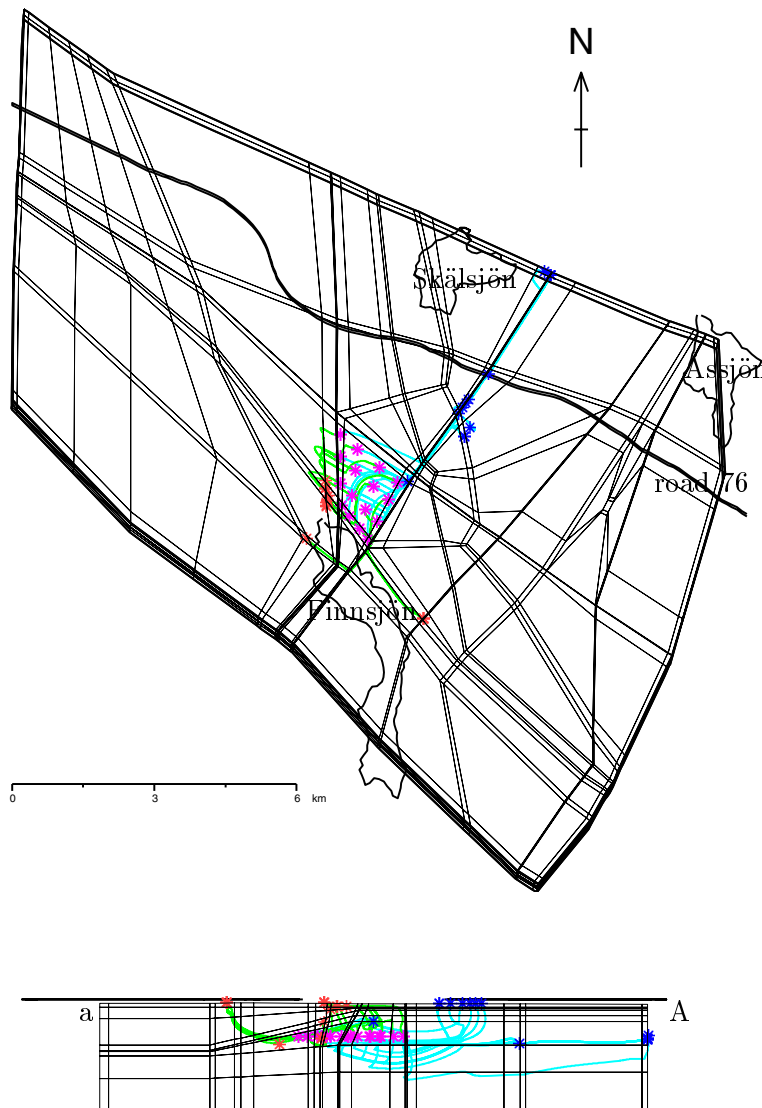


Figure 6.8: Forward (blue) and backward (green) pathlines for the RRD3 variant. A set of 16 pathlines are started from the northern block at a depth of $z = -600\text{m}$. Points of origin, discharge and recharge for each path are shown by an asterisk coloured pink, purple and orange, respectively.

The AltK variant is also very important for assessing groundwater pathways for the opposite reason to RRD3. This case has the longest travel times. Pathlines for the AltK variant are shown in Figure 6.9. Imundbo is now the dominant pathway for flow from the hypothetical repository, as suggest by the data in Subsection 5.3.11. There is only a single short path, and three long deep paths that follow Zone 1. The remaining twelve paths are long and deep along Imundbo, exiting the vertical northern boundary at about -1000masl. These results are similar to the X36 case in [Lindbom and Boghammar, 1992], which reflects the similarity in hydrogeological properties between AltK and that case. Travel times vary between 5,584 and 156,550 years. The reasons derive from the lower hydraulic conductivity in Zone 1. Zone 1 no longer dominates the site by draining the adjacent rock block. The dominant path is now Imundbo, but this is further away and not aligned with the head gradient.

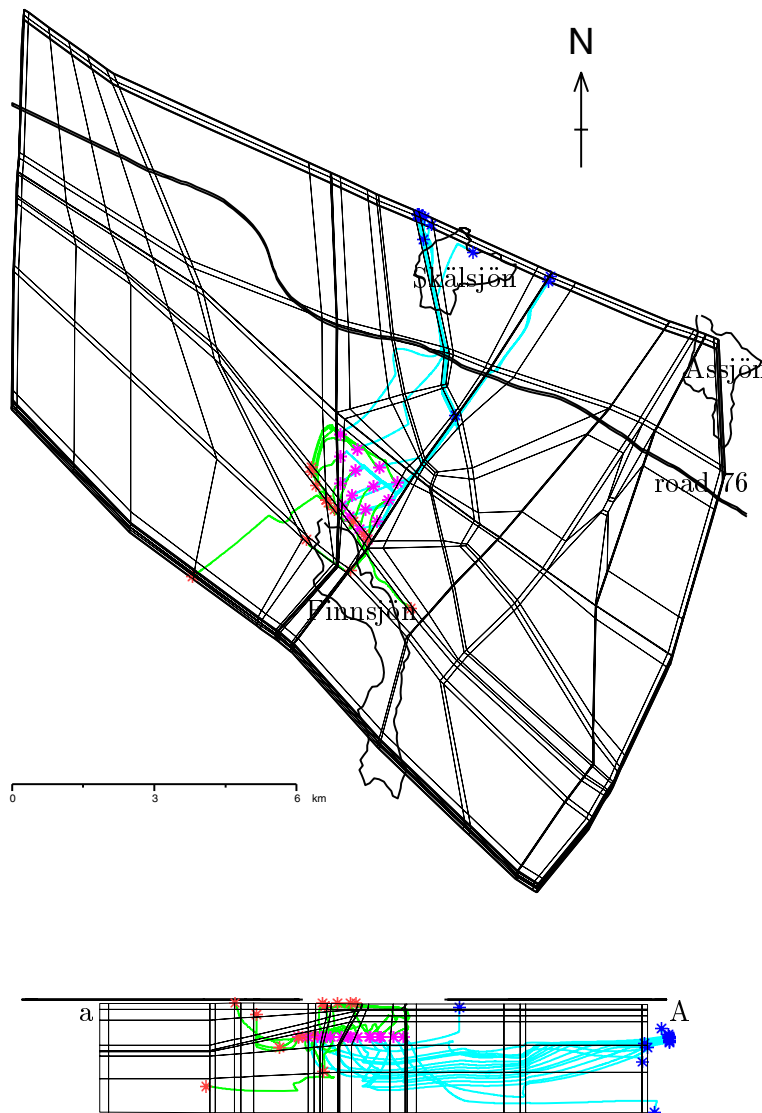


Figure 6.9: Forward (blue) and backward (green) pathlines for the AltK variant. A set of 16 pathlines are started from the northern block at a depth of $z = -600\text{m}$. Points of origin, discharge and recharge for each path are shown by an asterisk coloured pink, purple and orange, respectively.

6.1.3 Freshwater (Uniform density) Case

For comparison, pathlines are shown for the case of steady-state uniform density (freshwater) groundwater flow in Figure 6.10. The differences are significant. Firstly, pathlines starting in the west are much more shallow in the freshwater case. Secondly, all the paths are relatively short. All discharge occurs around Zone 1 or Giboda. Travel times are correspondingly shorter, 1 to 515 years. Thus, it would appear that for Beberg, salinity generally has a beneficial effect on repository performance.

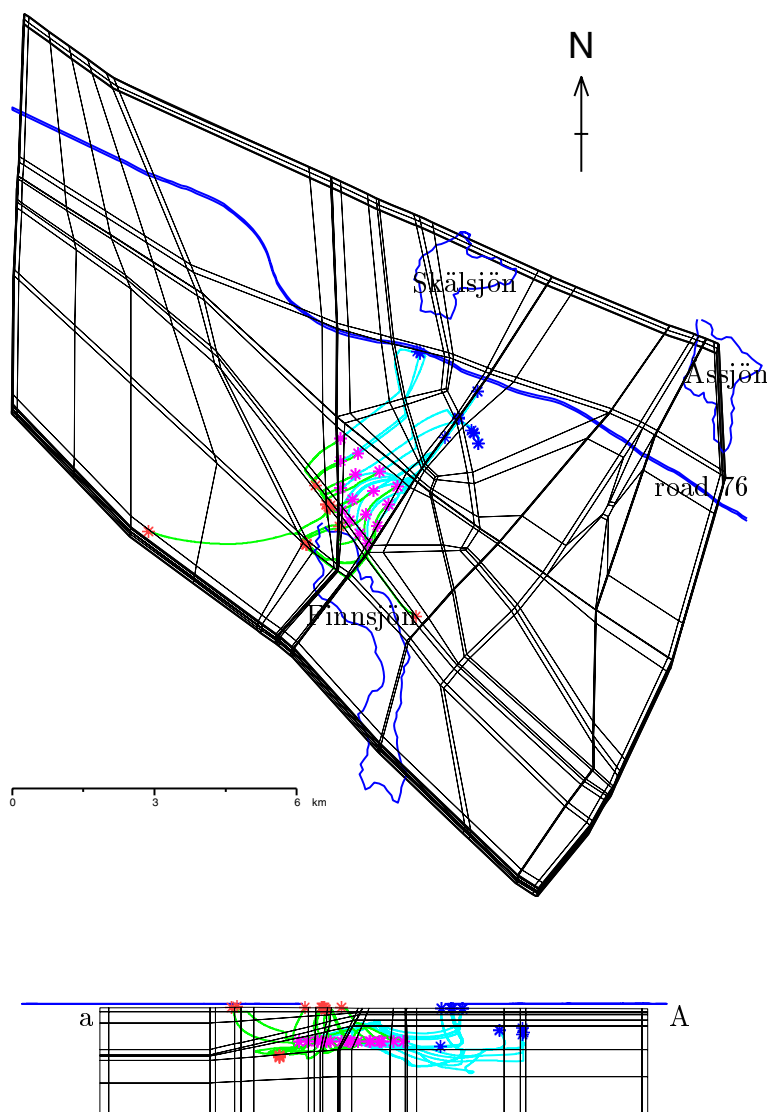


Figure 6.10: Forward (blue) and backward (green) pathlines for the freshwater variant. A set of 16 pathlines are started from the northern block at a depth of $z = -600\text{m}$. Points of origin, discharge and recharge for each path are shown by an asterisk coloured pink, purple and orange, respectively.

6.2 Choice of Local Scale Model and Summary

The choice of local scale model is driven by the requirement that it should contain the location of hypothetical repository and as much of the downstream region as is feasible. Ideally, it should include the relevant discharge regions. The results presented in Subsection 6.1 indicate the region bounded by Zone 14, Zone 12, Zone 1 and Giboda (see Figure 3.3) is the minimum domain for the local scale model at Beberg. This region does not include the discharge zones for the very long pathlines that exit the northern vertical boundary, but these paths are unlikely to contribute significantly to risk. The fact that the pathlines are found to be relatively insensitive to parameter variations implies the proposed local scale domain is appropriate for a large region of parameter space. Generally, recharge derives mostly from Zone 14 and discharge occurs in Zone 1 or Imundbo to the north east.

The minimum, average and maximum travel time for each variant are given in Table 6.1. The minimum travel time occurs for pathlines starting in the eastern side of the hypothetical repository adjacent to Zone 1. For this region Zone 1 is the dominant groundwater pathway, being highly transmissive and aligned with hydraulic gradient. Much longer travel times of over 800 years are experienced for pathlines starting in the west. In this case, the groundwater pathway is mainly through the rock mass, which leads to significant retardation. Although the minimum travel time is sensitive to changes, the average and maximum travel times are relatively invariant. Table 6.1 also indicates the number of 'short' paths, those less than 5km, and approximates the number of paths that discharge on the top surface south of Giboda. In most cases this is about 37-50%. The Dlow, Freshwater and AltK variants are notable exceptions. For Dlow and AltK pathlines stay deep in the saline region, and tend to exit the model on the vertical boundaries. For the Freshwater case all except one path is shallow and emerges south of Giboda.

Table 6.1: Summary of travel times for the sensitivity variants for 16 pathlines.

Variant	Travel time (years)			Number of short paths (< 5km)
	Minimum	Average	Maximum	
Base Case	10	271	882	6
Zsouth	10	287	765	10
ZlowK ϕ	15	331	661	6
Z11	10	273	876	6
Csouth	10	293	763	10
Dlow	2	446	1,869	13
Zlocal	2	202	762	8
RRD3	1	99	651	8
AltK	28	282	758	1
Freshwater	1	203	515	16

Since there are at least two distinct pathways, one along Zone 1 and the other through the rock mass, it would be useful to quantify the distribution of hypothetical repository

volume associated with each of these pathways. This requires a more detailed study than carried out here, and is best achieved using a local scale model.

6.3 Boundary Conditions

The local scale modelling is carried out with the Hydrastar stochastic continuum program. This solves the steady-state constant density groundwater flow equations for a stochastic permeability distribution. Such a model needs to be provided with boundary conditions for pressure which describe a hydraulic gradient consistent with the regional scale model. For a steady-state constant density regional scale model this is straightforward. Pressure is simply interpolated from the regional scale. For a transient variable density regional scale model the transfer of boundary condition is more problematic.

The first difficulty is that in general variable density flow cannot be described by the gradient of a single potential. Horizontal flows are given by the gradient in the residual pressure, p^r . Vertical flows are given by the gradient in the environmental pressure (density adjusted), p^e , [Luszczynski, 1961] given by

$$p^e(x, y, z) = p^r(x, y, z) - \int_z^{z_0} (\rho - \rho_0)g dz \quad .$$

In this, x , y , and z are Cartesian co-ordinates and z is measured vertically upwards. z_0 is some reference datum, usually chosen such that groundwater is fresh at this elevation, and hence $p^e(z_0) = p^r(z_0)$.

The consequence of using either one of these pressures to define boundary conditions for a constant density local scale model are as follows. Using residual pressure would predict consistent horizontal flows, but vertical flows would be over estimated. Environmental pressure would predict consistent vertical flows, but horizontal flows may be incorrect. A basis for selecting the most appropriate pressure to use is to consider the variations in density. If the density is near stratified, such that $\rho(x, y, z) \approx \rho(z)$, then environmental pressure is the correct potential to use. If density variations are dominantly horizontal then residual pressure is more appropriate.

For Beberg variations in salinity are generally greater in the vertical than horizontal direction, and hence the environmental pressure should give the best approximation of the boundary conditions to be used in the local scale model. Figure 6.11 compares three different descriptions of pressure: residual pressure, environmental pressure, and pressure for a steady-state freshwater calculation. For each plot the base case model was used. The most notable difference is that for residual pressure the flow beneath Zone 2 would be directed upwards; for environmental pressure it would have a significant downwards component; for freshwater pressure it would be mainly horizontal. It shall be interesting to see how these results compare with those for a constant density local scale model.

In summary, it is recommended that the environmental pressure (centre plot) is used

in defining the boundary conditions for the local scale. The alternative descriptions of pressure could be used to scope the sensitivity of the local scale results to assumptions made about the boundary conditions.

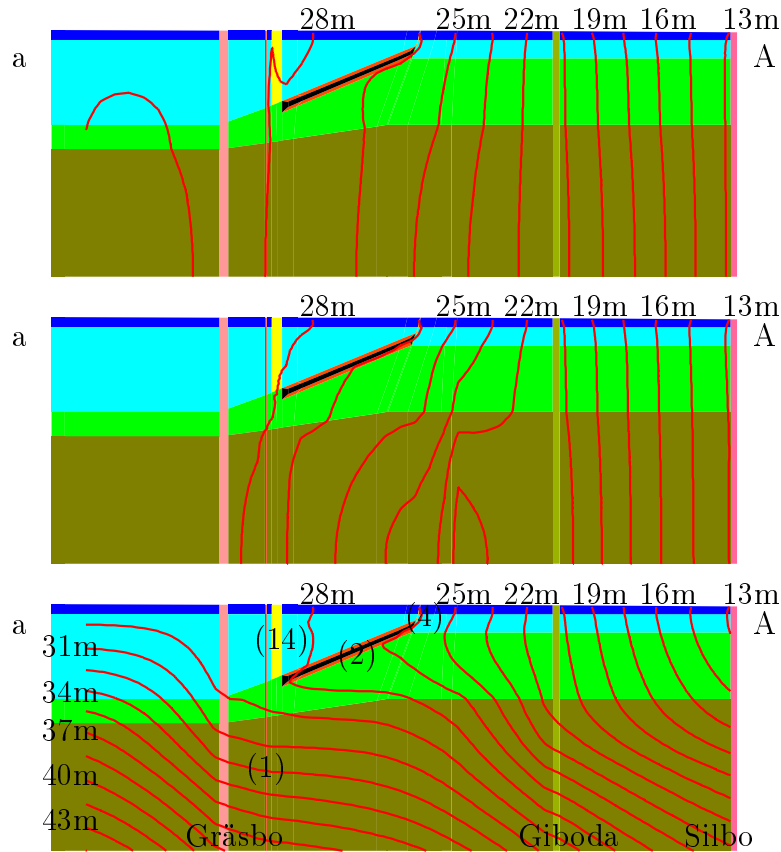


Figure 6.11: Three alternative prescriptions for defining pressure boundary conditions on the local scale model. Pressure contours are shown on the vertical slice a-A (see Figure 4.2). The plots are (bottom to top) for residual pressure, environmental pressure, and steady-state freshwater pressure. Contours of pressure are plotted in terms of the equivalent head $h = p/\rho_0g$ at intervals of 1.5m between 13m and 43m. Note the vertical scale is exaggerated by a factor of 2.

6.4 Comparison of Saline and Non-Saline Cases

In Subsection 6.1.3 it was shown that pathlines starting at the hypothetical repository location follow shorter and shallower trajectories when salinity is absent. The effects

of salinity at depth can also be illustrated by visualising the flow field. Plots of the three-dimensional velocity field for a saline case (the base case) and a non-saline case (the Freshwater variant) are shown in Figure 6.12. In each case velocity arrows are drawn for a horizontal slice at hypothetical repository depth and a vertical slice running N-S through the northern rock block. Velocity arrows are of constant length, but are projected onto a two-dimensional plane, so that arrows out of the plane appear short. The arrows are coloured according to the order of magnitude of the Darcy flow, $\log(|\mathbf{q}|)$. Dark blue is a slow flow. Light blue, Green, yellow and brown are progressively more rapid flows. Flows are clearly highest in the fracture zones, and the relatively large flows, $\sim 10^{-8}\text{ms}^{-1}$, along the highly conductive bands of Zone 2 can be seen. The most significant difference between the two cases are that flow below Zone 2 is vertically downwards and east for the saline case, but mainly upwards and northeast in the non-saline case. The general pattern of flow below Zone 2 and downstream is deeper in the saline case. This explains the short pathlines seen in Subsection 6.1.3 for the non-saline case, and demonstrates the important influence of salinity on the deep regional scale groundwater flow pattern.

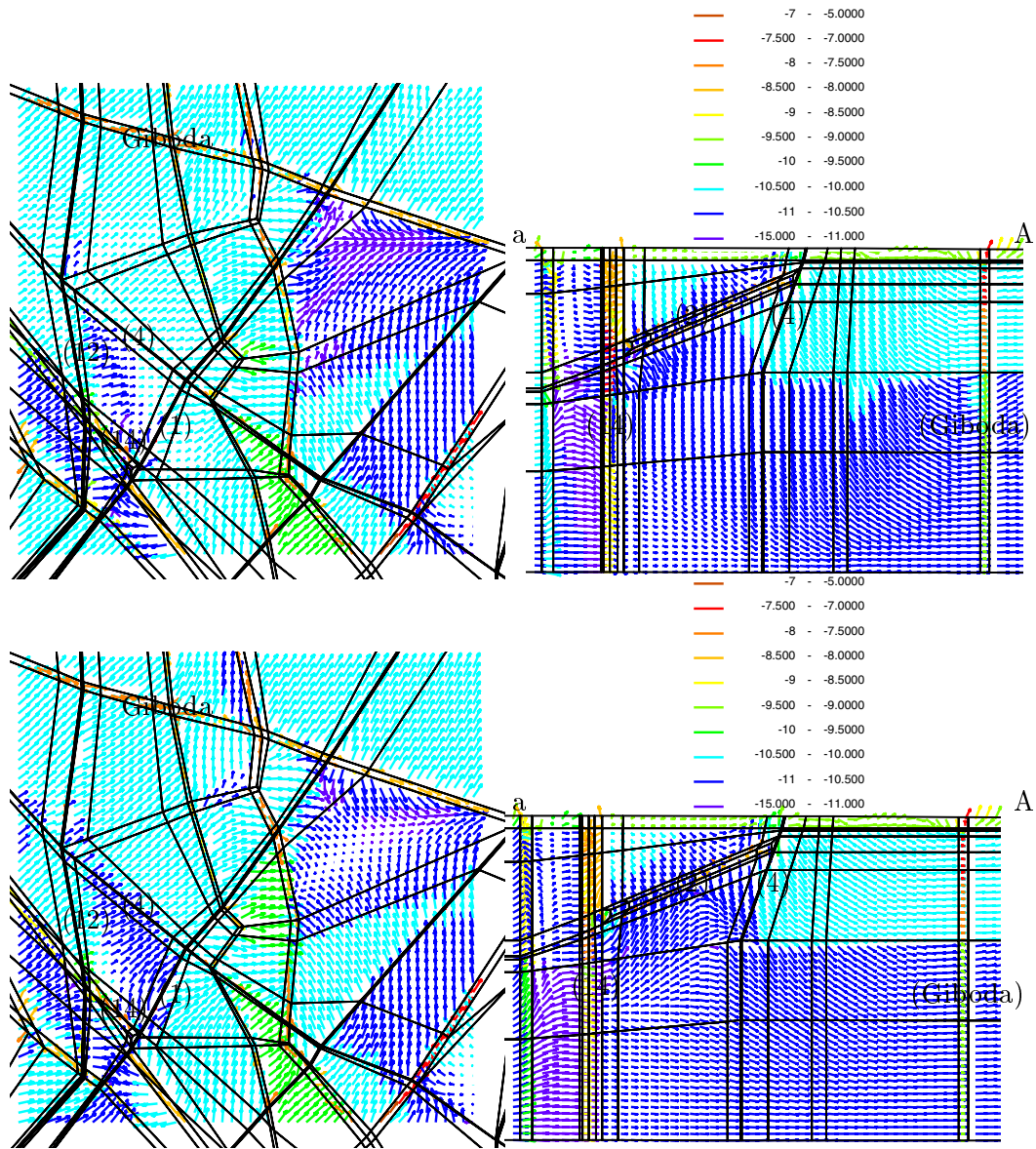


Figure 6.12: A comparison of velocity profiles for variable and constant density cases. The top profiles are the Darcy velocity at present day on a horizontal slice (left) at -600masl and on vertical slice a-A (right) for the base case. The bottom profiles are equivalent plots for the freshwater variant. The colours and key indicate the magnitude of velocity $\log(|\mathbf{q}|)$. The vertical scale in the right hand plots is exaggerated by a factor 2.

7 DETAILED MODEL WITH LAND-RISE

In this chapter a more detailed transient model is presented which examines whether any bias in the results given in Chapters 4-6 may have been introduced by the simplification of boundary conditions. This more detailed model focuses on the base case only. The boundary conditions for this model are more sophisticated than those used in the previous chapters (see Section 4.3) in the following three ways:

1. the head distribution on the top surface of the model is more detailed since topography is interpolated on a finer length scale;
2. the identification of recharge and discharge which determines the salt boundary condition on the top surface is performed automatically at each time-step (see Section 2.5.2);
3. the head boundary condition on the top surface evolves in time to represent the effects of land-rise over the last 4,000 years (see Section 2.5.1).

The set of boundary conditions used in this model give a more realistic description of transient geosphere as proposed in Section 2.4. Incorporation of the extra complexity has only been possible due to very recent developments to the functionality of NAMMU.

The numerical implementation of these boundary conditions and the effects on groundwater pathways are described below.

7.1 Finer Interpolation of Topography

The head distribution as shown in Figure 4.4, and used in the models described in Chapters 4-6, is based on a coarse interpolation of topography on the finite-element mesh. In these original models the interpolation was performed only at the corners of the finite-element patches (about 80 nodes in total). Mostly these are located at the intersections of the fracture zones. Head values at other nodes on the top surface

were calculated by bi-linear interpolation on the finite-element patches. This gives rise to the relatively smooth head distribution seen in Figure 4.4. A more detailed representation is obtained by interpolating topography at every node on the top surface of the finite-element mesh. This is about 1820 nodes, and hence there are many small local variations in the head distribution as seen in Figure 7.1.

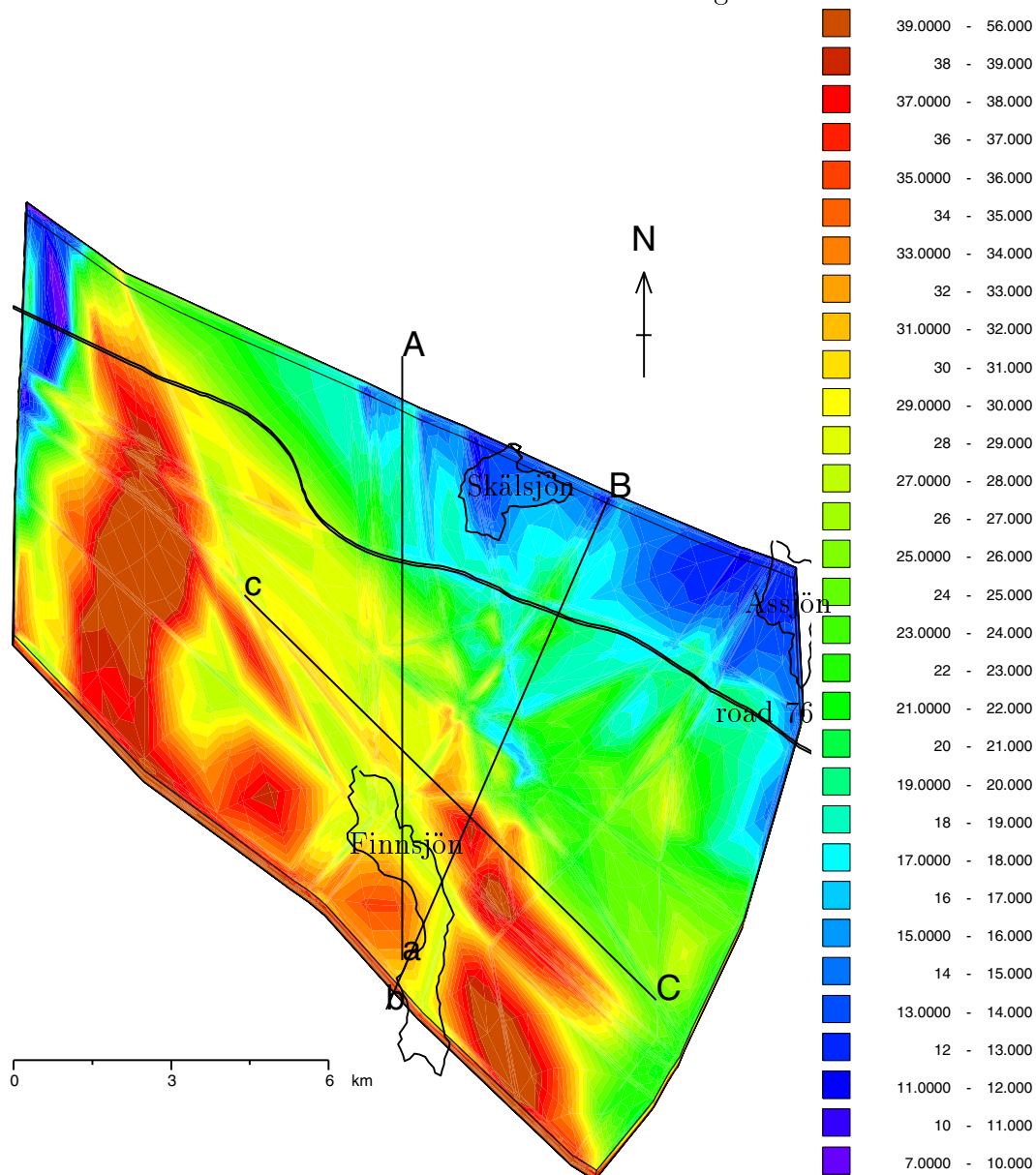


Figure 7.1: Distribution of head on the top surface of the model based on a fine scale interpolation of the present day topography. The numbers shown in the key are in units of metres. The positions of the 3 vertical slices a-A, b-B and c-C used in the calibration are indicated. Three lakes and road 76 are also shown as a reference.

Since the water table usually follows a smoother distribution than topography, one has to be careful in assuming that the head shown in Figure 7.1 is necessarily more realistic than that in Figure 4.4. However, it is important to evaluate whether local scale topographic features have an effect on flow. Hence, to see what effect topography

alone has, a variant with the more detailed head boundary condition is considered. Apart from the distribution of head set on the top surface the variant is exactly the same as the base. The same fixed distribution of recharge and discharge was used to set the salinity boundary condition on the top surface. The extra effects of land-rise are considered later in Section 7.2.

The groundwater pathways for this variant are shown in Figure 7.2.

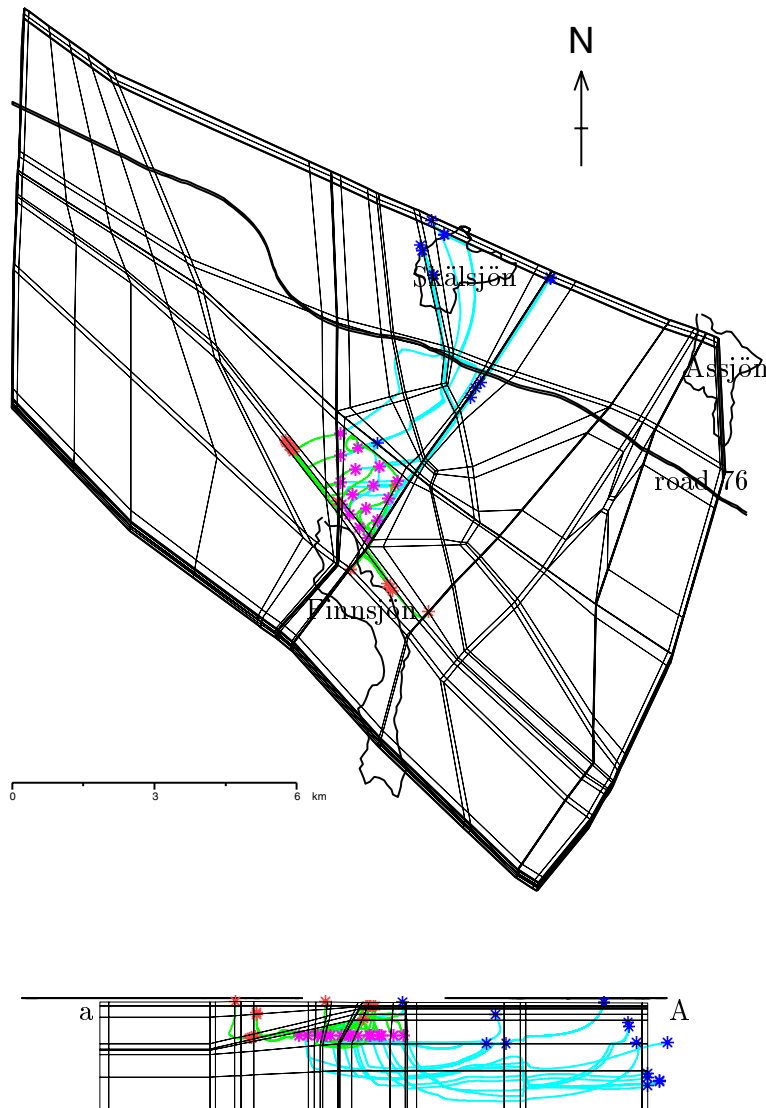


Figure 7.2: Forward (blue) and backward (green) pathlines detailed model without land-rise. A set of 16 pathlines are started from the northern block at a depth of $z = -600\text{m}$. Points of origin, discharge and recharge for each path are shown by an asterisk coloured pink, purple and orange, respectively.

Figure 7.2 shows that the localised topography has a substantial effect on the forward pathlines and discharge areas, but little effect on recharge areas. There are now more paths that remain deep and exit the model on the northern vertical boundary. Only four out of sixteen pathlines are short and discharge on the top surface. Table 7.1 shows

Table 7.1: Summary of travel times for the two detailed variants.

Variant	Travel time (years)			Number of short paths (< 5km)
	Minimum	Average	Maximum	
detailed topography	16	634	1534	4
land-rise	14	580	1268	4

how this effects the travel times. The average travel time has increased because there is a higher proportion of long paths. This is significant, since it suggests groundwater pathways will be sensitive to the localised water table surface northeast of the site. Interestingly, more of the long paths follow Imundbo in this variant, though the travel time for this path is similar to that along Zone 1.

7.2 Representation of Land-Rise

The effects of land-rise over the last 4,000 years are modelled by imposing a time-dependent head distribution on the top surface, as described in Section 2.5.1. The head value at any point is set to the current height of topography less 28 metres, and then increased according to a land-rise of 7mm/year. Of course this head value is negative for low lying areas at early times since the land would have been below sea level. In this case the head is reset to zero. Figure 7.3 shows the distribution of head on the top surface at three intervals in history: 4,000 years BP (the initial condition), 2,000 years BP and at present day. The same key is used to contour the surface head distribution, so the land-rise and coastal regression can be seen. The sea is shaded purple.

As can be seen in Figure 7.3 much of the model region was covered by sea 4,000 years BP, whereas today the coast is about 15km to the northeast. Due to this evolution of the coast the location of discharge areas can change in time. In Section 2.5.2 it was explained that the appropriate definition of salt boundary conditions on the top surface depends on the distribution of recharge and discharge, and so the salt boundary also needs to evolve in time when land-rise is modelled. What is required is to specify the salt boundary condition according to the recharge/discharge distribution at any given instant. There is a mathematical difficulty in formulating such a condition: where there is recharge one needs to specify a Dirichlet boundary condition ($c = 0$) for salt, where there is discharge a Neumann boundary condition (outflow condition). The solution is to specify a generalised non-linear Neumann boundary condition where the Dirichlet boundary condition is included as a penalty function. Specification of the mass flux, $F_c(\mathbf{x}, t)$, at time t out of a boundary is formulated as:

$$F_c = \begin{cases} \rho c \mathbf{q} \cdot \mathbf{n} & \mathbf{q}(\mathbf{x}, t) \cdot \mathbf{n}(\mathbf{x}) > 0 \\ \delta(c - c_0) & \mathbf{q}(\mathbf{x}, t) \cdot \mathbf{n}(\mathbf{x}) \leq 0 \end{cases}$$

where $\mathbf{q}(\mathbf{x}, t)$ is the Darcy velocity distribution, δ is a penalty weight, and c_0 is the specified value of salinity, zero in this case.

The penalty function ensures that a Dirichlet condition is set where $\mathbf{q}(t) \cdot \mathbf{n} \leq 0$ by introducing an appropriately large flux of salt to maintain salinity at approximately the specified value. If $c > c_0$ the boundary condition imposes a large outflow to reduce the salinity at the boundary. If $c < c_0$ the boundary condition imposes a large inflow. The higher the value of the penalty weight δ the closer the value of c to c_0 . To avoid any numerical ill-conditioning the penalty weight was set to

$$\delta = 10^3(\rho|\mathbf{q}|).$$

In order to get a stable numerical scheme using Newton-Raphson iterations it was necessary to base the non-linear boundary condition on the flow $\mathbf{q}(t)$ at the previous time-step. This ensured that the distribution of recharge and discharge was fixed between iterations at any one time-step, but could change between time-steps.

The way in which the recharge and discharge evolve is demonstrated in Figure 7.4. Flow arrows are coloured according to the vertical component on a slice near the surface at 3,600 years BP and at present. At 3,600 years BP the sea covered much of the model in the northeast. This is shown by the stagnant flow (dots) in this region. In this case where there is no vertical flow, the boundary condition becomes $F_c = 0$. That is, zero flux of salinity. Recharge and discharge for the rest of model appear to change much less, presumably because the head gradient in the near surface is not changing significantly.

The distribution of salinity for the detailed model is shown in Figure 7.5. The main differences from the base case are the reduced salinity above Zones 2 and 11, salinity is deeper in the southern rock block, and the saline transition across Zone 2 is slightly sharper. It is concluded that the model is well calibrated and more realistic in terms of the predicted salinity in the southern rock block. Pathlines corresponding to this case are shown in Figure 7.6. These are very similar to those shown in Figure 7.6, as are the travel times given in Table 7.1. It appears then that land-rise does not have a significant effect on pathlines started at the present day. This is probably because the coast retreated several kilometres away from the site at least 2,000 years BP. Land-rise is likely to be more important for a site situated closer to the present day coastline.

In summary:

- the results show sensitivity to local variations in topography;
- by including local variations in topography the number of short paths is reduced;
- it is possible to model the evolution of head and salinity boundary conditions appropriate to post-glacial land-rise at a near coastal site;
- the effects of land-rise are minimal for pathlines started at the present day;
- land-rise is likely to be more important for a site situated closer to the present day coastline.

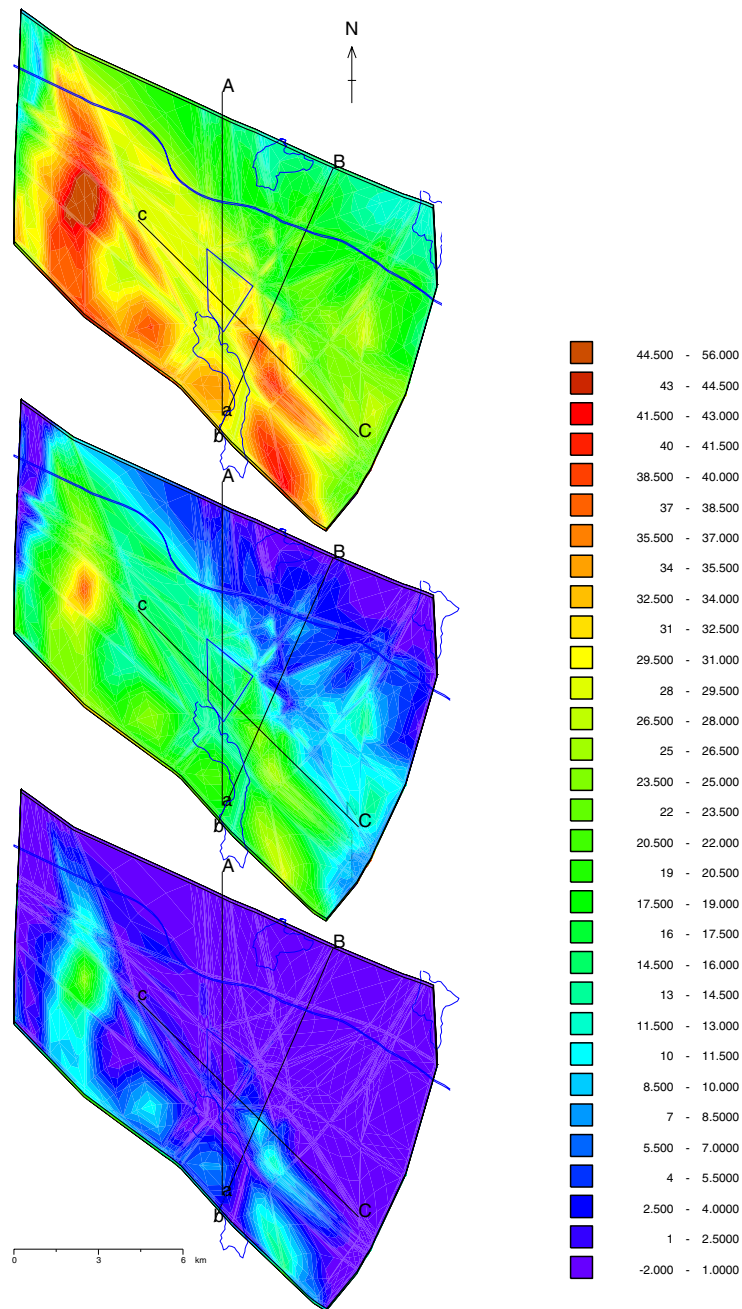


Figure 7.3: Distribution of head on the top surface of the model at 4,000 years BP (bottom), 2,000 years BP (centre) and at present (top). The numbers shown in the key are in units of metres. The same key is used for ewach time. The positions of the 3 vertical slices a-A, b-B and c-C used in the calibration are indicated. The northern rock block, three lakes and road 76 are also shown as a reference.

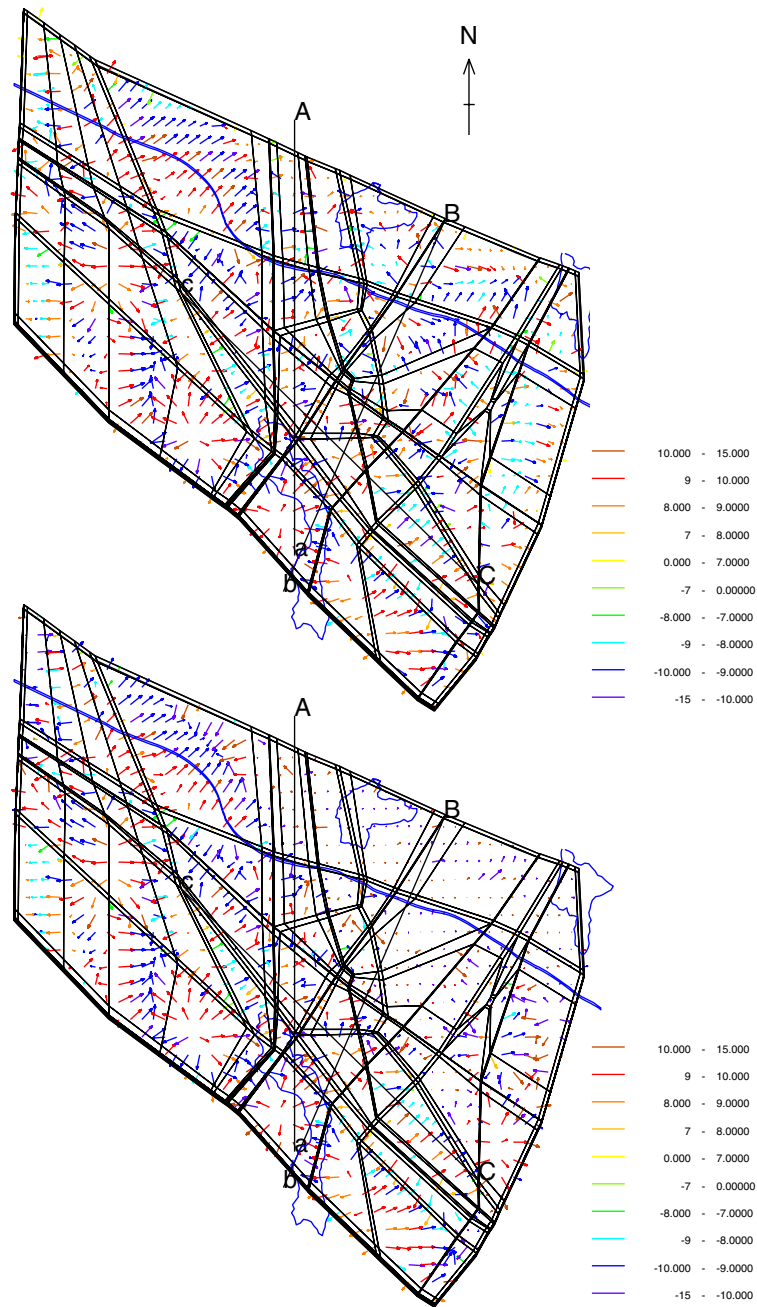


Figure 7.4: Plan view of the flow field for a slice near the top surface at 3,600 years BP (bottom) and at the present day (top). The key indicates the logarithm and sign of the vertical component of darcy velocity in units of ms^{-1} . Three lakes and road 76 are also shown as a reference.

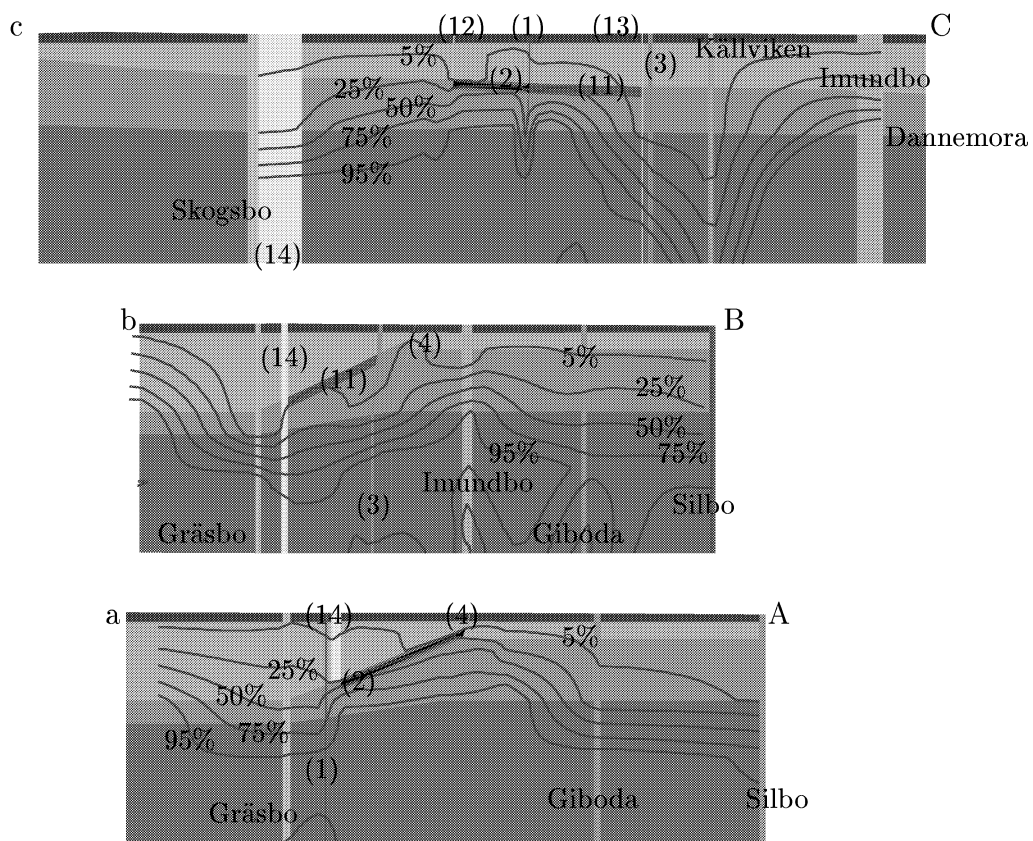


Figure 7.5: Salinity on vertical slices along a-A, b-B, c-C (see Figure 4.2) for the base case. The contours of salinity shown correspond to 5%, 25%, 50%, 75% and 95% of the maximum salinity (corresponding to 6, 500mg/l). Note the vertical scale is exaggerated by a factor of 2.

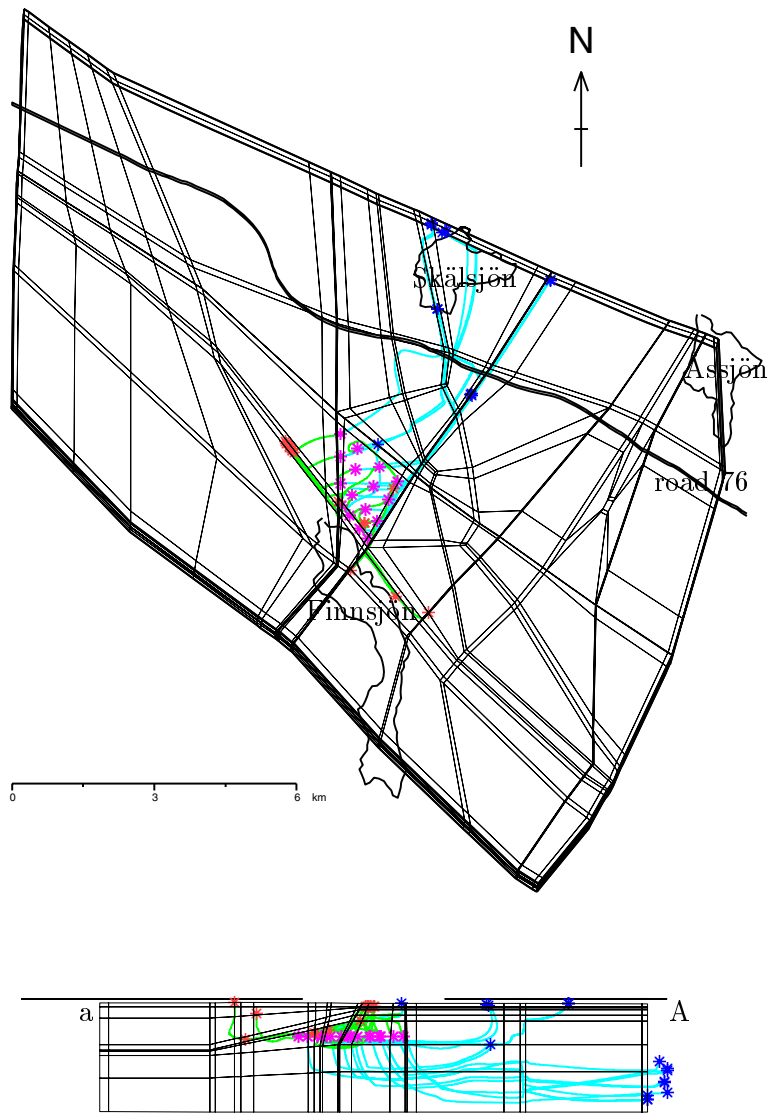


Figure 7.6: Forward (blue) and backward (green) pathlines for the detailed model with land-rise. A set of 16 pathlines are started from the northern block at a depth of $z = -600\text{m}$. Points of origin, discharge and recharge for each path are shown by an asterix coloured pink, purple and orange, respectively.

8 CONCLUSIONS

The present study addresses a number of objectives. The conclusions for each objective are discussed below.

Large-scale groundwater flow and salinity patterns: In order to understand the groundwater flow and salinity at present it is necessary to consider the history of the Finnsjön site over the last few thousand years. A numerical approach is developed to model a situation of transient variable density flow on a regional scale. The model is considered a reasonable representation of the real situation at the site, since it is consistent with the current conceptual understanding of the site and predictions of salinity are in broad agreement with field observations.

Salinity is found to be very important in determining the groundwater pathway for pathlines starting in the northern rock block beneath Zone 2. The model predicts that salinity is driving flow downwards here, while it is upwards in the non-saline case. Generally the pattern of groundwater flows is much deeper, -1kmasl or more, when salinity is present. The result is that pathlines tend to stay at depth below the saline transition zone giving pathlengths of 8km or more, compared to less than 5km for the non-saline case. All this has good implications for the contribution to safety from the salinity in the geosphere.

In all cases considered pathlines are directed to the north or north east of the hypothetical repository location. Zone 1 and the Imundbo regional zone are important features in determining the direction of flow. Their relative transmissivities determining which of these is the dominant flow path.

Examine the effects of natural transient processes: The effects of post-glacial uplift on the hydrogeological conditions are considered. It is assumed that the rock was completely infiltrated by saline groundwaters during the periods when the Yoldia and Litorina Seas covered the Finnsjön area. This provides an initial condition when the land rose above sea level about 4,000 years BP. The model represents the period from this time up to the present day. During which time the recharge of fresh water in the form of rainfall flushed or displaced saline water from the near-surface. It is found that the total porosity of the rock mass and the hydraulic conductivity of the fracture zones are the most important parameters in determining the rate at which the flow and salinity patterns evolve.

The results show that fractures zones are flushed of salt on a relatively short time-scale of 10-100 years. The equivalent time-scale for the rock mass is a few thousand years in the near-surface and on the order of 10,000 years for the deep rock.

Locations of significant recharge and discharge: The Lakes and surface drainage to the north and north east of the site are identified as likely discharge areas. However, due to the effects of salinity, many pathlines are found to exit the northern boundary of the model at depth. Hence, it is possible that discharge may occur 8km or more from the study site. All pathlines remain in the region between Zones 1 and 12.

The major recharge areas relevant to the site lie to the south and south west and are very localised. Zone 14 appears to be the main feature controlling recharge to the hypothetical repository location, though the low ridge to the south west also has some influence.

Determine boundary conditions appropriate to transient saline flow A prescription for boundary conditions on pressure and salinity appropriate to transient variable density flow is developed. Boundary conditions for pressure and salinity are applied on the vertical sides (the ‘far-field’) and on the top surface (the external environment) of the model. In reality, the pressure and salinity evolve in time as conditions change in the far field and external environment. Hence, a set of time-dependent boundary conditions are imposed which approximate this situation.

On vertical sides we impose hydrostatic pressure which varies in time as salinity changes on the boundary; and an advective outflow or inflow (depending on the direction of the normal component of velocity) of salt. On the top surface, pressure is specified as a function of ground elevation (and land-rise in the detailed model); where there is recharge salt is specified to be zero, where there is discharge an advective outflow of salinity is specified. Hence, the boundary conditions are both non-linear and transient. We believe that these boundary conditions give the most realistic mathematical description of the actual temporal and spatial variations of the system. Use of constant Dirichlet boundary conditions would be an over-simplification.

Calibrate the model to establish the combination of hydrogeological features and parameters that gives the best fit present day conditions: The main calibration of the model is to compare predictions of the current salinity distribution against that observed in the deep boreholes at the study site. The high values of salinity in and below Zone 2 can only be reproduced by including a semi-impermeable band within Zone 2, and reducing the hydraulic importance of the fracture Zones around the northern block below Zone 2.

Two alternative interpretations of the fracture zones [*Walker et al., 1997; Walker, 1998*] are considered. The case RCD1 has a constant hydraulic conductivity in the fracture zones. The alternative AltK has a decrease in hydraulic conductivity of about one order of magnitude below -100masl. RCD1 calibrates only if Zones 3, 12 and 14 are truncated above their intercept with Zone 2. AltK calibrates without any changes to its definition.

Of course, the model only represents an idealised situation. In a more general sense, the model indicates that the observed salinity profile can be reproduced with the following constraints on the structural model:

- the effective vertical hydraulic conductivity of Zone 2 on the regional scale is lower than the rock mass;
- Zone 2 is the dominant hydraulic feature at depth;
- and that other fracture zones have a transmissivity of similar or smaller magnitude to that of the surrounding rock mass blocks.

Clearly, this has important implications for the site characterisation.

The total porosity is also an important parameter to calibrate, since it determines the rate at which the salinity pattern evolves. The central values used are 2% for the rock mass and 5% for the fracture zones. These values are in good agreement with laboratory scale measurements.

A secondary calibration was to check that the recharge of groundwater at the surface was consistent with potential infiltration in the area. This was found to be the case for the central values of hydraulic conductivity provided by Walker et al. [1997].

Spatial extent of the regional model required: The size of the regional model required to model the evolution of the hydrogeological situation over the last 4,000 years has to be large. The model used in this work is about 16km by 10km. There is no firm basis on which the size of this model can be reduced significantly. Attempts to do so resulted in the boundary conditions having a strong influence on flow and salinity at the site. The main restriction being that any upstream (inflow) boundaries should be far from the site, as the salinity on this boundary is very uncertain.

Select the location of a site scale model: The results of pathline calculations suggest the site scale model should as a minimum include the region immediately to the north of the study site. Imundbo, Zones 1 and 3 all have an influence on pathlines originating in the northern block. Hence, it is recommended that the local scale model be bounded by Gräsbo in the south, Zone 13 in the east, Giboda in the north and Zone 12 in the west. Two distinct groundwater pathways were identified. A rapid pathway along Zone 1, and a slow path through the rock mass to the north of the site. The distribution of hypothetical repository volume associated with each of these pathways could be quantified using the local scale model.

The alternative structural model AltK gave much longer travel times and pathlines which mainly followed Imundbo rather than Zone 1. Hence, the uncertainty associated with the interpretation of the hydraulic conductivity of the local fracture zones, and its possible depth dependence, may have a significant impact on the performance assessment. In terms of travel times, the anisotropic case RRD3 has the shortest paths, and AltK the longest.

Supply such a model with appropriate boundary conditions: There is no exact method for defining the boundary conditions of a steady-state constant density site scale model based the results of transient variable density regional scale calculations. However, approximate boundary conditions can be defined if groundwater travel times are less than the time-scale on which salinity changes – a few thousand years. In the case where density variations are more significant in the vertical direction than the horizontal, the environmental pressure can be used to calculate variable density flows, and hence it should be used to define pressure boundary conditions for the site scale.

This condition appears to be valid for most of the model at Beberg, although there are some rapid horizontal density gradients around the intersect of Zones 1 and 2, for instance. Hence, the environmental pressure is still likely to give the best approximation to the forces driving flow. The sensitivity to this assumption could be quantified by also using the dynamic pressure or a pressure derived from a steady-state freshwater calculation to define the site scale boundary conditions.

The pathline calculations suggest that particle transport is relatively insensitive to the parameter variations considered in the variants based on RCD1. There are more significant differences for the alternative structural model AltK variant, but this is the ‘safest’ case. Even if this site interpretation is judged the more realistic, a case based on RCD1 should be assessed for reasons of conservatism. Travel times and groundwater pathways are far more sensitive to the particular location from which particles are started. Hence, the choice of variant used to transfer boundary conditions to the local scale model is not expected to be critical, and so it proposed that the base case is used.

8.1 Future Work

It is recommended that further work be considered to expand on the model and ideas developed in this study and to examine their validity. This includes:

Expand calibration: The calibration reported here is quantitative in nature and is focussed on the salinity distribution. There are several areas in which the assumptions made in the model could be checked. These include:

1. re-analysis of the conceptual model for Zone 2 to obtain large scale hydraulic properties along and across the permeable and impermeable bands;
2. calibrate the salinity predictions against any shallow wells with saline water in the region. This would particularly be useful in the north east where the model predicts discharge of saline groundwater;
3. assess the sensitivity of the calibration and pathlines to the hydraulic conductivities of Zones 1, 3, 4, 12, 14 and Imundbo within their range of uncertainty;

4. compare the distribution of discharge areas predicted by the model with the location of swamps in the region.

Long term transients: The current study has concentrated on the period when the land around the site emerged from the sea, about 4,000 years BP, to the present day. Safety assessments of nuclear waste facilities typically have to take into account changes in the environment over very long periods. Therefore, a more comprehensive study would be to model the evolution of the hydrogeology over a much longer time-scale, from perhaps the last ice age to the next. This would have to consider the infiltration of saline water from the precursors to the Baltic Sea, the present intrusion of fresh groundwater, and effects of the next glacial event.

Forwards modelling: a related issue is the sensitivity of particle transport to the actual time at which particles enter the geosphere. In this study all pathlines were calculated using the current groundwater flow distribution. Since the hydrogeological situation is clearly evolving it may be appropriate to consider transport at a range of times in the future.

9 REFERENCES

Ahlbom K., 1991. *The groundwater circulation in the Finnsjö area - the impact of density gradients. Part A: Saline Groundwater at the Finnsjö site and its surroundings.* **SKB TR 91-57.**

Ahlbom K., Andersson P., Ekman L., Tiren S., 1988. *Characterization of fracture zones in the Brandan area, Finnsjön study site, central Sweden.* **SKB AR 88-09.**

Ahlbom K., Andersson J.-E., Andersson P., Ittner T., Ljunggren C., Tiren S., 1992. *Finnsjön study site. Scope of activities and main results.* **SKB TR 92-33.**

Almen K.-E., Ekman L., Olkiewicz A., 1978, *Försöksområdet vid Finnsjön. Beskrivning till berggrunds- och jordarts kartor.*

Andersson J.-E., Nordqvist R., Nyberg G., Smellie J., Tiren S., 1989. *Hydrogeological conditions in the Finnsjön area.* **SKB AR 89-24.**

Andersson J.-E., Nordqvist R., Nyberg G., Smellie J., Tiren S., 1991. *Hydrogeological conditions in the Finnsjön area. Compilation of data and conceptual model.* **SKB TR 91-24.**

Boghammar A., Grundfelt B., Widen H., 1993, *Analysis of the regional groundwater flow in the Finnsjön area.* **SKB TR 93-15.**

Brandberg F., Skagius K., 1991, *Porosity, Sorption and diffusivity data compiled for the SKB 91 study.* **SKB TR 91-16.**

Carlsson L., Winberg A., Arnefors J., 1986, *Hydraulic modeling of the final repository for reactor waste (SFR). Compilation and conceptualization of available geological and hydrogeological data.* **SKB Progress Report SFR 86-03.**

Cliffe K.A., Jackson C. P., Morris S. T., 1995, *Assessment Model Validity Document; NAMMU: A program for calculating groundwater flow and transport through porous media.* **SKB AR 95-11.**

de Marsily G., 1981, *Quantitative Hydrogeology.* **Academic press, Inc. pp. 80–82.**

- Laaksoharju M., Gurban I., Skårman C., 1998, *SR97: Summary of Hydro-geochemical conditions at Aberg, Beberg, Ceberg*. **SKB TR 98-03**.
- Lindbom B., Boghammar A., Lindberg H., Bjelkås J., 1991, *Numerical groundwater flow calculations at the Finnsjön site*. **SKB TR 91-12**.
- Lindholm B., Boghammar A., 1992, *Numerical groundwater flow calculations at the Finnsjön study site – extended regional area*. **SKB TR 92-03**.
- Luszczynski N.J., 1961, *Head and flow of ground water of variable density*. **Journal of Geophysical Research, Vol.66, No. 12, pp. 4247-4256**.
- Smellie J. A. T., Wikberg P., 1983, *Characterization of fracture zone 2, Finnsjön study site*. **In: Ahlbom and Smellie (eds.) SKB TR 89-19**.
- Svensson U., 1991, *The groundwater circulation in the Finnsjö area - the impact of density gradients. Part C: A three-dimensional numerical model of groundwater flow and salinity distribution in the Finnsjö area*. **SKB TR 91-57**.
- Voss, C.I. and Andersson J., 1993, *Regional flow in the Baltic Shield during holocene coastal regression*. **Ground Water, Vol. 31, No. 6, pp.989–1006**.
- Walker D., Rhen I., Gurban I., 1997, *Summary of hydrogeologic conditions at Aberg, Beberg and Ceberg*. **SKB TR 97-23**.
- Walker D., 1998, *MEMO. Re: Supplementary parameter specifications for hydraulic conductivity at Beberg: depth-dependency in vertical fractures, anisotropy in rock mass*. **Memo, February 24, 1998**.

A COUPLED GROUNDWATER FLOW AND SALT TRANSPORT EQUATIONS

Coupled groundwater flow and solute transport with the density strongly dependent upon concentration is modelled in terms of the variables p^r and c using the following equations:

$$\frac{\partial}{\partial t}(\phi\rho) + \nabla \cdot (\rho\mathbf{q}) = 0, \quad (\text{A.1})$$

$$\mathbf{q} = -\frac{\mathbf{k}}{\mu}(\nabla p^r - [\rho - \rho_0]\mathbf{g}), \quad (\text{A.2})$$

and

$$\frac{\partial}{\partial t}(\phi\rho c) + \nabla \cdot (\rho\mathbf{q}c) = \nabla \cdot (\phi\rho\mathbf{D} \cdot \nabla c), \quad (\text{A.3})$$

where \mathbf{k} is the permeability tensor, μ is the fluid viscosity and ϕ is the total porosity. The Equations (A.1) and (A.2) are combined into a single second-order partial differential equation for p^r , which we call the pressure equation.

The dependence of density upon the salt variable, c is given by

$$\frac{1}{\rho} = \frac{1-c}{\rho_0} + \frac{c}{\rho_s}. \quad (\text{A.4})$$

It can be seen then that variable c represents a mass fraction of saline water to fresh water. If the density difference is small ($(\rho_s - \rho_0)/\rho_s \ll 1$), then density can be approximated by a linear expression

$$\rho \sim \rho_0 \left(1 + \frac{(\rho_s - \rho_0)c}{\rho_s} \right). \quad (\text{A.5})$$

For Beberg, the values $\rho_0 = 998.3\text{kg m}^{-3}$ and $\rho_s = 1006.3\text{kg m}^{-3}$ are used. Hence, density can be expressed in terms of a linear relationship to the mass fraction c :

$$\rho \sim 998.3(1 + 0.008c). \quad (\text{A.6})$$

Equivalently, density can be related to the concentration of Chloride, $X(\text{mg/l})$,

$$\rho \sim 998.3 + 0.00123X, \quad (\text{A.7})$$

or salinity, $S(\%)$,

$$\rho \sim 998.3 + 7.46S. \quad (A.8)$$

Salinity, S , is related to Chloride concentration, X , according to the relative molecular weight NaCl of Chloride

$$S = \frac{W_{NaCl}}{W_{Cl}} \frac{X}{10^4} = \frac{58.44}{35.45} \frac{X}{10^4} = 1.65 \cdot 10^{-4} X. \quad (A.9)$$

The maximum salinity can therefore be expressed in any of the following ways

$$\begin{aligned} c &= 1 \\ X &= 6,500\text{mg/l} \\ S &= 1.07\% \\ \rho &= 1008.3\text{kg m}^{-3} \end{aligned} \quad (A.10)$$

The hydrodynamic dispersivity \mathbf{D} is given by

$$D_{ij} = \frac{D_m}{\tau} \delta_{ij} + \alpha_T v \delta_{ij} + (\alpha_L - \alpha_T) \frac{v_i v_j}{v}, \quad (A.11)$$

where the porewater velocity is given by

$$\mathbf{v} = \frac{\mathbf{q}}{\phi} \quad \text{and} \quad v = (\mathbf{v} \cdot \mathbf{v})^{\frac{1}{2}}. \quad (A.12)$$

B DATA

Table B.1: Summary of hydrogeological data used in the modelling.

Subject	Comments	References
Grid	Digitised from structural map Topography interpolated on to mesh from SKB GIS database RAK coordinate system is used throughout Depth of sub-horizontal zones approximated Grid created using NAMMU. Fracture zones represented explicitly	TR 92-33 TR 92-33, data TR 97-23 AR 95-11
Concepts	Post-glacial events define the initial condition and the time-scale considered in the model. Initial condition 4,000 years BP with bedrock filled with saline water Land rise about 6-7mm/year	[<i>Almen et al., 1978</i>], TR 89-19 TR 92-38, TR 97-23
Hydrogeological parameters	Regional fracture zone widths and hydraulic conductivities provided Rock mass properties from 3m sections up-scaled to SGU data scale (100m). Small variation with depth. Storativity of limited significance Total porosity calibrated in range 0.5-3% for rock mass, 1-5% for fracture zones Flowing porosity consistent with Aberg and Ceberg 10^{-4} Dispersivity uncertain 1-100m Zone 2 split in to horizontal bands of low and high permeability	TR 97-23 TR 97-23 AR 88-09, AR 89-24 TR 91-16 TR 97-23 TR 92-33 TR 91-24
Salinity	0.8% density contrast used for deep groundwater Salinity present at many shallow wells in region Salinity profiles calibrated against borehole data	TR 97-23 TR 97-23 TR 98-03

Table B.2: Hydrogeological parameters used in the modelling.

Hydrogeological unit	Hydraulic conductivity ms^{-1}	Total porosity	Longitudinal dispersion m	Transverse dispersion m
Near Surface	$1.55 \cdot 10^{-7}$	2%	80	40
Above Zone 2	$1.28 \cdot 10^{-8}$	2%	80	40
Below Zone 2	$1.58 \cdot 10^{-8}$	2%	80	40
Basement	$6.00 \cdot 10^{-9}$	2%	80	40
Zone 1	$4.68 \cdot 10^{-5}$	5%	80	40
Zone 1 (deep)	$1.50 \cdot 10^{-6}$	5%	80	40
Zone 2 (high K)	$1.45 \cdot 10^{-5}$	5%	20	10
Zone 2 (low K)	$1.00 \cdot 10^{-9}$	5%	20	10
Zone 3	$2.34 \cdot 10^{-6}$	5%	80	40
Zone 3 (deep)	$8.00 \cdot 10^{-8}$	5%	80	40
Zone 4	$6.92 \cdot 10^{-6}$	5%	80	40
Zone 4 (deep)	$2.30 \cdot 10^{-7}$	5%	80	40
Zone11	$1.58 \cdot 10^{-8}$	2%	80	40
Zone12	$1.23 \cdot 10^{-5}$	5%	80	40
Zone12 (deep)	$4.00 \cdot 10^{-7}$	5%	80	40
Zone13	$4.68 \cdot 10^{-5}$	5%	80	40
Zone13 (deep)	$1.50 \cdot 10^{-6}$	5%	80	40
Zone14	$3.25 \cdot 10^{-6}$	5%	80	40
Zone14 (deep)	$1.10 \cdot 10^{-7}$	5%	80	40
Imundbo	$6.92 \cdot 10^{-6}$	5%	80	40
Imundbo (deep)	$2.30 \cdot 10^{-7}$	5%	80	40
Gräsbo	$3.25 \cdot 10^{-6}$	5%	80	40
Gräsbo (deep)	$1.10 \cdot 10^{-7}$	5%	80	40
Skogsbo	$6.92 \cdot 10^{-6}$	5%	80	40
Skogsbo (deep)	$2.30 \cdot 10^{-7}$	5%	80	40
Silbo	$1.23 \cdot 10^{-5}$	5%	80	40
Silbo (deep)	$4.00 \cdot 10^{-7}$	5%	80	40
Örbyhus	$1.23 \cdot 10^{-5}$	5%	80	40
Örbyhus (deep)	$4.00 \cdot 10^{-7}$	5%	80	40
Källviken	$4.68 \cdot 10^{-5}$	5%	80	40
Källviken (deep)	$1.50 \cdot 10^{-6}$	5%	80	40
Dannemora	$1.23 \cdot 10^{-5}$	5%	80	40
Dannemora (deep)	$4.40 \cdot 10^{-7}$	5%	80	40
Giboda	$1.04 \cdot 10^{-5}$	5%	80	40
Giboda (deep)	$3.50 \cdot 10^{-7}$	5%	80	40
NS2	$1.23 \cdot 10^{-5}$	5%	80	40
NS2 (deep)	$4.00 \cdot 10^{-7}$	5%	80	40

C QUALITY ASSURANCE

This appendix records the file locations and edit records for the main NAMMU input data files.

C.1 File Locations

All files are stored on AEA Technology's UNIX fileserver abel (151.182.148.103). Copies of the NAMMU input data sets are also stored on SKB's UNIX workstation sultan (192.36.18.209).

The NAMMU input files (.dat) for the regional model are located in
/net/abel/vp0/lee/nammu/2119sr97/beberg/grl/dat (on abel)

/export/nammu/2119sr97/beberg/grl/nam (on sultan)

The NAMMU output files (.out) for the regional model are located in
/net/abel/vp0/lee/nammu/2119sr97/beberg/grl/out (on abel)

The NAMMU postscript files (.ps) for the regional model are located in
/net/abel/vp0/lee/nammu/2119sr97/beberg/grl/ps (on abel)

The NAMMU model files (.mdl) for the regional model are located in
/net/abel/vp0/lee/nammu/2119sr97/beberg/grl/ml (on abel)

The NAMMU solution files (.gf) for the regional model are located in
/net/abel/vp0/lee/nammu/2119sr97/beberg/grl/gf (on abel)

C.2 NAMMU Input Files

Table C.1 gives the NAMMU input data files for each of the variants. For each variant NAMMU a dataset was used to create the model, calculate an initial condition, carry out a transient solve and post-process the results.

Table C.1: Input files for main cases

Variant	Transient solve	Last edit	Model	Initial condition	Post-processing
Base case	grltrans52	07/12/97	grlmdls52	grlslvs52	grlposts52_g
Zdeep	grltrans51	09/12/97	grlmdls51	grlslvs51	grlposts51_g
Zsouth	grltrans54	11/12/97	grlmdls54	grlslvs54	grlposts54_g
Z2highK	grltrans56	12/12/97	grlmdls52	grlslvs56	grlposts56_g
ZlowK	grltrans55	12/12/97	grlmdls55	grlslvs55	grlposts55_g
ZlowK ϕ	grltrans55a	12/12/97	grlmdls55	grlslvs55	grlposts55a_g
Z11	grltrans53	09/12/97	grlmdls52	grlslvs53	grlposts53_g
Csouth	grltrans57	15/12/97	grlmdls52	grlslvs52	grlposts57_g
ϕ low	grltrans58	13/12/97	grlmdls52	grlslvs52	grlposts58_g
Dlow	grltrans59	13/12/97	grlmdls52	grlslvs52	grlposts59_g
Zlocal	grltrans60	15/12/97	grlmdls60	grlslvs60	grlposts60_g
RRD3	grltrans61	23/02/98	grlmdls61	grlslvs61	grlposts61_g
AltK	grltrans62a	06/03/98	grlmdls62	grlslvs62	grlposts62a_g
Fresh	grlfresh52	16/12/97	grlmdls52	N/A	N/A
detailed top	grltrans73	15/12/97	grlmdls72	grlslvs72	grlposts73_g
land-rise	grltrans75	12/01/98	grlmdls74	grlslvs75	grlposts75_g

List of SKB reports

Annual Reports

1977-78

TR 121

KBS Technical Reports 1 – 120

Summaries

Stockholm, May 1979

1979

TR 79-28

The KBS Annual Report 1979

KBS Technical Reports 79-01 – 79-27

Summaries

Stockholm, March 1980

1980

TR 80-26

The KBS Annual Report 1980

KBS Technical Reports 80-01 – 80-25

Summaries

Stockholm, March 1981

1981

TR 81-17

The KBS Annual Report 1981

KBS Technical Reports 81-01 – 81-16

Summaries

Stockholm, April 1982

1982

TR 82-28

The KBS Annual Report 1982

KBS Technical Reports 82-01 – 82-27

Summaries

Stockholm, July 1983

1983

TR 83-77

The KBS Annual Report 1983

KBS Technical Reports 83-01 – 83-76

Summaries

Stockholm, June 1984

1984

TR 85-01

Annual Research and Development Report 1984

Including Summaries of Technical Reports Issued during 1984. (Technical Reports 84-01 – 84-19)

Stockholm, June 1985

1985

TR 85-20

Annual Research and Development Report 1985

Including Summaries of Technical Reports Issued during 1985. (Technical Reports 85-01 – 85-19)

Stockholm, May 1986

1986

TR 86-31

SKB Annual Report 1986

Including Summaries of Technical Reports Issued during 1986

Stockholm, May 1987

1987

TR 87-33

SKB Annual Report 1987

Including Summaries of Technical Reports Issued during 1987

Stockholm, May 1988

1988

TR 88-32

SKB Annual Report 1988

Including Summaries of Technical Reports Issued during 1988

Stockholm, May 1989

1989

TR 89-40

SKB Annual Report 1989

Including Summaries of Technical Reports Issued during 1989

Stockholm, May 1990

1990

TR 90-46

SKB Annual Report 1990

Including Summaries of Technical Reports Issued during 1990

Stockholm, May 1991

1991

TR 91-64

SKB Annual Report 1991

Including Summaries of Technical Reports Issued during 1991

Stockholm, April 1992

1992

TR 92-46

SKB Annual Report 1992

Including Summaries of Technical Reports Issued during 1992

Stockholm, May 1993

1993

TR 93-34

SKB Annual Report 1993

Including Summaries of Technical Reports Issued during 1993

Stockholm, May 1994

1994

TR 94-33

SKB Annual Report 1994

Including Summaries of Technical Reports Issued during 1994

Stockholm, May 1995

1995

TR 95-37

SKB Annual Report 1995

Including Summaries of Technical Reports Issued during 1995

Stockholm, May 1996

1996

TR 96-25

SKB Annual Report 1996

Including Summaries of Technical Reports Issued during 1996

Stockholm, May 1997

List of SKB Technical Reports 1998

TR 98-01

Global thermo-mechanical effects from a KBS-3 type repository. Summary report

Eva Hakami, Stig-Olof Olofsson, Hossein Hakami, Jan Israelsson

Itasca Geomekanik AB, Stockholm, Sweden

April 1998

TR 98-02

Parameters of importance to determine during geoscientific site investigation

Johan Andersson¹, Karl-Erik Almén², Lars O Ericsson³, Anders Fredriksson⁴, Fred Karlsson³, Roy Stanfors⁵, Anders Ström³

¹ QuantiSci AB

² KEA GEO-Konsult AB

³ SKB

⁴ ADG Grundteknik KB

⁵ Roy Stanfors Consulting AB

June 1998

TR 98-03

Summary of hydrochemical conditions at Aberg, Beberg and Ceberg

Marcus Laaksoharju, Iona Gurban, Christina Skärman

Intera KB

May 1998

TR 98-04

Maqarin Natural Analogue Study: Phase III

J A T Smellie (ed.)

Conterra AB

September 1998

TR 98-05

The Very Deep Hole Concept – Geoscientific appraisal of conditions at great depth

C Juhlin¹, T Wallroth², J Smellie³, T Eliasson⁴, C Ljunggren⁵, B Leijon³, J Beswick⁶

¹ Christopher Juhlin Consulting

² Bergab Consulting Geologists

³ Conterra AB

⁴ Geological Survey of Sweden

⁵ Vattenfall Hydropower AB

⁶ EDECO Petroleum Services Ltd.

June 1998

TR 98-06

Indications of uranium transport around the reactor zone at Bagombe (Oklo)

I Gurban¹, M Laaksoharju¹, E Ledoux², B Made², A L Salignac²,

¹ Intera KB, Stockholm, Sweden

² Ecole des Mines, Paris, France

August 1998

TR 98-07

PLAN 98 – Costs for management of the radioactive waste from nuclear power production

Swedish Nuclear Fuel and Waste Management Co

June 1998

TR 98-08

Design premises for canister for spent nuclear fuel

Lars Werme

Svensk Kärnbränslehantering AB

September 1998

TR 98-09

Test manufacturing of copper canisters with cast inserts Assessment report

Claes-Göran Andersson

Svensk Kärnbränslehantering AB

Augusti 1998

TR 98-10
Characterization and Evaluation of Sites for Deep Geological Disposal of Radioactive Waste in Fractured Rocks

Proceedings from The 3rd Äspö International Seminar, Oskarshamn, June 10–12, 1998-11-10
Svensk Kärnbränslehantering AB
September 1998

TR 98-11
Leaching of 90-year old concrete mortar in contact with stagnant water

Jan Trägårdh, Björn Lagerblad
Swedish Cement and Concrete Research Institute
July 1998

TR 98-12
Geological-structural models used in SR 97

Uncertainty analysis
Pauli Saksa, Jorma Nummela
FINTACT Ltd
October 1998

TR 98-13
Late Quaternary changes in climate

Karin Holmgren and Wibjörn Karlén
Department of Physical Geography
Stockholm University
December 1998

TR 98-14
Partitioning and transmutation (P&T) 1997

Åsa Enarsson, Anders Landgren, Jan-Olov Liljenzin, Mats Skålberg, Lena Spjuth
Department of Nuclear Chemistry, Chalmers University of Technology, Gothenburg
and
Waclaw Gudowski, Jan Wallenius
Department of Nuclear and Reactor Physics, Royal Institute of Technology, Stockholm
May 1998

TR 98-15
Studies of surface complexation of H⁺, NpO₂⁺, Co²⁺, Th⁴⁺ onto TiO₂ and H⁺, UO₂²⁺ onto alumina

Anna-Maria Jakobsson, Yngve Albinsson
Department of Nuclear Chemistry, Chalmers University of Technology, Sweden
and
Robert S Rundberg
Los Alamos National Laboratory, USA
November 1998

TR 98-16
Backfilling with mixtures of bentonite/ballast materials or natural smectitic clay?

Roland Pusch
Geodevelopment AB
October 1998

TR 98-17
Groundwater degassing in fractured rock:

Modelling and data comparison
Jerker Jarsjö and Georgia Destouni
Water Resources Engineering
Royal Institute of Technology, Stockholm
November 1998

TR 98-18
The interaction of sorbing and non-sorbing tracers with different Äspö rock types
Sorption and diffusion experiments in the laboratory scale

Johan Byegård, Henrik Johansson, Mats Skålberg
Department of Nuclear Chemistry, Chalmers University of Technology, Gothenburg, Sweden
and
Eva-Lena Tullborg
Terralogica AB, Gråbo, Sweden
November 1998

TR 98-19
Äspö Hard Rock Laboratory Annual Report 1997

Svensk Kärnbränslehantering AB
May 1998

TR 98-20
The biosphere at Aberg, Beberg and Ceberg – a description based on literature concerning climate, physical geography, ecology, land use and environment

Tobias Lindborg, Regina Schöldt
NaturRådet
December 1998

TR 98-21
Crustal structure and regional tectonics of SE Sweden and the Baltic Sea

Alan Geoffrey Milnes
Department of Geology, University of Bergen, Norway
David G Gee and Carl-Erik Lund
Department of Earth Sciences, Uppsala University
November 1998

TR 98-22

**Development of a kinetic model for the
dissolution of the UO₂ spent nuclear
fuel**

**Application of the model to the minor
radionuclides**

Jordi Bruno, Esther Cera, Lara Duro, Jordi Pon
QuantiSci SL, Barcelona, Spain

Joan de Pablo

Department Enginyeria Quimica, UPC, Barcelona,
Spain

Trygve Eriksen

Department Nuclear Chemistry, KTH, Stockholm

May 1998

TR 98-23

**Site-scale groundwater flow
modelling of Aberg**

Douglas Walker

Duke Engineering & Services

Björn Gylling

Kemakta Konsult AB

December 1998

ISSN 0284-3757

CM Gruppen AB, Bromma, 1999